GEOLOGICA ULTRAIECTINA

MEDEDELINGEN VAN DE
FACULTEIT GEOWETENSCHAPPEN
UNIVERSITEIT UTRECHT

No. 264

Biogeochemical Cycling of Nutrients and Trace Metals in the Sediment of Haringvliet Lake: Response to Salinization

Richard W. Canavan

Promotor:	Prof. dr. P. Van Cappellen Department of Earth Science – Geochemistry Faculty of Geosciences, Utrecht University
Co-promotor:	Dr. C. P. Slomp Department of Earth Science – Geochemistry Faculty of Geosciences, Utrecht University

Members of the dissertation assessment committee:

Prof. dr. S.B. Joye	University of Georgia, Athens, Georgia USA
Prof. dr. G.J. de Lange	Utrecht University, Utrecht, The Netherlands
Prof. dr. J.J. Middelburg	Utrecht University & NIOO-KNAW, Yerseke, The Netherlands
Prof. dr. C. Rabouille	LSCE/IPSL, Gif-sur-Yvette, France
Prof. dr. A. Tessier	INRS-ETE, Université du Québec, Sainte-Foy, Québec Canada

Cover design: Sue Canavan
Printing: Grafisch bedrif Ponsen & Looijen, Wageningen

Biogeochemical Cycling of Nutrients and Trace Metals in the Sediment of Haringvliet Lake: Response to Salinization

Biogeochemische kringlopen van nutriënten en spoormetalen in sediment van het Haringvliet en gevolgen van verzilting
(met een samenvatting in het Nederlands)

PROEFSCHRIFT

ter verkrijging van de graad van doctor aan de Universiteit Utrecht op gezag van de rector magnificus, prof.dr.W.H. Gispen, ingevolge het besluit van het college voor promoties in het openbaar te verdedigen op dinsdag 17 oktober 2006 des ochtends te 10.30 uur

door
Richard William Canavan IV
geboren op 6 februari 1971
te Putnam, Connecticut,
Verenigde Staten van Amerika

This thesis was accomplished with financial support from RIZA (Institute for Inland Water Management and Waste Water Treatment) as part of the joint RIZA-Utrecht University project RESIN (Restoration of Estuarine Systems In the Netherlands: response of biogeochemical processes).

ISBN-10: 90-5744-128-4
ISBN-13: 978-90-5744-128-8

For Anouk, Isabella, and Lucas

Contents

Summary

Biogeochemical processes in sediments of shallow waterbodies are strongly coupled to processes in the overlying water. A quantitative understanding of the interactions and controls of sediment biogeochemistry is needed to determine the long-term fate of nutrients and pollutants that accumulate in aquatic sediments. The ability of sediments to retain nutrients and pollutants may be reduced by changing environmental conditions, such as salinization, anoxia, algae blooms, or changes in the benthic community structure. In areas subject to environmental change, sediments may then represent a so-called chemical time bomb, through the potential remobilization of previously stored nutrients and pollutants.

This thesis examines sediment redox processes associated with organic matter degradation and their impact on the cycling of nutrients (N, P) and trace metals (Cd, Co, Ni, Pb, Zn). Our study site, Haringvliet Lake, is located in the Rhine-Meuse River Delta in the southwest of The Netherlands. This waterbody was formerly a tidal and brackish estuary but was separated from the North Sea in 1970 by a dam, as part of the Delta Works program. Currently, a partial restoration of estuarine conditions in the lake is planned, which can be achieved by altering the management of the sluice gates within the dam. Concern that salinization of the recently deposited freshwater sediment in Haringvliet Lake could result in a release of nutrients and trace metals motivated this study. Salinization of coastal fresh waters is a phenomenon that is not limited to this particular site, however, as sea-level rise, intense coastal storms, climate change, and increased fresh water usage is increasing the risk of the salinization of coastal fresh waterbodies at the global scale.

The deposition of organic matter to aquatic sediments drives a series of interconnected redox reactions, as microorganisms oxidize the organic carbon. The oxidation of organic matter is coupled to the reduction of terminal electron acceptors, which include O_2, NO_3^-, Mn-(hydr)oxides, Fe-(hydr)oxides, SO_4^{2-}, and CO_2. The rapid degradation of organic matter can result in the formation of steep redox gradients in sediments. The mixing of sediment and pore water by benthic organisms results in the transport of solids and solutes across these redox gradients creating further opportunities for microbial and abiotic reactions. In Chapter 2 we use a multi-component reactive transport model (RTM) to infer the rates of organic carbon mineralization pathways in Haringvliet sediment. The model is calibrated using field measurements of solid phases and dissolved concentrations, and experimental determinations of reaction rates. We find that the most important terminal electron acceptors for organic carbon oxidation are O_2 (55%), NO_3^- (21%), and SO_4^{2-} (17%). Model simulations conducted

to approximate estuarine restoration show that the increased relative importance of sulfate reduction leads to a long-term conversion of sediment Fe(III) minerals to pyrite.

The sediment nitrogen cycle was examined with both experimental techniques (Chapter 3) and reactive transport modeling (Chapter 4). Potential nitrate reduction and denitrification rates were determined using flow through reactors (FTRs). Experiments suggest that denitrification accounts for only half of the total potential nitrate reduction rate in Haringvliet sediment. The remaining nitrate reduction is due to incomplete denitrification and alternative reaction pathways, most likely dissimilatory nitrate reduction to ammonium (DNRA). Increasing the salinity of the inflow solution in FTR experiments increases the release of ammonium and dissolved organic carbon from the sediment. It also enhances the rates of nitrate reduction and nitrite production, but not that of denitrification. In Chapter 4, the RTM developed in Chapter 2 is adapted to explicitly include both denitrification and DNRA. Sediment N-removal declines by 40% when nitrate reduction occurs via DNRA in place of denitrification. The net sediment-water exchange of dissolved inorganic nitrogen was more sensitive to the relative distribution of denitrification versus DNRA, than to other changes expected to accompany estuarine restoration. When DNRA is the dominant nitrate reduction pathway, N removal is limited to sediment burial and becomes less sensitive to additional environmental change.

Extraction results provide evidence that a reducible iron-phosphate mineral is a major pool for phosphorus in the sediment (Chapter 5). Phosphorus diagenesis is added to the RTM to examine the existing early diagenetic P cycle and changes that may result from estuarine restoration. The dissolution of the iron-phosphate phase and organic-P mineralization are important pathways for the release of PO_4 in the sediment. The sediment retains only 50% of the depositional P flux. Restoration of estuarine conditions in the Haringvliet is expected to decrease sediment retention of the iron phosphate phase.

Concentrations of Cd, Co, Ni, Pb, and Zn are reported for sediment pore water and sediment extractions (Chapter 6). Sediment trace metal concentrations are elevated, due to anthropogenic influences in the Rhine and Meuse Rivers. Results suggest that metals, which enter the sediment associated with oxides, become associated with sulfides. Extraction results show that Ni and Co ultimately associate with pyrite. Pore waters are generally saturated for trace metal mono-sulfides of Zn, Pb, Co, and Cd. The RTM developed in Chapter 2 is further adapted to include Zn and Ni. The model results are able to reproduce some of the trends observed in pore water and sediment data. Model calculations suggest that diffusive release of dissolved Zn and Ni to the overlying water is more important than bioirrigation. Processes controlling the dissolved trace metal concentrations in the upper millimeters of sediment, such as trace metal scavenging by newly formed oxides, and sulfide oxidation, are important

in controlling the diffusive release to the overlying water. The relative importance of sulfides in trace metal speciation is expected to increase following restoration, allowing for trace metal retention in the reduced sediment.

Modeled and experimental evidence of nutrient and trace metal release from the sediment in response to salinization are summarized in Chapter 7. Experimental results suggest that the initial response to salinization will be a pulsed release of ammonium, phosphorus, and trace metals from the sediments. The estimated change in sediment efflux is combined with the proposed restoration area and water flow rates to derive simple estimates of the changes in concentrations in the overlying water. The high flow rates at the site mean that under most conditions increased sediment effluxes will have minimal impact. Lower flow through the Haringvliet would decrease this dilution effect and also increase the chances of salinity stratification and bottom water anoxia.

Samenvatting

Biogeochemische processen in waterbodems en het bovenstaande water zijn sterk gekoppeld. Op de lange termijn zijn sedimenten vooral een opslagplaats voor materiaal uit de waterkolom. Om het definitieve lot van nutriënten en spoormetalen in sedimenten te voorspellen is kwantitatief inzicht in de biogeochemische processen in sedimenten vereist. Dit geldt met name voor locaties waar omgevingsfactoren sterk veranderen. Belangrijk zijn bijvoorbeeld wijzigingen in het zout- of zuurstofgehalte in het bovenstaande water en de intensiteit en duur van algenbloeien en de samenstelling van de benthische gemeenschap. Vanwege het potentieel voor remobilisatie van grote hoeveelheden nutriënten en verontreinigingen kunnen sedimenten zelfs een "chemische tijd-bom" vormen.

Dit proefschrift beschrijft onderzoek naar de redox processen in sedimenten geassocieerd met de afbraak van organisch materiaal en de invloed daarvan op de omzettingen en sediment-water uitwisseling van nutriënten (N, P) en spoormetalen (Cd, Co, Ni, Pb, Zn). De onderzoekslocatie, het Haringvliet, bevindt zich in de Rijn-Maas delta in het zuidwesten van Nederland. Het Haringvliet was voorheen een estuarium met getijdewerking en brak water. In het kader van de Delta Werken werd in 1970 door de plaatsing van een dam een zoetwatermeer gecreëerd. Momenteel zijn er plannen voor een gedeeltelijk herstel van de estuariene condities in het meer. Dit herstel kan bereikt worden door een wijziging in het beheer van de sluizen in de Haringvlietdam. Er bestaat echter enige zorg dat de verzilting van het Haringvliet zou kunnen leiden tot het vrijkomen van nutriënten en spoormetalen uit het sediment. Dit was een belangrijke reden om dit onderzoek uit te voeren.Verzilting van zoetwater in kustgebieden is echter niet beperkt tot deze specifieke locatie. Er is een toenemend risico van verzilting in de kustzone op mondiale schaal vanwege de rijzende zeespiegel, verhoogde intensiteit van stormen veroorzaakt door klimaatverandering en een toename in het gebruik van zoetwater in kustgebieden.

De depositie van organisch materiaal op waterbodems leidt tot een reeks van redox reacties die gedreven worden door microbiële afbraakprocessen. De oxidatie van organisch materiaal is gekoppeld aan de reductie van O_2, NO_3^-, Mn-(hydr)oxides, Fe-(hydr)oxides, SO_4^{2-} en CO_2. Een snelle afbraak van het organisch materiaal kan leiden tot de vorming van steile redox gradiënten in het sediment. Organismen in de waterbodem (benthische fauna) kunnen zorgen voor transport van zowel vaste als opgeloste stoffen over deze redox gradienten, wat verdere microbiële en anorganische reacties mogelijk maakt. In Hoofdstuk 2 wordt een "multi-component" reactief transport model (RTM) gebruikt om de diverse afbraakroutes van organisch koolstof in Haringvliet sediment te kwantificeren. Het model is gekalibreerd aan

veldmetingen van opgeloste en vaste stoffen in het sediment en experimentele bepalingen van reactiesnelheden. De resultaten wijzen erop dat O_2 (55%), NO_3^- (21%), en SO_4^{2-} (17%) de belangrijkste elektronacceptoren voor de afbraak van het organisch materiaal in Haringvliet sediment zijn. Model simulaties suggereren tevens dat herstel van het estuarium zal leiden tot een toename van de rol van sulfaatreductie en tot de omzetting van Fe(III)-mineralen tot pyriet over een zeer lange termijn.

De stikstofomzettingen in het sediment zijn zowel met experimentele technieken (Hoofdstuk 3) als met het reactief transport model (Hoofdstuk 4) onderzocht. Potentiële nitraatreductie en denitrificatie snelheden zijn bepaald met behulp van doorstroomreactoren. De resultaten van de experimenten suggereren dat denitrificatie slechts voor de helft van de nitraatreductie in het Haringvliet sediment verantwoordelijk is. De resterende nitraatreductie is het resultaat van onvolledige denitrificatie en alternatieve routes, waarvan dissimilatieve reductie van nitraat tot ammonium (DNRA) het meest waarschijnlijk is. Een verhoogd zoutgehalte in de toevoer van de reactoren leidde tot het vrijkomen van ammonium en oplosbaar koolstof uit het sediment. Het resulteerde ook in een verhoging van de nitraatreductie snelheid en de productie van nitriet, maar niet in een verhoging van de denitrificatie snelheid. In hoofdstuk 4 is het eerder ontwikkelde RTM uitgebreid met een beschrijving van denitrificatie en DNRA. De verwijdering van stikstof door het sediment daalde met 40% wanneer nitraat gereduceerd werd tot ammonium (DNRA) in plaats van via denitrificatie. De netto sediment-water uitwisseling van oplosbaar stikstof was gevoeliger voor veranderingen in de relatieve verhouding tusssen denitrificatie en DNRA dan voor andere veranderingen die verwacht worden naar aanleiding van het estuariene herstel. Wanneer DNRA de dominante nitraatreductie route is zal de N verwijdering beperkt zijn tot opslag in het sediment en is de opgeslagen N minder gevoelig zijn voor omgevingsveranderingen.

In Hoofdstuk 5 wordt de cyclus van fosfor (P) in Haringvliet sediment beschreven. Resultaten van sediment-extracties laten zien dat een reduceerbaar ijzer-fosfaat mineraal een belangrijke vorm van fosfaat in het sediment is. Het RTM is uitgebreid met fosfor diagenese om de huidige cyclus van P in het sediment te kwantificeren en om de mogelijke veranderingen door het estuariene herstel te bestuderen. Mineralisatie van organisch P en reductie van ijzer-fosfaat zijn de belangrijkste bronnen van opgelost fosfaat in het sediment. Het sediment houdt slechts 50% van het inkomende fosfaat vast. Herstel van de estuariene condities in het Haringvliet zal waarschijnlijk leiden tot een afname van de retentie van fosfaat in de vorm van ijzer-fosfaat.

Poriewater en vaste fase profielen van Cd, Co, Ni, Pb, and Zn in Haringvliet sediment worden beschreven in Hoofdstuk 6. De concentraties van deze spoormetalen in het sediment zijn hoog vanwege de invloed van de mens op de rivieren Rijn en Maas. De resultaten

suggereren dat de metalen in de vorm van oxides in het sediment terecht komen en vervolgens geassocieerd raken met sulfides. De resultaten van extracties laten zien dat Ni en Co uiteindelijk opgeslagen worden in pyriet. Het poriewater is over het algemeen verzadigd wat betreft monosulfiden van Zn, Pb, Co, and Cd. Het RTM dat gepresenteerd is in Hoofdstuk 2 is verder uitgebreid met een beschrijving van de diagenese van Zn en Ni. Een aantal van de concentratieprofielen in het poriewater en sediment worden goed gereproduceerd door het model. Model berekeningen suggereren dat diffusie van Zn en Ni naar het overliggende water belangrijker is dan bioirrigatie. Processen die de spoormetaal-concentraties in de bovenste millimeters van het sediment beïnvloeden, zoals het wegvangen van opgeloste sporen metalen door de vorming van oxides en sulfideoxidatie, bepalen sterk de diffuse uitwisseling met het bovenstaande water. Het is te verwachten dat het esturariene hestel zal leiden tot een toename van de rol van sulfiden voor de vastlegging van spoormetalen en daarmee een sterkere retentie van spoormetalen in het gereduceerde sediment.

De resultaten van de experimenten en het modelleerwerk wijzen erop dat bij herstel van het estuarium zowel nutriënten als spoormetalen uit het sediment zullen vrijkomen. Deze resultaten zijn samengevat in Hoofdstuk 7. De experimentele resultaten suggereren een initiële fase waarbij ammonium, fosfaat en spoormetalen in een kortdurende "puls" uit het sediment zullen vrijkomen. De veranderingen in de sediment-water uitwisseling zijn gecombineerd met het verwachte oppervlakte van het restoratiegebied om een schatting te maken van de concentratieveranderingen in het bovenstaande water. Vanwege de hoge stroomsnelheden in het Haringvliet zal de toename in de sediment-water uitwisseling meestal een beperkt effect op de samenstelling van het bovenstaande water hebben. Bij lage stroomsnelheden in het Haringvliet zal het "verdunningseffect" een minder grote rol spelen en zal de kans ook groter zijn dat verzilting leidt tot stratificatie en zuurstofloosheid van het bodemwater.

Chapter 1
Introduction

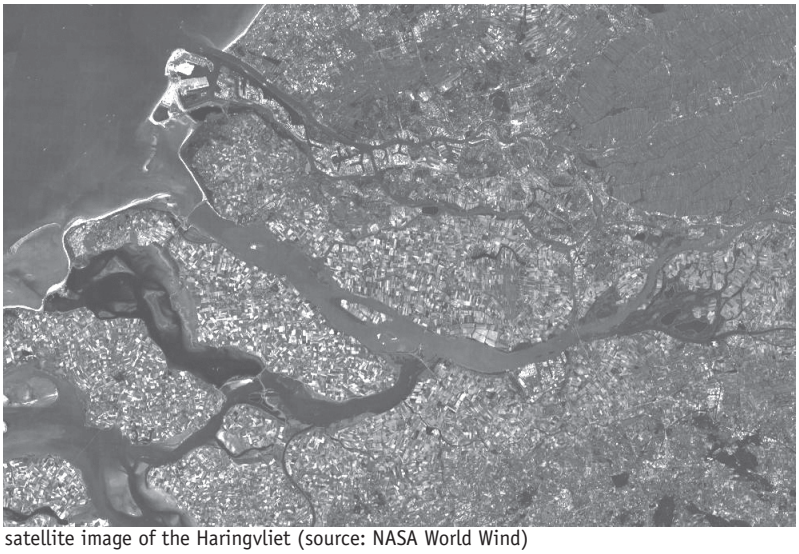

satellite image of the Haringvliet (source: NASA World Wind)

Sediment-water interactions play an important role in determining the water quality of shallow freshwater and marine systems. Sediments act as a repository of suspended particulate matter (SPM) settling from the overlying water. Degradation of the deposited organic matter drives a return flux of dissolved components, which may profoundly affect the biogeochemical and ecological functioning of the water column (Middelburg and Soetaert 2005; Sondergaard et al. 2003). In addition to releasing solutes, sediments may also act as a sink with nutrients or trace metals remaining in the sediment after deposition. Sediments pose a risk to surface water quality and ecosystem health if environmental changes lead to release of nutrients or trace metals stored in the sediments (Salomons and Förstner 1984). An example of such an environmental change is the intrusion of salt water in coastal freshwater bodies. Coastal ecosystems are increasingly encroached by saline waters, mainly as a result of increasing demands for fresh water. Salinization is expected to intensify worldwide due to increased demands for freshwater in coastal areas, sea-level rise and changing weather patterns accompanying global warming (Jacobs et al. 2000; Smith et al. 2005; Wigley 2005).

The goal of this thesis is to obtain quantitative insight into the biogeochemical cycles of C, N, P, Fe, S, Mn and trace metals (Zn, Pb, Cd, Ni, Co) in freshwater sediments and their response to salinization. To meet this goal this study combined three major efforts: collection and analysis of field samples, experimentation to determine biogeochemical reaction rates, and reaction-transport modeling. The study site is Haringvliet Lake, a coastal freshwater body located in the southwest of the Netherlands that is targeted for estuarine restoration in 2008. The following sections provide background information on the biogeochemistry of freshwater sediments, and the expected effects of their salinization. A review of the recent history of Haringvliet Lake and a review of preliminary studies examining the effects of restoration is presented. Finally, an outline of the content of the remaining chapters of the thesis is given.

1.1 Biogeochemistry of freshwater sediments

Many biogeochemical processes in sediments are fueled by the input of organic material from the overlying water. This organic matter may be derived from primary production in the surface water or external sources such as terrestrial inputs of plant remains and wastewater. Degradation of organic matter by microorganisms drives many important redox reactions in the sediment and releases organically-bound elements into solution. Microorganisms couple the oxidation of organic carbon with the reduction of a terminal electron acceptor (TEA); these reactions are referred to as primary redox reactions (Van Cappellen and Wang 1996). Common TEAs utilized in sediments include: O_2, NO_3^-, Mn-(hydr)oxides, Fe-(hydr)oxides, SO_4^{2-} and organic carbon (methanogenesis) (Table 1.1). The utilization of TEAs occurs roughly

in the order of decreasing free energy yield. The reduction of the TEAs produces new reduced compounds, which can be involved in subsequent secondary redox or precipitation reactions (Table 1.1).

Table 1.1 Simplified reactions of organic matter degradation (primary redox reactions) and examples of secondary redox and precipitation reactions.

OM degradation reactions[a]	
Aerobic respiration	$OM + O_2 \rightarrow DIC + H_2O$
Denitrification	$OM + 0.8NO_3^- + 0.8H^+ \rightarrow DIC + 1.4H_2O + 0.4N_2$
DNRA[b]	$OM + 0.5NO_3^- + H^+ \rightarrow DIC + H_2O + 0.5NH_4^+$
Mn-oxide reduction	$OM + 2MnO_2 + 4H^+ \rightarrow DIC + 3H_2O + 2Mn^{2+}$
Fe-oxide reduction	$OM + 4Fe(OH)_3 + 8H^+ \rightarrow DIC + 7H_2O + 4Fe^{2+}$
Sulfate reduction	$OM + 0.5SO_2^{2-} + H^+ \rightarrow DIC + 3H_2O + HS^-$
Methanogenesis	$OM \rightarrow 0.5DIC + 0.5CH_4$
Secondary redox reaction (example)	
Nitrification	$NH_4^+ + 2O_2 \rightarrow NO_3^- + H_2O + H^+$
Mineral precipitation reaction (example)	
FeS formation	$Fe^{2+} + H_2S \rightarrow FeS + 2H^+$

(a) OM represents organic matter with the general formula $(CH_2O)_x(NH_3)_y(PO_4)_z$. The degradation of OM results in the release of $y/x(NH_4^+)$ and $z/x(PO_4^{3-})$ where x:y:z is the C:N:P ratio of the OM. DIC is dissolved inorganic carbon which includes (CO_2, HCO_3^-, and CO_3^{2-}). The consumption and production of protons by DIC and the release of NH_4^+ and PO_4^{3-} are omitted from the equations for the sake of simplicity. (b) DNRA is Dissimilatory Nitrate Reduction to Ammonium

The primary redox reactions produce various dissolved reduced compounds, including NH_4^+, Mn^{2+}, Fe^{2+}, CH_4, and sulfides. These reduced solutes diffuse toward the sediment surface where they can be re-oxidized. The re-oxidation of reduced species can account for a major proportion of total O_2 consumption in sediments (Sweerts et al. 1991). Frequent cycling between oxidized and reduced states can result in high rates of organic matter mineralization by relatively less abundant TEAs such as Fe-oxides and sulfate (Thomsen et al. 2004; Urban et al. 1994). Freshwater environments present a wide range of sedimentary conditions and TEA availability. However, freshwaters generally have a much lower SO_4^{2-} concentration than seawater (Holmer and Storkholm 2001), while for a number of freshwater sediments a limited availability of reactive Fe(III) phases has been proposed (Hyacinthe and Van Cappellen 2004; Wersin et al. 1991).

Nitrogen is often the limiting nutrient for primary production in coastal waters. Nitrate can be used as a TEA by microorganisms, where in the process of denitrification N_2 gas is

produced. Denitrification is an important removal process of dissolved inorganic nitrogen from aquatic ecosystems. Additional microbially-mediated N processes include the release of NH_4^+ from OM mineralization (ammonification) and the oxidation of NH_4^+ to NO_3^- (nitrification; see chapters 3 and 4 for more details). Phosphorus is also an important nutrient for primary production and is often limiting in freshwater environments. In addition to organic-P, solid inorganic phases of P, such as Fe(III)-P are also important reactive P-species. This means that P release in sediment can relate to OM mineralization and Fe(III) reduction. Fe and S cycling are reviewed in Chapter 2 and P cycling is treated in Chapter 5. Concentrations of trace metals such as Zn, Pb, Cd, Ni, and Co can be elevated relative to natural background concentrations in freshwater sediments due to anthropogenic activities (Gallon et al. 2004; van den Berg et al. 1999). The decomposition of OM and the associated increase in reducing conditions leads to changes in trace metal speciation. More reducing conditions typically results in a greater importance of sulfides relative to oxides and organic matter for trace metal binding (Huerta-Diaz et al. 1998).

In addition microorganisms, macroinvertebrates play an important role in sediment biogeochemistry. Macroinvertebrates alter conditions in the sediment through a variety of processes including burrowing, flushing of burrows, particle ingestion and excretion (Heip et al. 2001; Matisoff and Wang 2000; Matisoff and Wang 1998). These activities result in the mixing of sediment and pore water across steep redox gradients, which greatly affects biogeochemical reactions and cycling (Aller and Aller 1998; Meysman et al. 2003; Meysman et al. 2006), as well as sediment water exchange of solutes (Meile and Van Cappellen 2003).

1.2 Salinization of freshwater sediments

Increasing salinity in freshwaters can result from seawater intrusion and profoundly affects sediment biogeochemical processes. Increased salinity influences microbial physiology and diversity (Bernhard et al. 2005; Hopkinson et al. 1999; Rysgaard et al. 1999). Changes in electrolyte chemistry also affect aquatic chemistry, for example increased Cl^- concentrations can increase the solubility of NH_4^+ and Cd^{2+} through the formation of ion pairs (Gardner et al. 1991; Paalman et al. 1994). Salinization increases sulfate concentrations in sediment, allowing sulfate reduction to replace methanogenesis (Capone and Kiene 1988; Weston et al. 2006), thereby enhancing the precipitation of Fe and trace metals as sulfides. This may also result in the release of Fe(III) bound P in the sediment through reductive dissolution by sulfide (Blomqvist et al. 2004). Increasing salinity has also been associated with increased rates of OM mineralization which may relate to both the changing concentrations of TEAs and salinity-induced mobilization of dissolved organic matter (Nyvang 2003; Weston et al. 2006).

Changing salinity also causes changes in the macrobenthic community (Van Nes and Smit 1993), further altering the mixing and flushing regime of the sediment.

1.3 The Haringvliet: from tidal estuary to freshwater lake and back

Haringvliet Lake is a freshwater lake in the Rhine-Meuse river delta (The Netherlands). The location was a tidal, brackish estuary before its conversion to a fresh water lake in 1970 by the construction of a storm surge barrier (dam) as part of the Dutch Delta Project. Haringvliet Lake is approximately 30 km long and 1 km wide. The lake maintains a fluvial nature with a mean residence time of approximately 10 days, although this varies based on the stage of the source rivers and management of the dam (Smit et al. 1997). The chemistry of the lake water generally reflects that of the source rivers. The Rhine is the dominant source and accounts for approximately 80% of the total water input (Table 1.2). The Rhine and Meuse river watersheds are densely populated (304 people km^{-2}) and highly managed (Revenga et al. 1998). Water quality in the Haringvliet has improved over the past decades in response to measures implemented in the Rhine and Meuse. Concentrations of trace metals in suspended matter declined to current values in the period 1970-1987 (Fig. 1.1). Phosphate and ammonium concentrations also declined in this period, although nitrate did not (Fig 1.2).

Table 1.2 Physical description of the Rhine and Meuse Rivers

Measure	Unit	Rhine	Meuse
length	km	1320	935
watershed area	km^2	185000	36000
average discharge	m^3sec^{-1}	2300	230
countries		5	3

Source: (Middelkoop and Haselen 1999)

The abrupt conversion of the estuary to a lake following the completion of the dam in 1970 led to ecological impacts for the resident fish, bird, and macroinvertebrate communities (Ferguson and Wolff 1984; Smit et al. 1997). Changes in tide and salinity resulted in the loss of vegetation on the banks and subsequent bank erosion. The modified flow regime within the lake led to the deposition of suspended solids containing elevated levels of P and trace metals (Paalman 1997; van de Meent et al. 1985; van Eck 1982). This material accumulated in the deeper channels of the former riverbed, while the shallower parts of the basin experienced lower accumulation rates (van Wijngaarden et al. 2002a; 2002b). The species density and diversity of the macrobenthic community has been found to relate to both the increase of fine-grained sediment and to increased pollutant levels (Peeters et al. 2001; Reinhold-Dudok van Heel and den Besten 1999; Smit et al. 1995).

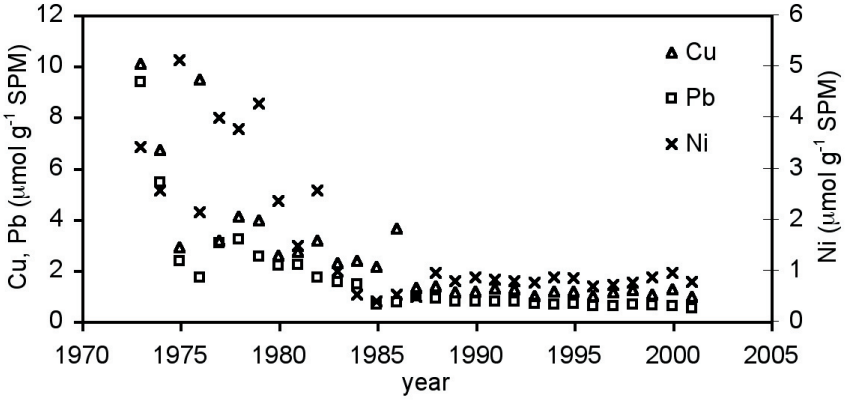

Figure 1.1 The concentrations of Cu (△), Pb (▫), and Ni (x) in suspended particulate matter (SPM) in the Haringvliet. Values estimated as the difference between total and dissolved concentrations before 1987, after that date values from direct measurement. Annual values are average values of monthly sampling performed by the RIZA and available at www.waterbase.nl.

Large areas of formerly brackish and tidal waters in the Netherlands have been closed from the North Sea over the last century. These areas include the Zuiderzee (1932), the Lauwerszee (1969) and other parts of the south western delta, in addition to the Haringvliet (Delta Project 1960-1986; de Jonge and de Jong 2002). These projects were undertaken to provide protection from flooding, for land reclamation, and development of freshwater resources. The recognition of the negative ecological impacts that result from estuary closure led to a revision of the plans for a closed barrier at the mouth of the eastern Scheldt. At this location an open storm surge barrier that allows for tidal water exchange was constructed, and completed in 1986. Restoration of tide and salinity gradients is now being considered for several closed water bodies in the Netherlands. This includes Haringvliet Lake where such restoration can be easily implemented by changing the management of the sluices in the dam separating the lake from the North Sea. Since its completion in 1970, the barriers in the dam are only open at low tide to allow fresh water to be released to the sea. At high tide and low river flow conditions, the barriers are always closed thus keeping sea water from entering the lake.

In 1998, an Environmental Impact Assessment (EIA) was prepared to examine different alternatives for the restoration of estuarine conditions in the Haringvliet (Anonymous 1998). The EIA report concluded that a greater opening of the dam, would lead a more sustainable and diverse estuarine system. However, due to the high demand on the freshwater resources in the vicinity of the lake, complete restoration of the estuary would be too expensive. Following a revision of restoration plans made in 2004, a controlled, relatively limited opening of the

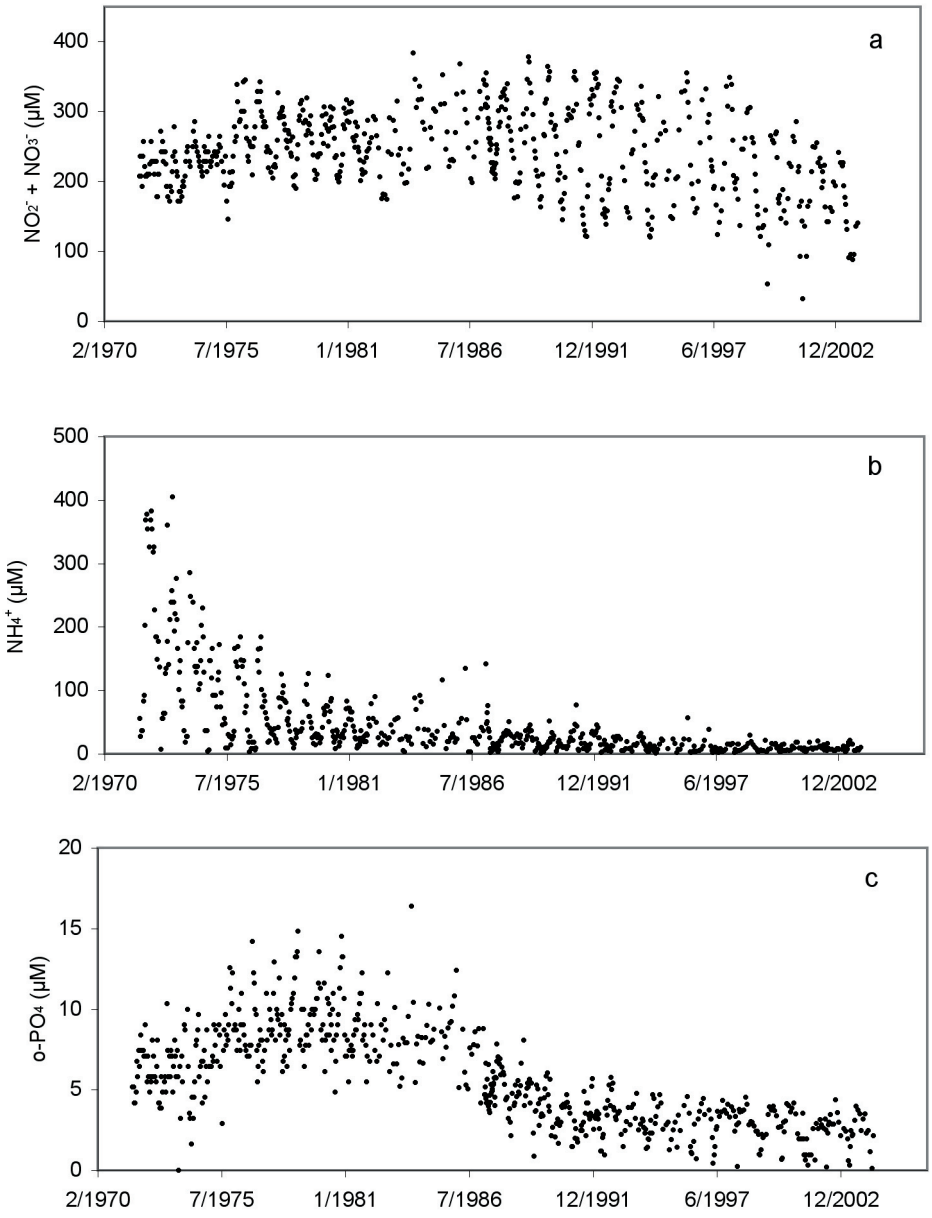

Figure 1.2 Surface water concentrations of nitrate + nitrite (a), ammonium (b), and dissolved ortho-phosphorus (c) in the period between 1971 and 2003 from periodic water quality monitoring (Rijkswaterstaat, www.waterbase.nl).

dam is planned to begin in 2008. This will allow for brackish conditions to be established until approximately 10 km inward from the dam. As part of the preparation for restoration a test opening of the Haringvliet dam was conducted over a five day period in March, 1997 (Jacobs et al. 2003). Salinity stratification was observed and a further study of oxygen consumption in saline bottom water was recommended. It was found that greater opening of the dam increases flow velocity and mixing of salt and fresh water, however this also increased the risk of sediment erosion and resuspension. After the completion of the test-opening, Cl^- concentrations rapidly returned to background levels. Additional water quality monitoring during this test opening provided evidence for salinity induced release of phosphorus, ammonium, dissolved organic carbon, and the trace metals Cd, Cr, Cu, Ni, and Zn, even for a moderate salinity increase of approximately 2‰ (van den Berg and Zwolsman 2000). A mesocosm study with Haringvliet sediments indicated that trace metals (Cd, Ni, and Zn) and nutrients (NO_3^-, NH_4^+, and PO_4^{3-}) could be released from sediment upon exposure to saline water (Wijdeveld 1999).

The findings of the mesocosm study and the analysis during the test-opening prompted the development of the RESIN project (Restoration of Estuarine Systems In the Netherlands: response of biogeochemical processes), to further examine the sediment biogeochemical processes and their response to salinization. This study of the impact of estuarine restoration on sediment geochemical processes in the Haringvliet helps to create the scientific basis for environmental monitoring during the restoration process. The study of fresh water sediment geochemistry and its response to salinization is also more broadly relevant as this process may occur throughout the coastal zone. Long term water management plans include further restoration of former estuarine locations in the Netherlands. Thus, restoration of the Haringvliet may serve as an example for future projects.

1.4 Thesis outline

The work in this thesis was conducted as part of the RESIN project, which was a joint project of the Institute for Inland Water Management and Waste Water Treatment (RIZA) and the geochemistry group at Utrecht University. The following chapters combine the results of field sampling, experimental reaction rate determination, and reaction-transport modeling to quantify sediment biogeochemical processes and their response to salinization.

In **Chapter 2**, a multi-component reactive transport model is developed to describe organic matter mineralization for a 1-D sediment profile. The model is used to interpret sediment and pore water data at a study site near the dam in Haringvliet Lake and to assess changes in TEA –pathways that may result from estuarine restoration. Model results indicate that oxic degradation (55 %), denitrification (21 %), sulfate reduction (17 %), and methanogenesis (5 %)

are currently the most important organic carbon degradation pathways in the upper 30 cm of sediment. Model sensitivity analyses demonstrate the importance of biologically mediated transport processes (bioirrigation and bioturbation). Simulations of estuarine conditions predict that sulfate reduction would rapidly suppress methanogenesis, and lead to a long-term reduction of Fe(III) minerals present in the sediment.

Flow through reactors (FTRs) are used to study nitrogen transformations in the sediment (**Chapter 3**). Potential for NO_3^- reduction is found in all samples. Rates of nitrate reduction display a temperature dependence typical for biologically mediated reactions. This temperature dependence can not account for all of the observed seasonal variation, and, other factors such as organic substrate availability likely also play a role. The addition of increased salinity in FTR experiments leads to a transient release of ammonium and dissolved organic carbon from the sediment and enhanced rates of nitrate reduction and nitrite production. The measurement of potential denitrification in FTRs using the acetylene block technique suggests that processes other than denitrification, such as DNRA and incomplete denitrification, are also important in NO_3^- reduction.

In **Chapter 4**, the model developed in Chapter 2 is adapted to examine N transformations in Haringvliet sediment, quantify N removal rates, and to assess the response to salinization. Model results show that both sediment-water exchange fluxes of dissolved inorganic nitrogen (DIN) and N removal are very sensitive to the competition between denitrification and DNRA (Table 1.1). The salinity-induced release of adsorbed ammonium is also simulated.

Sediment phosphorus cycling is examined in **Chapter 5**, using of field data, sediment extractions, and modeling. Results show that P cycling in the sediment is closely coupled to the iron and sulfur cycles. Model sensitivity analyses show that increased sulfate reduction leads to decreased P retention in the sediment. The rate of sulfate reduction is not only limited by sulfate concentration but may also be limited by organic substrate availability deeper in the sediment (Chapter 2). This means that sediment P retention is also sensitive to changes in the mixing regime, which leads to a redistribution of organic matter. The changes expected from restoration, will likely lead to increased Fe reduction and decreasing P retention in the sediment.

Pore water and solid phase profiles of Cd, Co, Ni, Pb, and Zn in Haringvliet sediment are reported in **Chapter 6**. Results of sediment extractions show that the pool of trace metals associated with Fe and Mn-oxides declines with depth in the reduced sediments, but is not completely consumed at 20 cm depth. Extraction results show that Ni and Co are associated with pyrite, while Mn, Pb, and Cd are not. Pore waters are generally saturated for trace metal mono-sulfides of Zn, Pb, Co, and Cd but not for those of Mn and Ni. These results suggest a

shift in trace metal speciation in the sediment from oxide-bound to sulfide-bound. Results for Zn and Ni are further examined with a reactive transport model. Model results suggest that trace metal scavenging by newly formed oxides at the sediment surface, and sulfide oxidation are important in controlling the diffusive release to the overlying water.

In **Chapter 7** results of previous chapters are synthesized to quantify the changes in sediment-water exchange of nutrients and trace metals that can be expected to result from restoration. Although some results suggest increased sediment efflux will result from estuarine restoration, this is expected to have little effect on the surface water concentrations at average water flows, given the limited restoration area and large discharge volumes. However, in periods of low flow in the Rhine and Meuse Rivers, water residence time in the Haringvliet increases, which would result in a greater effect of sediment efflux of nutrients or trace metals on surface water concentrations. Therefore future monitoring efforts to address the influence of sediment-water exchange should focus on periods of low flow, or when salinity stratification results in stagnant saline bottom waters.

References

Aller, R. C., and J.Y. Aller. 1998. The effect of biogenic irrigation intensity and solute exchange on diagenetic reaction rates in marine sediments. Journal of Marine Research 56**:** 905-936.

Anonymous. 1998. MER beheer Haringvlietsluizen report (Environmental Impact Report- Haringvliet dam management). Rijkswaterstaat directie Zuid-Holland, APV 98.186. (in Dutch).

Bernhard, A. E., T. Donn, A. E. Giblin, and D. A. Stahl. 2005. Loss of diversity of ammonia-oxidizing bacteria correlates with increasing salinity in an estuary system. Environmental Microbiology 7**:** 1289-1297.

Blomqvist, S., A. Gunnars, and R. Elmgren. 2004. Why the limiting nutrient differs between temperate coastal seas and freshwater lakes: A matter of salt. Limnology and Oceanography 49**:** 2236-2241.

Capone, D. G., and R. P. Kiene. 1988. Comparison of microbial dynamics in marine and fresh-water sediments - contrasts in anaerobic carbon catabolism. Limnology and Oceanography 33**:** 725-749.

de Jonge, V. N., and D. J. de Jong. 2002. Ecological restoration in coastal areas in the Netherlands: concepts, dilemmas and some examples. Hydrobiologia 478**:** 7-28.

Ferguson, H. A., and W. J. Wolff. 1984. The Haringvliet-Project: The development of the Rhine-Meuse Estuary from tidal inlet to stagnant freshwater lake. Water Science and Technology 16**:** 11-26.

Gallon, C., A. Tessier, C. Gobeil, and M. C. Alfaro-De La Torre. 2004. Modeling diagenesis of lead in sediments of a Canadian Shield lake. Geochimica et Cosmochimica Acta 68**:** 3531-3545.

Gardner, W. S., S. P. Seitzinger, and J. M. Malczyk. 1991. The effects of sea salts on the forms of nitrogen released from estuarine and freshwater sediments: Does ion pairing affect ammonium flux. Estuaries 14**:** 157-166.

Heip, C. H. R., G. Duineveld, E. Flach, G. Graf, W. Helder, P. M. J. Herman, M. Lavaleye, J. J. Middelburg, O. Pfannkuche, K. Soetaert, T. Soltwedel, H. De Stigter, L. Thomsen, J. Vanaverbeke, and P. De Wilde. 2001. The role of the benthic biota in sedimentary metabolism and sediment-water exchange processes in the Goban Spur area (NE Atlantic). Deep-Sea Research Part Ii-Topical Studies in Oceanography 48**:** 3223-3243.

Holmer, M., and P. Storkholm. 2001. Sulphate reduction and sulphur cycling in lake sediments: a review. Freshwater Biology 46**:** 431-451.

Hopkinson, C. S., A. E. Giblin, J. Tucker, and R. H. Garritt. 1999. Benthic metabolism and nutrient cycling along an estuarine salinity gradient. Estuaries 22**:** 863-881.

Huerta-Diaz, M. A., A. Tessier, and R. Carignan. 1998. Geochemistry of trace metals associated with reduced sulfur in freshwater sediments. Applied Geochemistry 13**:** 213-233.

Hyacinthe, C., and P. Van Cappellen. 2004. An authigenic iron phosphate phase in estuarine sediments: composition, formation and chemical reactivity. Marine Chemistry 91**:** 227-251.

Jacobs, P., G. Blom, and M. Van Der Linden. 2000. Climatological changes in storm surges and river discharges: the impact on flood protection and salt intrusion in the Rhine-Meuse delta, p. 13. *In* J. Beersma, M. Hulme, E. Kaas and D. Viner [eds.], Climate scenarios for water-related and coastal impact.

Jacobs, P., B. P. C. Steenkamp, and S. De Goederen. 2003. Van zoet naar zout in 5 dagen? RIZA, RIZA rapport 2003.001. (in Dutch).

Matisoff, G., and X. Wang. 2000. Particle mixing by freshwater infaunal bioirrigators: Midges (Chironomidae: Diptera) and mayflies (Ephemeridae: Ephemeroptera). Journal of Great Lakes Research 26**:** 174-182.

Matisoff, G., and X. S. Wang. 1998. Solute transport in sediments by freshwater infaunal bioirrigators. Limnology and Oceanography 43**:** 1487-1499.

Meile, C., and P. Van Cappellen. 2003. Global estimates of enhanced solute transport in marine sediments. Limnology and Oceanography 48**:** 777-786.

Meysman, F. J. R., B. P. Boudreau, and J. J. Middelburg. 2003. Relations between local, nonlocal, discrete and continuous models of bioturbation. Journal of Marine Research 61**:** 391-410.

Meysman, F. J. R., O. S. Galaktionov, B. Gribsholt, and J. J. Middelburg. 2006. Bioirrigation in permeable sediments: Advective pore-water transport induced by burrow ventilation. Limnology and Oceanography 51**:** 142-156.

Middelburg, J. J., and K. Soetaert. 2005. The role of sediments in shelf ecosystem dynamics, p. 353-374. *In* Robinson and Brink [eds.], The Sea. Harvard University Press.

Middelkoop, H., and V. Haselen. 1999. Twice a River: Rhine and Meuse in the Netherlands. RIZA, RIZA report n. 99.003.

Nyvang, V. 2003. Redox processes at the salt-/freshwater interface in an anaerobic aquifer. PhD Thesis. Technical University of Denmark.

Paalman, M. A. A. 1997. Processes affecting the distribution and speciation of heavy metals in the Rhine/Meuse Estuary. PhD Thesis. Utrecht University.

Paalman, M. A. A., C. H. van der Weijden, and J. P. G. Loch. 1994. Sorption of cadmium on suspended matter under estuarine conditions - competition and complexation with major sea-water ions. Water Air and Soil Pollution 73**:** 49-60.

Peeters, E., A. Dewitte, A. A. Koelmans, J. A. van ver Velden, and P. J. den Besten. 2001. Evaluation of bioassays versus contaminant concentrations in explaining the macroinvertebrate community structure in the Rhine-Meuse delta, the Netherlands. Environmental Toxicology and Chemistry 20**:** 2883-2891.

Reinhold-Dudok van Heel, H. C., and P. J. den Besten. 1999. The relation between macroinvertebrate assemblages in the Rhine-Meuse delta (The Netherlands) and sediment quality. Aquatic Ecosystem Health and Management 2**:** 19-38.

Revenga, C., S. Murray, J. Abramovitz, and A. Hammond. 1998. Watersheds of the World: Ecological Value and Vulnerability. World Resources Institute,

Rysgaard, S., P. Thastum, T. Dalsgaard, P. B. Christensen, and N. P. Sloth. 1999. Effects of salinity on NH_4^+ adsorption capacity, nitrification, and denitrification in Danish estuarine sediments. Estuaries 22(1)**:** 21-30.

Salomons, W., and U. Förstner. 1984. Metals in the Hydrocycle. Springer-Verlag.

Smit, H., H. C. Reinhold-Dudok van Heel, and S. M. Wiersma. 1995. Sublittoral macrozoobenthic assemblages in the enclosed sediment-polluted Rhine-Meuse Delta; their relationship to environmental conditions. Netherlands Journal of Aquatic Ecology 29**:** 31-47.

Smit, H., R. Smits, G. van der Velde, and H. Coops. 1997. Ecosystem responses in the Rhine-Meuse delta during two decades after enclosure and steps toward estuary restoration. Estuaries 20**:** 504-520.

Smith, S. J., A. M. Thomson, N. J. Rosenberg, R. C. Izaurralde, R. A. Brown, and T. M. L. Wigley. 2005. Climate change impacts for the conterminous USA: an integrated assessment. Climatic Change 69**:** 7.

Sondergaard, M., J. P. Jensen, and E. Jeppesen. 2003. Role of sediment and internal loading of phosphorus in shallow lakes. Hydrobiologia 506**:** 135-145.

Sweerts, J.-P. R. A., M.-J. Bar-Gilissen, A. A. Cornelese, and T. E. Cappenberg. 1991. Oxygen-consuming processes at the profundal and littoral sediment-water interface of a small meso-eutrophic lake (Lake Vechten, The Netherlands). Limnology and Oceanography 36**:** 1124-1133.

Thomsen, U., B. Thamdrup, D. A. Stahl, and D. E. Canfield. 2004. Pathways of organic carbon oxidation in a deep lacustrine sediment, Lake Michigan. Limnology and Oceanography 49(6)**:** 2046-2057.

Urban, N. R., P. L. Brezonik, L. A. Baker, and L. A. Sherman. 1994. Sulfate reduction and diffusion in sediments of Little Rock Lake, Wisconsin. Limnology and Oceanography 39(4)**:** 797-815.

Van Cappellen, P., and Y. F. Wang. 1996. Cycling of iron and manganese in surface sediments: A general theory for the coupled transport and reaction of carbon, oxygen, nitrogen, sulfur, iron, and manganese. American Journal of Science 296**:** 197-243.

van de Meent, D., J. W. de Leeuw, P. A. Schenck, and W. Salomons. 1985. Geochemistry of suspended particulate matter in two natural sedimentation basins of the river Rhine. Water Research 19**:** 1333.

van den Berg, G. A., J. P. G. Loch, L. M. van der Heijdt, and J. J. G. Zwolsman. 1999. Mobilisation of heavy metals in contaminated sediments in the river Meuse, The Netherlands. Water Air and Soil Pollution 116**:** 567-586.

van den Berg, G. A., and J. J. G. Zwolsman. 2000. Gedrag van zware metalen and fosfaat tijdens de proef met de Haringvlietsluizen (maart 1997). RIZA, werkdocument 2000.121X.

van Eck, G. T. M. 1982. Forms of phosphorus in particulate matter from the Hollands Diep/Haringvliet, The Netherlands. Hydrobiologia 92**:** 665-681.

Van Nes, E. H., and H. Smit. 1993. Multivariate-Analysis Of Macrozoobenthos In Lake Volkerak-Zoommeer (The Netherlands) - Changes In An Estuary Before And After Closure. Archiv Fur Hydrobiologie 127**:** 185-203.

van Wijngaarden, M., L. B. Venema, and R. J. de Meijer. 2002a. Radiometric sand mud characterisation in the Rhine-Meuse estuary part B. In situ mapping. Geomorphology 43**:** 103-116.

van Wijngaarden, M., L. B. Venema, R. J. de Meijer, J. J. G. Zwolsman, B. van Os, and J. M. J. Gieske. 2002b. Radiometric sand-mud characterisation in the Rhine-Meuse estuary part A. Fingerprinting. Geomorphology 43**:** 87-101.

Wersin, P., P. Hohener, R. Giovanoli, and W. Stumm. 1991. Early Diagenetic Influences on Iron Transformations in a Fresh-Water Lake Sediment. Chemical Geology 90**:** 233-252.

Weston, N. B., R. E. Dixon, and S. B. Joye. 2006. Ramifications of increased salinity in tidal freshwater sediments: Geochemistry and microbial pathways of organic matter mineralization. Journal of Geophysical Research 111**:** G01009.

Wigley, T. M. L. 2005. The climate change commitment. Science 307**:** 1766-1769.

Wijdeveld, A. J. 1999. Invloed verzouting Haringvliet op mobilisatie zware metalen en fosfaat. WL/Delft Hydraulics, T2387. (in Dutch).

Chapter 2

Organic matter mineralization in sediment of a coastal freshwater lake and response to salinization

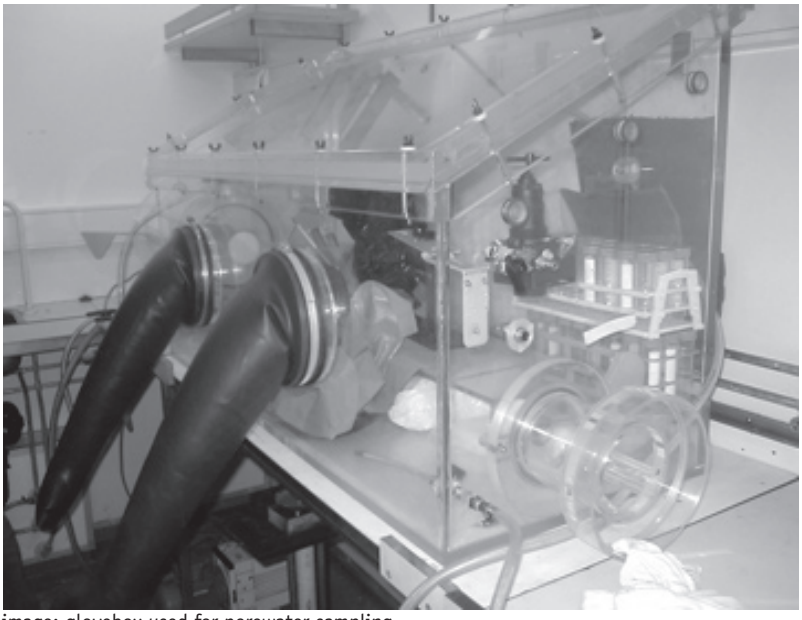

image: glovebox used for porewater sampling

R.W. Canavan, C.P. Slomp, P. Jourabchi, P. Van Cappellen, A.M. Laverman and G.A. van den Berg (2006) Geochimica et Cosmochimica Acta 70:2836-2855 ...Acta 70:2836-2855. Reprinted with permission from Elsevier.

ABSTRACT

Solid phase and pore water chemical data collected in a sediment of the Haringvliet Lake are interpreted using a multi-component reactive transport model. This freshwater lake, which was formed as the result of a river impoundment along the southwestern coast of the Netherlands, is currently targeted for restoration of estuarine conditions. The model is used to assess the present-day biogeochemical dynamics in the sediment, and to forecast possible changes in organic carbon mineralization pathways and associated redox reactions upon salinization of the bottom waters. Model results indicate that oxic degradation (55 %), denitrification (21 %), and sulfate reduction (17 %) are currently the main organic carbon degradation pathways in the upper 30 cm of sediment. Unlike in many other freshwater sediments, methanogenesis is a relatively minor carbon mineralization pathway (5%), because of significant supply of soluble electron acceptors from the well-mixed bottom waters. Although ascorbate-reducible Fe(III) mineral phases are present throughout the upper 30 cm of sediment, the contribution of dissimilatory iron reduction to overall sediment metabolism is negligible. Sensitivity analyses show that bioirrigation and bioturbation are important processes controlling the distribution of organic carbon degradation over the different pathways. Model simulations indicate that sulfate reduction would rapidly suppress methanogenesis upon seawater intrusion in the Haringvliet, and could lead to significant changes in the sediment's solid-state iron speciation. The changes in Fe speciation would take place on time-scales of 20-100 years.

2.1 INTRODUCTION

The degradation of organic matter in sediments drives the release of nutrients and pollutants from sediments to surface waters, and can profoundly influence the biogeochemical cycling of C, N, O, S, P, Fe, Mn, and trace metals in aquatic environments (Hamilton-Taylor et al., 1996; Wetzel, 2001). Organic carbon (C_{org}) oxidation in sediments is coupled to the utilization of terminal electron acceptors (TEAs), primarily O_2, NO_3^-, Mn-(hydr)oxides, Fe-(hydr)oxides, and SO_4^{2-}. When these TEAs are completely consumed, degradation of C_{org} continues via methanogenesis. The corresponding C_{org} degradation reactions, often referred to as the primary redox reactions, roughly succeed one another vertically in order of decreasing free energy yield (Froelich et al., 1979). In sediments receiving large inputs of reactive organic matter, however, the various mineralization processes may exhibit significant overlap (Wersin et al., 1991; Canfield et al., 1993; Holmer and Storkholm, 2001). The primary redox reactions also produce reduced species (e.g. NH_4^+, Fe^{2+}, H_2S, CH_4), which can participate in other, so-called secondary, redox reactions. The network of primary and secondary redox reactions usually leads to a characteristic zonation of redox conditions in sediments.

The relative importance of the different primary redox reactions depends on the availability of both the organic matter and the TEAs. Key determining factors are the input fluxes of C_{org} and TEAs from the overlying water column, organic matter quality, rates of physical transport of solids and solutes in the sediment, and rates of secondary redox reactions that regenerate or consume TEAs. In eutrophic lake sediments, TEAs are frequently in low supply relative to the influx of C_{org}. In these depositional settings, aerobic degradation of C_{org} may be limited by O_2 consumption due to secondary oxygenation reactions, particularly the oxidation of CH_4 (Sweerts et al., 1991). Furthermore, reactive Fe(III) mineral phases are often preserved in fresh water sediments (Wersin et al., 1991; Gallon et al., 2004; Hyacinthe and Van Cappellen, 2004), while low SO_4^{2-} concentrations in freshwater environments limit sulfate reduction (Holmer and Storkholm, 2001). As a consequence, methanogenesis is generally a dominant C_{org} degradation process (Capone and Kiene, 1988; Peretyazhko et al., 2005). However, efficient recycling of TEAs may increase the importance of specific primary redox pathways, as observed for sulfate reduction (Urban et al., 1994) and dissimilatory iron reduction (Thomsen et al., 2004) in oligotrophic lake sediments.

Total organic carbon mineralization rates, and the relative contributions of the different primary redox reactions, can be estimated directly via incubation experiments (Canfield et al., 1993; Dauwe et al., 2001; Thomsen et al., 2004), or they can be quantified by applying reactive transport models (RTMs) to geochemical data sets. Multi-component RTMs have been used successfully to estimate kinetic parameters and rates of primary and secondary redox reactions (Van Cappellen and Wang, 1996). These models have mostly been applied to marine sediments, and less frequently to freshwater sediments (Van Cappellen and Wang, 1995; Furrer and Wehrli, 1996; van den Berg et al., 2000).

The focus of this study is to quantify the rates of organic carbon mineralization in the sediment of Haringvliet Lake (The Netherlands). Reaction rates are determined both experimentally and with a RTM calibrated with pore water and sediment chemistry data. In addition, the RTM is used to examine how biogeochemical cycling may change in response to salinization induced by restoration of estuarine conditions in the lake.

2.2 STUDY SITE

Haringvliet Lake is a eutrophic freshwater lake, which was created as a result of the damming of the mouth of an estuary in 1970 (Fig. 2.1), as part of the Dutch Delta Project (Ferguson and Wolff, 1984). Prior to dam construction, the Haringvliet was a tidal estuary and an outlet of the Meuse-Rhine river system to the North Sea. The closure of the Haringvliet caused physical and chemical changes in the water body, including the rapid conversion to a

freshwater lake, increased shore-line erosion, and the accumulation of river derived suspended matter (Ferguson and Wolff, 1984; Smit et al., 1997; van Wijngaarden et al., 2002). The latter has negatively affected the benthic fauna, because of the high pollutant loading associated with suspended matter from the Rhine and Meuse (Reinhold-Dudok van Heel and den Besten, 1999). Thermal stratification and bottom water anoxia are not observed due to the shallow water depth and short residence time of water in the lake (Smit et al., 1997).

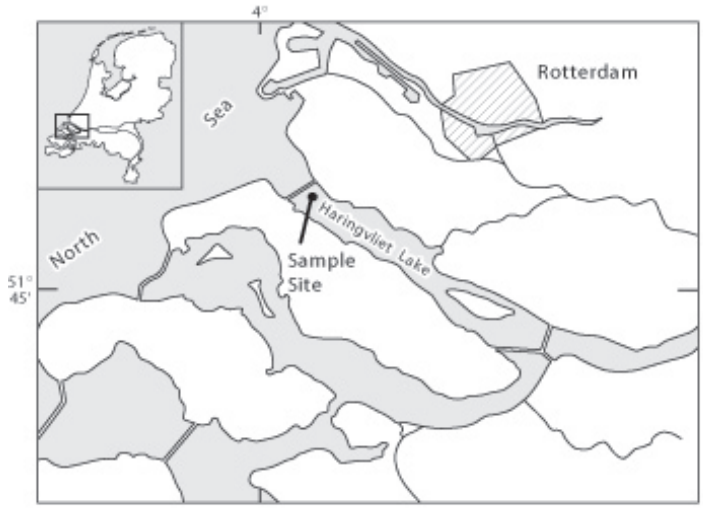

Figure 2.1 The sampling location in Haringvliet Lake. The inset map shows The Netherlands with a box denoting the location of the detail section. The Rhine-Meuse river complex flows into the lake from the east, and the lake discharges through the dam at the western limit of the lake.

Current Dutch water management policy aims at the development of a broad range of tidal systems with a high ecological diversity (de Jonge and de Jong, 2002). Within the framework of this policy, a proposed partial restoration of estuarine conditions in the Haringvliet would begin in 2008 and be achieved by changing the opening and closing of the gates in the dam that separates the lake from the North Sea (Anonymous, 1998). The present study is part of a larger effort to assess how benthic biogeochemistry and ecology may respond to a possible future intrusion of seawater in the lake. We selected a location near the dam as our study site (Fig. 2.1), within the area that will be most impacted by salinization. This location is characterized by fine-grained sediments, which are the main reservoir of pollutants in the lake, as reported for other Rhine and Meuse-derived sediments in the Netherlands (van den Berg et al., 1999; van den Berg et al., 2001). The water depth at the sampling site is 7.5 meters.

2.3 METHODS

2.3.1 Sample collection

Field sampling was carried out in November 2001, September 2002, and April 2003. These sampling times are referred to in the text as fall, late-summer, and spring, respectively. Sediment was collected using a cylindrical box corer (31 cm i.d.) deployed from RV Navicula. Each box core contained approximately 40 cm of surface sediment and 30 cm of overlying water. Sub-cores were taken with polycarbonate tubes (10 cm i.d.). Sub-cores for pore water and solid phase analyses were taken from a single box core. The sub-cores were immediately sectioned in a N_2 purged glove box on board the ship in a temperature-controlled laboratory. Sediment was centrifuged at 2500 *g* for 10 to 30 minutes in polyethylene tubes to collect pore water.

2.3.2 Pore water analyses

After centrifugation, tubes were transferred to a N_2 purged glove box, the pore water was filtered through 0.2 or 0.45 μm pore size filters, and pH was measured immediately with an ion selective field effect transistor electrode (ISFET, Sentron). Pore water was then sub-divided and preserved for analysis in the laboratory. Sub-samples for NO_3^-, NH_4^+, Cl^-, and SO_4^{2-} were stored frozen until analysis: NO_3^- and NH_4^+ were determined colorimetrically on a nutrient auto-analyzer (Bran and Luebbe), Cl^- and SO_4^{2-} were determined by ion chromatography (Dionex DX-120). Sub-samples for total dissolved Mn and Fe were acidified with HNO_3 (50 μl conc. suprapur HNO_3 per ml) and stored at 4 °C until analysis by ICP-MS (Agilent 7500 series). Sub-samples for major constituents, such as Na^+, were preserved with HNO_3 (10 μl conc. suprapur HNO_3 per ml) and stored at 4 °C until analysis by ICP-OES (Perkin Elmer Optima 3000).

During the spring and late-summer sampling, sulfide (Cline, 1969) and alkalinity (Sarazin et al., 1999) were determined on board the ship colorimeterically using a UV-Vis spectrophotometer (Unicam UV1). Sub-samples for sulfide analysis included a base preservative (10 μl 1M NaOH per ml). A sulfide pore water profile was also measured in late-summer using the Diffusive Gradient in Thin Films (DGT) method (Teasdale et al., 1999; Naylor et al., 2004). With this method, sulfide is determined by quantifying the color change resulting from the reaction of a AgI (yellow) containing gel with pore water sulfide, producing AgS_2 (black). Sulfide concentrations in the pore water were calculated using the calibration of Naylor et al. (2004).

During fall sampling, dissolved inorganic carbon (DIC) was measured as the difference of total and organic dissolved carbon. The latter was measured with a Shimadzu TOC-5050A analyzer. Dissolved oxygen microprofiles were obtained on board using a Clark-type

oxygen sensor with an internal reference and a guard cathode (Revsbech, 1989) attached to a micromanipulator. Perspex cores (4.2 cm i.d.) with 10 cm sediment and 5 cm overlying water were collected from a box core. The surface of each core was sparged with air and profiling was completed within 30 minutes of core retrieval.

2.3.3 Solid phase analyses

The water content and density of the sediment were determined from the weight loss upon freeze drying. Grain size was measured using a laser diffraction technique (Malvern Mastersizer S) on freeze dried sediment, after HCl and H_2O_2 pre-treatment. Total carbon, total sulfur, and organic carbon (following carbonate removal with 1 M HCl) were determined on freeze-dried sediments using an elemental analyzer (LECO SC-1440H). Total Mn and Fe were determined by ICP-MS after HF-$HClO_4$-HNO_3 digestion of freeze dried sediment as described in Hyacinthe and Van Cappellen (2004). Near-neutral pH ascorbate extractions were performed on wet sediment following the procedure of Hyacinthe and Van Cappellen (2004). This extraction releases the most chemically reactive reducible pool of Mn and Fe (Kostka and Luther, 1994, Hyacinthe and Van Cappellen, 2004).

Acid Volatile Sulfide (AVS) was determined by the method described in van den Berg et al. (1998), with some modifications. Approximately 1 gram of wet sediment was transferred to a reaction vessel in an Ar filled glove bag. The reaction vessel was weighed and then attached to an Ar purged analysis train. Samples were acidified with 10 ml 6M HCl and purged for 1 hour. The H_2S released from the sample was trapped in a 1 M NaOH solution and determined colorimetrically (Cline, 1969).

Chloropigments were extracted from wet sediment with 90% acetone, at a 1:2 sediment to solvent ratio. Sediments were mixed with a vortex stirrer and sonicated for ten minutes (Sun et al., 1991). Following sonication, the extractant was collected by centrifugation and stored at 0 °C until analysis. Determination of Chlorophyll-*a* (Chl-*a*) and Pheophytin-*a* (Pheo-*a*) in the extracts was performed spectrophotometrically (APHA, 1985). Solid phase data presented are from the late-summer sampling unless otherwise indicated.

2.3.4 Rate measurements

Rates of total carbon mineralization were determined by monitoring CO_2 accumulation in the headspace of oxic and anoxically incubated slurries, following the procedure of Dauwe et al. (2001). Slurries containing approximately 20 ml wet sediment and 10 ml filtered, de-oxygenated lake water were placed in 100 ml glass vials sealed with rubber septa. The vials were shaken and the headspace was purged for ten minutes with either air for oxic incubations,

or N_2 for anoxic incubations. The purging procedure was repeated three times for each vial. The CO_2 concentration in the headspace was monitored using gas chromatography. Potential rates of denitrification and sulfate reduction were determined using flow-through reactors (FTRs), following methods described in detail elsewhere (Roychoudhury et al., 1998; Laverman et al., 2006; Pallud and Van Cappellen, 2006).

2.4 MODEL FORMULATION

The model presented in this paper follows the general approach outlined in Van Cappellen and Wang (1996); this section therefore focuses on the implementation of processes described in more recent studies, and the derivation of parameter values and boundary conditions from field data. The reaction-transport model calculations were carried out with the Biogeochemical Reaction Network Simulator (BRNS), a flexible modeling environment for one-dimensional simulations (Regnier et al., 2003; Jourabchi et al., 2005; Aguilera et al., 2005). In the BRNS, the chemical species, reaction stoichiometries, kinetic parameters, boundary conditions, and transport parameters are specified by the user through a MAPLE software or web-based interface (Chilakapati, 1995; Amberg et al., 1999; Regnier et al., 2002; 2003). An executable program, which consists of a set of standard routines for iteratively solving the reaction and transport equations, is then generated automatically. The model output consists of the species concentrations, reaction rates, and fluxes as a function of depth. Both steady-state and transient simulations can be performed.

2.4.1 Species and reactions

The model developed here considers 24 chemical species (Table 2.1) and 32 reaction pathways (Table 2.2). The mineralization of organic carbon is modeled using the multi-G approach (Westrich and Berner, 1984). Three pools of organic carbon are included in the model: OM1, the most reactive C_{org} fraction, OM2, a less reactive fraction, and OM3, the non-reactive or refractory pool. The decomposition kinetics are first-order and controlled by the rate constants, kOM1 and kOM2. To account for increased degradation efficiencies of C_{org} under oxic versus anoxic conditions (e.g., Hedges and Keil, 1995; Kristensen, 2000; Dauwe et al., 2001; Bastviken et al., 2004; Meile and Van Cappellen, 2005), a dimensionless acceleration factor (accel) is included (Table 2.2).

Total C_{org} decomposition is distributed over the different degradation pathways following the approach of Van Cappellen and Wang (1996). This approach is based on a Michaelis-Menten kinetic formulation for the utilization of the TEAs, where a set of limiting concentration values (K_m) determines the fractions (f_{TEA}) of total C_{org} occurring via the various degradation pathways.

The redox zonation and overlap between primary redox processes has been successfully reporduced for a variety of subsurface environments using this approach (Van Cappellen and Wang, 1995; 1996; Hunter et al., 1998; Berg et al., 2003; Fossing et al., 2004).

Table 2.1 Solutes and solids included in the model and their boundary conditions at the sediment surface. Solute concentrations are determined experimentally or estimated, solid fluxes are derived from model fitting (see section 2.4.3).

Solutes	μM	*Solids*	μmol cm^{-2} yr^{-1}
O_2	238	OM1	630
NO_3^-	154	OM2	315
SO_4^{2-}	638	OM3	546
NH_4^+	14.5	MnO_2A	4.2
Mn^{2+}	0.2	$Fe(OH)_3A$	14.7
Fe^{2+}	0	MnO_2B	2.1
H_2S, HS^-	0	$Fe(OH)_3B$	23.1
HCO_3^-	405	FeS	0
CO_2	17.3	FeS_2	0
CO_3^{2-}	0	$NH_{4\ ads}^+$	0
CH_4 (aq), (g)	0		
H^+	7.9[a]		

(a) pH units

The rate parameters controlling C_{org} decomposition (kOM1, kOM2, and accel) were constrained by the experimental rate measurements and the model fits (Table 2.3). Initial guesses of the parameter values were based on the global relationships reported by Tromp et al. (1995). The value of the acceleration factor imposed in the model calculations (accel = 25) falls in between that obtained from the CO_2 production rates in oxic versus anoxic slurry incubations (oxic:anoxic = 17), and the maximum potential rates of denitrification and sulfate reduction measured in FTRs on intact sediment slices (denitrification:sulfate reduction = 34). The K_m values of Van Cappellen and Wang (1995) were used, except for dissimilatory iron reduction, for which a higher K_m value had to be imposed in order to reproduce the limited microbial reduction of iron in the sediment.

In sediments, the build-up of methane may result in the formation of gas bubbles. This process is simulated using the approach of Martens et al. (1998), where methanogenesis

produces $CH_4(aq)$ until the pore water concentration equals the saturation concentration. Further methanogenesis then produces $CH_4(g)$. A unitless parameter, *f*m, is introduced to switch between $CH_4(aq)$ and $CH_4(g)$ production (R12 and R13, Table 2.2):

$$fm = 1 - 1/(1+ e^{\delta}) \quad (1)$$
$$\text{with } \delta = S_m (CH_4(aq) - CH_4^*)$$

where CH_4^* is the methane solubility (mM) and S_m (mM^{-1}) is an adjustable parameter. This formulation insures that the value of *f*m rapidly approaches 1 when $CH_4(aq) > CH_4^*$, and 0 when $CH_4(aq) < CH_4^*$. The use of a continuous *f*m function (eq. 1) avoids numerical oscillations in model output. It is assumed that $CH_4(g)$ is transported to the sediment-water interface (SWI) without further reaction in the sediment. For the sake of simplicity, effects of gas production on porosity and compaction are not considered in the model.

All secondary redox reactions are assigned bimolecular rate laws (Table 2.2). As in Berg et al. (2003), two pools of reactive Mn and Fe oxides are considered. The first, or bioavailable, pool can be reduced microbially as well as chemically, while the second pool can only be reduced chemically. Chemical reduction of reactive Mn and Fe oxides by sulfide is assumed to yield SO_4^{2-} as the final oxidized S-species (R22-R25, Table 2). That is, intermediate sulfur species are assumed to be short-lived (Elsgaard and Jørgensen, 1992) and are not represented explicitly. Initial values of secondary reaction rate constants were obtained from previous studies (Table 2.3), and then adjusted to obtain better fits to the field data. In particular, the values of k_{tsmn}, k_{tsfe}, and k_{ch4so4} used here are lower than reported previously.

The rates of FeS dissolution and precipitation (R30-31, Table 2.2) are dependent on the degree of FeS under- or supersaturation of the pore water, using the formulations of Van Cappellen and Wang (1996). Formation of pyrite (FeS_2) is described as a reaction of FeS and H_2S, using the bimolecular rate equation of Rickard (1997). Dissolution of pyrite is not included in the model.

Adsorption of NH_4^+ to cation exchange sites is represented by a linear equilibrium isotherm, with a constant adsorption coefficient, K_N. The model further includes homogenous carbonate and sulfide equilibrium reactions (R27-29), which are assumed to be the major aqueous pH buffers in this system. The concentration of H^+ is explicitly computed from the equilibrium conditions (Jourabchi et al., 2005). Reactions with sulfide are written with H_2S as the reactive species, however the inclusion of the H_2S dissociation equilibrium (R29) means that both H_2S and HS^- species concentrations respond to sulfide producing and consuming reactions.

Table 2.2. The reaction network and kinetic formulations used in the model. Reaction parameters are defined in Table 2.3.

Description	Reaction	Kinetic or equilibrium formulation	Reaction number
Primary redox reactions [a,b]			
aerobic respiration [c]	$OM + xO_2 + (-y+2z)HCO_3^- \rightarrow (x-y+2z)CO_2 + yNH_4^+ + zHPO_4^{2-} + (x+2y+2z)H_2O$	fO_2 kOM1 [OM1] accel	R1, R7
denitrification [c]	$OM + 0.8xNO_3^- \rightarrow 0.4xN_2 + (0.2x-y+2z)CO_2 + (0.8x+y-2z)HCO_3^- + yNH_4^+ + zHPO_4^{2-} + (0.6x-y+2z)H_2O$	fNO_3 kOM1 [OM1] accel	R2, R8
Mn oxide reduction	$OM + 2xMnO_2 + (3x+y-2z)CO_2 + (x+y-2z)H_2O \rightarrow 2xMn^{2+} + (4x+y-2z)HCO_3^- + yNH_4^+ + zHPO_4^{2-}$	$fMnO_2$ kOM1 [OM1]	R3, R9
Fe oxide reduction	$OM + 4xFe(OH)_3 + (7x+y-2z)CO_2 \rightarrow 4xFe^{2+} + (8x+y-2z)HCO_3^- + yNH_4^+ + zHPO_4^{2-} + (3x+y-2z)H_2O$	$fFe(OH)_3$ kOM1 [OM1]	R4, R10
sulfate reduction	$OM + 0.5xSO_4^{2-} + (y-2z)CO_2 + (y-2z)H_2O \rightarrow 0.5xH_2S + (x+y-2z)HCO_3^- + yNH_4^+ + zHPO_4^{2-}$	fSO_4 kOM1 [OM1]	R5, R11
methanogenesis-(aq) [d]	$OM + (y-2z)H_2O \rightarrow 0.5xCH_4\,(aq) + (0.5x-y+2z)CO_2 + (y-2z)HCO_3^- + yNH_4^+ + zHPO_4^{2-}$	fOM kOM1 [OM1] fm	R6, R12
methanogenesis-(g) [d]	$OM + (y-2z)H2O \rightarrow 0.5xCH_4\,(g) + (0.5x-y+2z)CO_2 + (y-2z)HCO_3^- + yNH_4^+ + zHPO_4^{2-}$	fOM kOM2 [OM2] (1-fm)	R13
Secondary redox reactions			
NH_4^+ oxidation by O_2	$NH_4^+ + 2O_2 + 2HCO_3^- \rightarrow NO_3^- + 2CO_2 + 3H_2O$	knh4ox $[NH_4^+][O_2]$	R14
H_2S oxidation by O_2	$H_2S + 2O_2 + 2HCO_3^- \rightarrow SO_4^{2-} + 2CO_2 + 2H_2O$	ktsox $[H_2S][O_2]$	R15
FeS oxidation by O_2	$FeS + 2O_2 \rightarrow SO_4^{2-} + Fe^{2+}$	kfesox $[FeS][O_2]$	R16
Mn^{2+} oxidation by O_2	$Mn^{2+} + 0.5O_2 + 2HCO_3^- \rightarrow MnO_2 + 2CO_2 + H_2O$	kmnox $[Mn^{2+}][O_2]$	R17
Fe^{2+} oxidation by O_2	$Fe^{2+} + 0.25O_2 + 2HCO_3^- + H_2O \rightarrow Fe(OH)_3 + 2CO_2$	kfeox $[Fe^{2+}][O_2]$	R18
CH_4 oxidation by O_2	$CH_4 + O_2 \rightarrow CO_2 + H_2O$	kch4ox [CH4][O_2]	R19
Fe^{2+} oxidation by Mn oxide	$2Fe^{2+} + MnO_2 + 2HCO_3^- + 2H_2O \rightarrow 2Fe(OH)_3 + Mn^{2+} + 2CO_2$	kfemn $[Fe^{2+}][MnO_2]$	R20

Table 2.2 continued

Description	Reaction	Kinetic or equilibrium formulation	Reaction number
Secondary redox reactions (continued)			
CH_4 oxidation by SO_4^{2-}	$CH_4 + SO_4^{2-} + CO_2 \rightarrow H_2S + 2HCO_3^-$	kch4so4 $[CH_4][SO_4^{2-}]$	R21
H_2S oxidation by Mn oxide [e]	$H_2S + 6CO_2 + 4\,MnO_2 + 2H_2O \rightarrow 4Mn^{2+} + SO_4^{2-} + 6HCO_3^-$	ktsmn $[H_2S][MnO_2]$	R22,R23
H_2S oxidation by Fe oxide [e]	$H_2S + 14CO_2 + 8FeOH_3 \rightarrow 8Fe^{2+} + SO_4^{2-} + 14HCO_3^- + 6H_2O$	ktsfe $[H_2S][Fe(OH)_3]$	R24,R25
Adsorption and equilibrium reactions			
NH_4^+ adsorption	$NH_4^+ \leftrightarrow NH_{4\,ads}^+$	K_N $[NH_4^+]$	R26
carbonate equilibria	$H^+ + HCO_3^- \leftrightarrow CO_2 + H_2O$	Keqc1	R27
	$CO_3^{2-} + H^+ \leftrightarrow HCO_3^-$	Keqc2	R28
sulfide equilibrium	$H^+ + HS^- \leftrightarrow H_2S$	Keqs	R29
Precipitation and dissolution reactions (non-redox)			
FeS dissolution [f]	$FeS + 2H^+ \rightarrow Fe2+ + H_2S$	kfesdis [FeS] (1- ΩFeS)	R30
FeS precipitation [g]	$Fe2+ + H_2S \rightarrow FeS + 2H^+$	kfespre (ΩFeS -1)	R31
pyrite precipitation	$FeS + H_2S \rightarrow FeS_2 + H_2$	Kpyrpre [FeS] $[H_2S]$	R32

(a) OM = $(CH_2O)_x(NH_3)_y(H_3PO_4)_z$ where x,y,z represent the CNP ratios given in Table 3; (b) For reactions R1-R6 k_{OM1} and CNP_{OM1} are used, for R7-R13 k_{OM2} and CNP_{OM2} are used; the f_{TEA} terms are the fractions of total carbon mineralization assigned to the different TEA pathways; (c) the accel term is only used in R1 and R2; (d) the term *fm* is defined by Eq. 1, and controls the switching between R12 and R13, *fm* is not included in R6 which does not produce methane in excess of saturation in this system; (e) R23 with MnO_2B, R25 with $Fe(OH)_3$B; (f) ΩFeS = Fe^{2+} H_2S /$(H^+)^2$ Kfes, R30 = 0 when ΩFeS > 1; (g) R31 = 0 when ΩFeS < 1.

Table 2.3 Reaction parameter values used in the model. The source of the parameter values are indicated by the following code: C = constrained from experimental data, M = derived by model fitting, I = independently determined from field data, L = literature value, with references given at the bottom of the table. A range of literature values for the secondary reaction rate constants is provided.

Parameter	Value	Unit	Source	Ref.	Description
Primary redox reactions					
kOM1	1	yr^{-1}	C, M		degradation rate constant OM1
kOM2	0.01	yr^{-1}	C, M		degradation rate constant OM2
kOM3	0	yr^{-1}	M		OM3 not reactive
accel	25	-	M, C		acceleration factor: R1 - R2
f_{TEA}	0-1	-	M		fraction of total OM degradation by each TEA pathway
CNP_{OM1}	112:20:1	-	C, L	1	CNP for OM1 (highly reactive)
CNP_{OM2}	200:20:1	-	C		CNP for OM2 (less reactive)
K_m O_2	8	µM	L	2	limitation for oxic respiration
K_m NO_3^-	10	µM	L	2	limitation for denitrification
K_m MnO_2	16	µmol g^{-1}	L	3	limitation for Mn reduction
K_m $FeOH_3$	200	µmol g^{-1}	M		limitation for Fe reduction
K_m SO_4^{2-}	100	µM	C, L	2	limitation for SO_4^{2-} reduction
CH_4^*	2.66	mM	I		saturation conc. at study site
fm	0-1	-	M	4	methane switch (see eq.1)
S_m	3.0	mM^{-1}	M, L	4	methane switch (see eq. 1)
Secondary redox reaction			range from (2,3,5,6)		
knh4ox	2×10^1	μM^{-1} yr^{-1}	$5 - 7.9 \times 10^1$		R14, nitrification
ktsox	1×10^3	μM^{-1} yr^{-1}	1.6×10^{-1} - 1.6×10^3		R15, sulfide oxidation by O_2
kfesox	2×10^1	μM^{-1} yr^{-1}	1.9×10^{-1} - 2×10^1		R16, FeS oxidation by O_2
kmnox	1.0	μM^{-1} yr^{-1}	3.5×10^{-1} - 2×10^3		R17, Mn^{2+} oxidation by O_2
kfeox	5×10^1	μM^{-1} yr^{-1}	3.5×10^{-1} - 1.6×10^4		R18, Fe^{2+} oxidation by O_2
kch4ox	1×10^4	μM^{-1} yr^{-1}	1×10^4		R19, methane oxidation by O_2
kfemn	1×10^{-1}	μM^{-1} yr^{-1}	2.4×10^{-3} - 3		R20, Fe^{2+} oxidation by Mn-oxides
kch4so4	1×10^{-4}	μM^{-1} yr^{-1}	1×10^{-2} - 1×10^4		R21, methane oxidation by SO_4^{2-}
ktsmn	7.5×10^{-3}	μM^{-1} yr^{-1}	1×10^{-2} - 6.3×10^{-1}		R22, R23 sulfide oxidation by Mn-oxides
ktsfe	2.5×10^{-3}	μM^{-1} yr^{-1}	8×10^{-3} - 9.5×10^{-2}		R24, R25 sulfide oxidation by Fe-oxides, see also (7)
Adsorption, equilibrium, dissolution, and precipitation constants					
K_N	1.4	-	L	3	ammonium adsorption constant
Keqc1	3.0×10^{-7}	-	I	8	carbonate equilibrium constant
Keqc2	3.6×10^{-13}	-	I	8	bicarbonate equilibrium constant
Keqs	6.3×10^{-8}	-	I	9	Sulfide equilibrium constant
Kfes	9.6×10^3	-	L	10	FeS stability constant
kfespre	1.5×10^{-3}	mol g^{-1} yr^{-1}	M		FeS precipitation rate constant
kfesdis	1.0×10^{-3}	yr^{-1}	L	3	FeS dissolution rate constant
Kpyrpre	3.3×10^{-3}	μM^{-1} yr^{-1}	L	11	FeS_2 precipitation rate constant

1. Koelmans (1998); 2. Van Cappellen and Wang (1995); 3. Van Cappellen and Wang (1996); 4. Martens *et al.* (1998); 5. Berg *et al.* (2003); 6. Fossing *et al.* (2004); 7. Poulton *et al.* (2004); 8. Cai and Wang (1998); 9. Pilson (1998); 10. Davison *et al.* (1999); 11. Rickard (1997).

2.4.2 Transport

Solute transport processes included are molecular diffusion, bioirrigation, bioturbation, and sediment advection, while solid species are transported by bioturbation and sediment advection. Molecular diffusion coefficients at 0 °C and temperature correction factors are taken from Van Cappellen and Wang (1995), and references therein, and corrected for tortuosity effects after Boudreau (1996). Porosity, φ ($cm^3\ cm^{-3}$), varies with depth as defined by the equation given in Table 2.4 and shown in Fig. 2.2. The advection velocity accounts for the variations in porosity (Berner, 1980).

Table 2.4 Depth distributions and parameter values for physical properties and transport processes.

Depth distributions				Description
$\varphi(x) = \varphi_\infty + (\varphi_o - \varphi_\infty)e^{-(\tau x)}$				porosity distribution (Fig. 2.2)
$\alpha = \begin{cases} \alpha_0 \left(1 - e^{(x-17)}\right) & (x \le 17\,cm) \\ 0 & (x > 17\,cm) \end{cases}$				distribution of bioirrigation coefficient α (Fig. 2.3)
$D_b = D_b 0\ e^{-(x/\lambda)}$				distribution of bioturbation coefficient D_b (Fig. 2.4)
Parameter definitions and values				
Parameter	Value	Unit	Source	Description
φ_0	0.89	$cm^3\ cm^{-3}$	measured	porosity at SWI
φ_∞	0.79	$cm^3\ cm^{-3}$	measured	porosity at infinite depth
τ	0.2	cm^{-1}	data fitting	porosity attenuation
x	0-30	cm	measured	sediment depth
ω	1.0	$cm\ yr^{-1}$	literature[a]	sediment accumulation rate at SWI
α	0-10	yr^{-1}	data fitting	bioirrigation coefficient
α_0	10	yr^{-1}	data fitting	value of α at SWI
D_b	0-5	$cm^2\ yr^{-1}$	data fitting	bioturbation coefficient
$D_b 0$	5	$cm^2\ yr^{-1}$	data fitting	value of D_b at SWI
λ	2.5	cm	data fitting	D_b attenuation
ρ	2.1	$g\ cm^{-3}$	measured	sediment density
temp.	12	°C	measured	mean sediment temperature

(a) van Wijngaarden et al. (2002)

The pore water profiles of many species, including the conservative ions Na^+ and Cl^-, show evidence of bioirrigation (Fig. 2.3). As can be seen in Fig. 2.3, the concentrations of Na^+ and Cl^- increase with depth below 17 cm. It is unlikely that these concentration profiles reflect the ongoing replacement of remnant saline pore waters by freshwater. The age of the lake (created in 1970) and the sedimentation rate (~1 cm yr^{-1}, see below), imply that the sediment in the

upper 30 cm was deposited in freshwater conditions. The increasing salinity in the lower half of the cores thus indicates salt diffusion from a deeper source, probably related to subterranean seawater intrusion. The near-constant concentrations of Na^+ and Cl^- in the upper 17 cm then require enhanced pore water transport to counteract the upward salt diffusion. This enhanced pore water transport is attributed to bioirrigation.

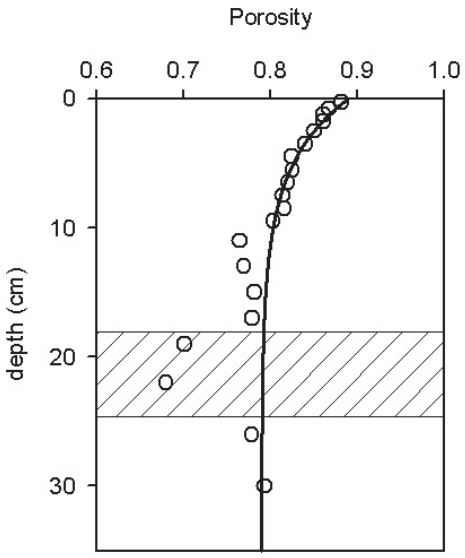

Figure 2.2 Depth distribution of sediment porosity in late-summer. The solid line is the exponential fit used to represent porosity in the model (see equation in Table 2.4). The shaded area between approximately 18 and 24 cm depth denotes a zone of coarser-grained sediment.

The depth distribution of the bioirrigation coefficient α (Table 2.4) was derived by fitting the Na^+ and Cl^- profiles to the steady state diffusion-irrigation equation, with the concentrations at the SWI and at 30 cm depth fixed to the measured values. Note that this approach yields a minimum estimate of the irrigation intensity. The selected form of the depth distribution (Fig. 2.3c, Table 2.4) produced a better fit to the pore water Na^+ and Cl^- profiles than a linearly or exponentially attenuating bioirrigation coefficient distribution. It is also preferred over the simpler step-function distribution, as it avoids a sharp discontinuity of α at the bottom of the irrigated zone. The value of α_0 obtained (10 yr^{-1}) is similar to irrigation coefficients reported for freshwater sediment microcosms inhabited by deposit feeding tubificid worms (5-10 yr^{-1}, Wang and Matisoff, 1997), at comparable population densities as those found by Smit et al. (1995) in fine-grained Haringvliet Lake sediments (on the order of 10^3 organisms m^{-2}).

All solutes are assigned the bioirrigation coefficient distribution shown in Table 2.4, except Mn^{2+} and Fe^{2+}. Net vertical transport of Mn^{2+} and Fe^{2+} by irrigation is strongly impeded, because these pore water species oxidatively precipitate near flushed burrow walls, and are

therefore prevented from escaping via the burrows (Berg et al., 2003; Meile et al., 2005). The value of α for Fe^{2+} is reduced by 100% (no bioirrigation) while α for Mn^{2+} is reduced by 40%. The reduced α values produce modeled pore water profiles that are consistent with the data. The variable adjustments to the irrigation coefficients of Mn^{2+} and Fe^{2+} are also in agreement with Berg et al. (2003) who found that, in contrast to Fe^{2+}, pore water distributions of Mn^{2+} show evidence of transport by irrigation, most likely because of slower oxidation rates compared to Fe^{2+}.

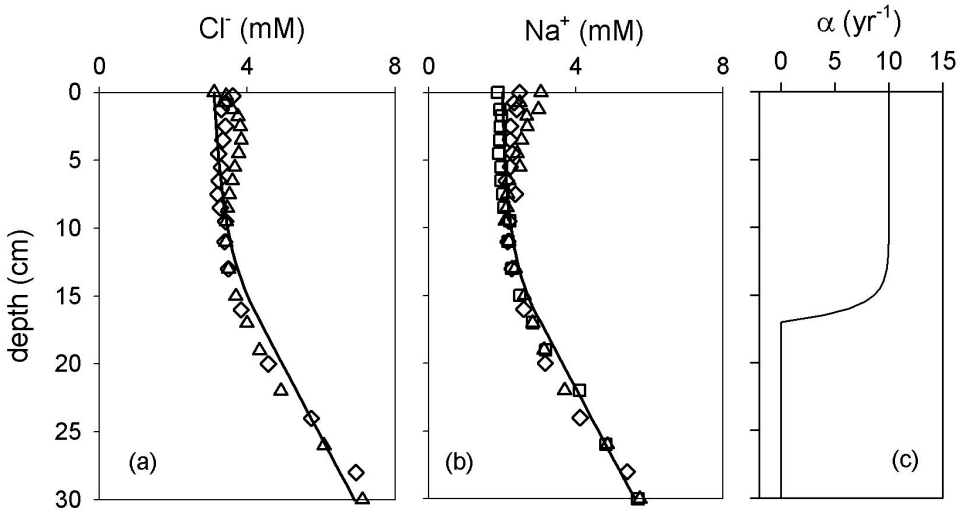

Figure 2.3. Pore water profiles of Cl^- in (a) fall (◇) and spring (△), and Na^+ in (b) fall (◇), late-summer (□) and spring (△). The solid lines represent a model fit for fixed boundary concentrations (at 0 and 30 cm), and the bioirrigation distribution given in Table 2.4. The depth distribution of the irrigation coefficient is depicted in panel (c).

Particle mixing is represented as a diffusion process (Berner, 1980). It results mainly from the activity of benthic macrofauna (bioturbation), although some effect of sediment resuspension cannot be excluded at the shallow water depth of the sampling site (7.5 m). The bioturbation coefficient, D_b ($cm^2\,yr^{-1}$) is defined by an exponentially decaying depth distribution (Table 2.4; Wijsman et al., 2002). The magnitude and depth distribution of the biodiffusion coefficient were constrained by fitting the measured profiles of Pheo-*a*, a breakdown product of Chl-*a* (Fig. 2.4). Sediment profiles of Chl-*a* have been previously used to quantify sediment mixing (e.g. Sun et al., 1994; Boon and Duineveld, 1998; Wijsman et al., 2002). The depth distribution of D_b was obtained assuming steady state and a degradation rate constant of 0.05 yr^{-1} for Pheo-*a* (Table 2.4, Fig. 2.4b). A major source of uncertainty in this estimation is the value of

the degradation rate constant imposed in the calculations. For refractory Pheo-*a* in marine sediments the reported values exhibit a considerable range, from 0.002 to 0.15 yr^{-1} (Stephens et al., 1997). Bioturbation is described as a diffusion process for the sake of simplicity; however, actual sediment mixing processes may be more complex as evidenced by the pigment data from late-summer (Fig. 2.4) which suggests non-local sediment transport.

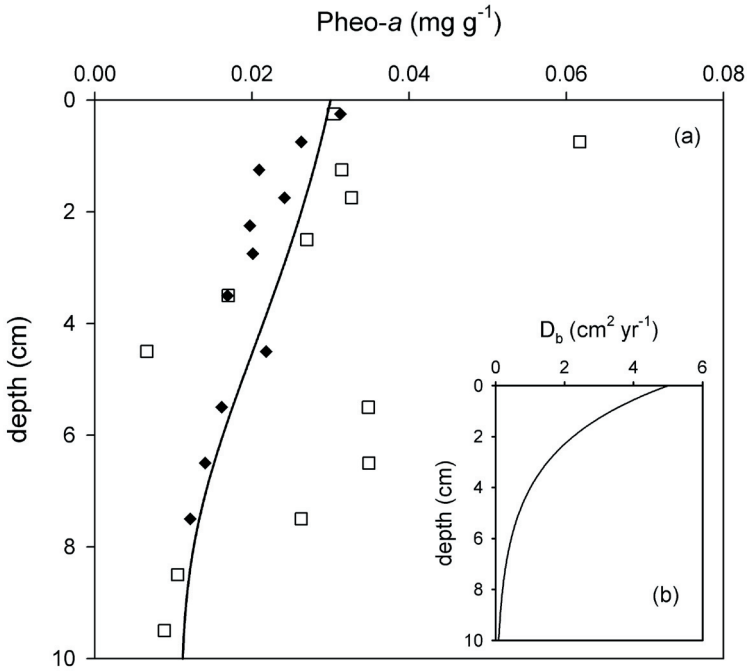

Figure 2.4 Pheo-*a* sediment profiles for fall (♦) and late-summer (□). The solid line in (a) is the modeled fall Pheo-*a* distribution obtained using the D_b depth distribution depicted in the inset (b). The D_b depth distribution is given in Table 2.4.

2.4.3 Boundary conditions

Upper boundary conditions for solutes and solids at the SWI are summarized in Table 2.1. All chemical species are assigned a zero concentration gradient as lower boundary condition. The model depth (100 cm) extends well below the depth interval examined in this study (0-30 cm), in order to minimize computational artifacts associated with the lower boundary conditions.

In the absence of direct measurements, initial estimates of particulate depositional fluxes were derived from suspended matter concentrations and the sedimentation rate. The latter was estimated at 1 cm yr^{-1}, based on the radiometric age determinations of van Wijngaarden

et al. (2002). The initial flux estimates were then adjusted by trial and error in order to fit measured concentration profiles. The deposition fluxes of Mn and Fe oxides were adjusted to optimize the simultaneous fit of the concentration distributions of both solid-phase and pore water Mn and Fe. The model-calculated pore water O_2 distribution is particularly sensitive to the deposition flux of the most reactive organic matter, OM1. Hence, the measured O_2 microprofiles were used primarily to constrain the flux of OM1. The pore water profiles of NH_4^+ and DIC were used in a similar manner to determine the flux of OM2. Once the fluxes of OM1 and OM2 were fixed, the flux of non-reactive organic matter, OM3, was adjusted to reproduce the measured total organic carbon concentrations.

2.5 RESULTS

Sediment porosity approached 90% at the SWI, and decreased near-exponentially with depth to values of around 80% (Fig. 2.2). The anomalously low porosities in depth interval 18-24 cm corresponded to an increase in sediment grain size (not shown). This change in sediment grain size may be the result of lake shore erosion. Concentrations of C_{org}, total Fe, and total Mn were also lower in the 18-24 cm depth range due to dilution by coarser grained sediment (Figs. 2.5 and 2.6).

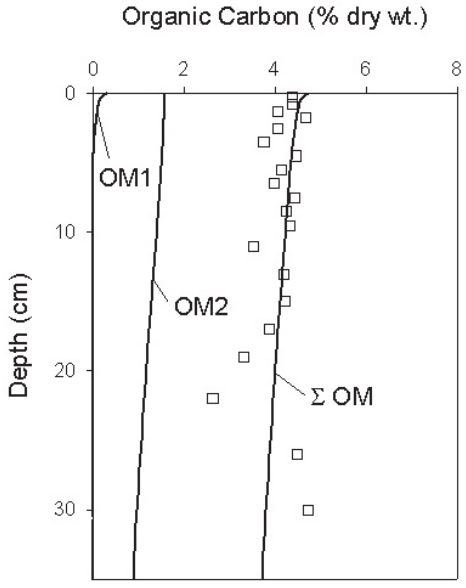

Figure 2.5 Depth distribution of the measured total organic carbon (□), and model distributions of the reactive organic carbon pools OM1, OM2, and the sum of the three OM pools (Σ OM) (solid lines).

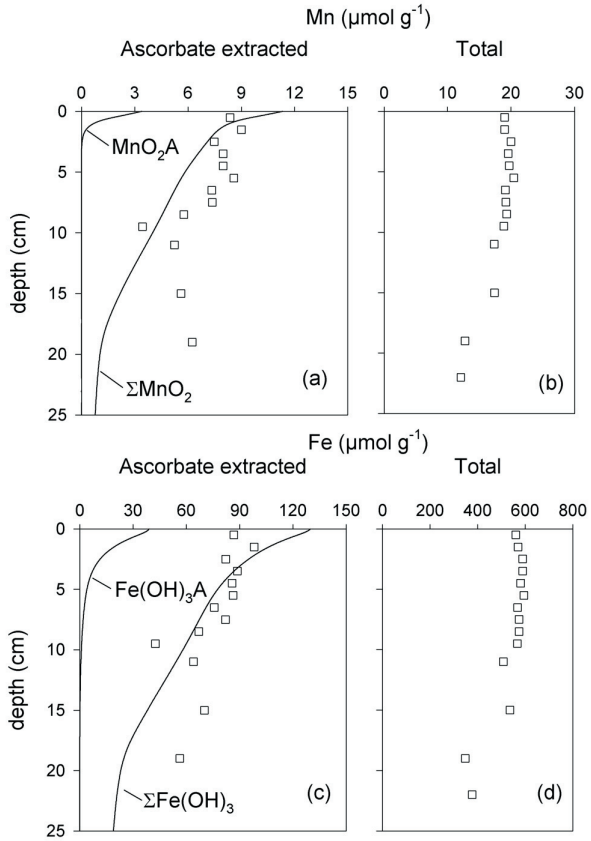

Figure 2.6 Depth distributions of total and reducible Mn and Fe. Reducible Mn and Fe are obtained by chemical extraction with ascorbate at near-neutral pH. This method releases the reactive fractions of oxidized Mn and Fe (Hyacinthe and Van Cappellen, 2004). Also shown are the model distributions of MnO_2A, $MnO_2A + MnO_2B$ (ΣMnO_2), $Fe(OH)_3A$, and $Fe(OH)_3A + Fe(OH)_3B$ ($\Sigma Fe(OH)_3$). Model distributions are depicted as solid lines, extraction data are indicated with (□) symbols.

The particulate C_{org} concentration profile shows little change with depth in the upper 18 cm of sediment, suggesting that the major part of organic matter is refractory (Fig 2.5). The profiles of total Mn and Fe do not exhibit distinct changes with depth. However, the concentrations of easily reducible Mn_{asc} and Fe_{asc} pools were highest near the SWI and declined with depth (Fig. 2.6). Reactive Mn_{asc} represented approximately 45% of the total Mn concentration near the SWI, while Fe_{asc} represented less than 20% of total Fe near the SWI. AVS concentrations were lower in spring than in late-summer in depth interval 4-15 cm. In late-summer, AVS accounted for 22-48% of the total sulfur measured below 4 cm depth (Fig. 2.7).

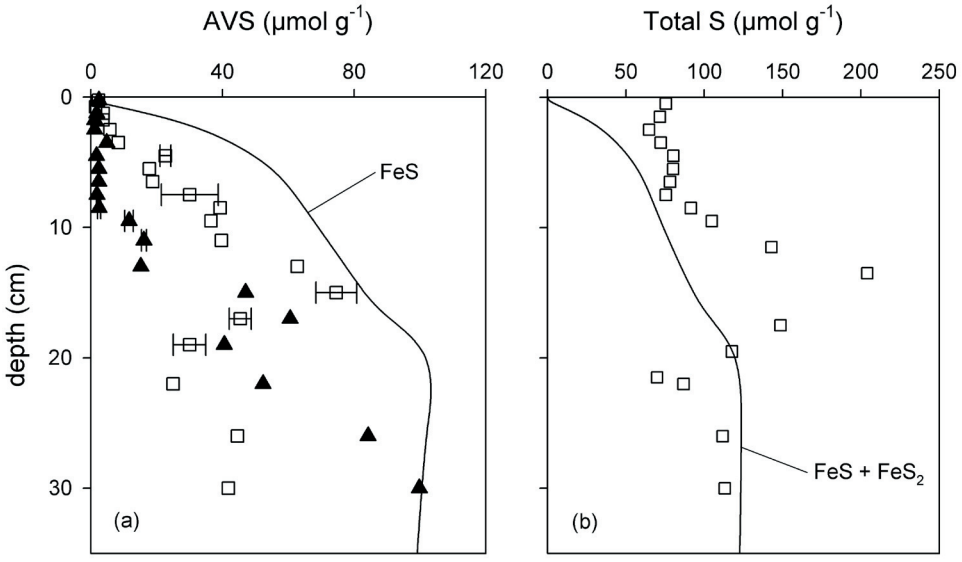

Figure 2.7 Acid Volatile Sulfide (AVS) distributions for late-summer (□) and spring (▲); the solid line represents the modeled FeS concentrations (a). Total sulfur distribution for late-summer (□), the solid line represents the sum of modeled FeS and FeS_2 concentrations (b). Errors bars are +/- one standard deviations on duplicate or triplicate analyses.

Pore water O_2 and NO_3^- were depleted within the uppermost centimeter of sediment (Fig. 2.8), implying high rates of oxygen and nitrate reduction. Dissolved Mn concentrations exhibited a subsurface peak at approximately 3 cm. The peak in dissolved Mn concentrations was greater in spring than at the other two sampling dates. The concentrations of dissolved Fe were fairly constant in the upper 13 cm and then increased steadily with depth. Measurable pore water concentrations of sulfate persisted down to 20 cm depth in fall. In spring and late-summer, the penetration depth of SO_4^{2-} was shallower, although in late-summer concentrations of approximately 60 µM were measured between 5 and 17 cm depth. Colorimetric sulfide analysis of centrifuged pore water never resulted in detectable concentrations. The sulfide pore water profile obtained with the AgI DGT probe gave S(-II) concentrations in the range of 5-10 µM in the 2-10 cm depth interval. Concentrations of NH_4^+ and alkalinity increased with depth, providing evidence that C_{org} mineralization occurred at least down to 30 cm. Pore water pH was most variable in the upper 10 cm of sediment; below this depth pH values displayed a gradually decreasing trend with depth.

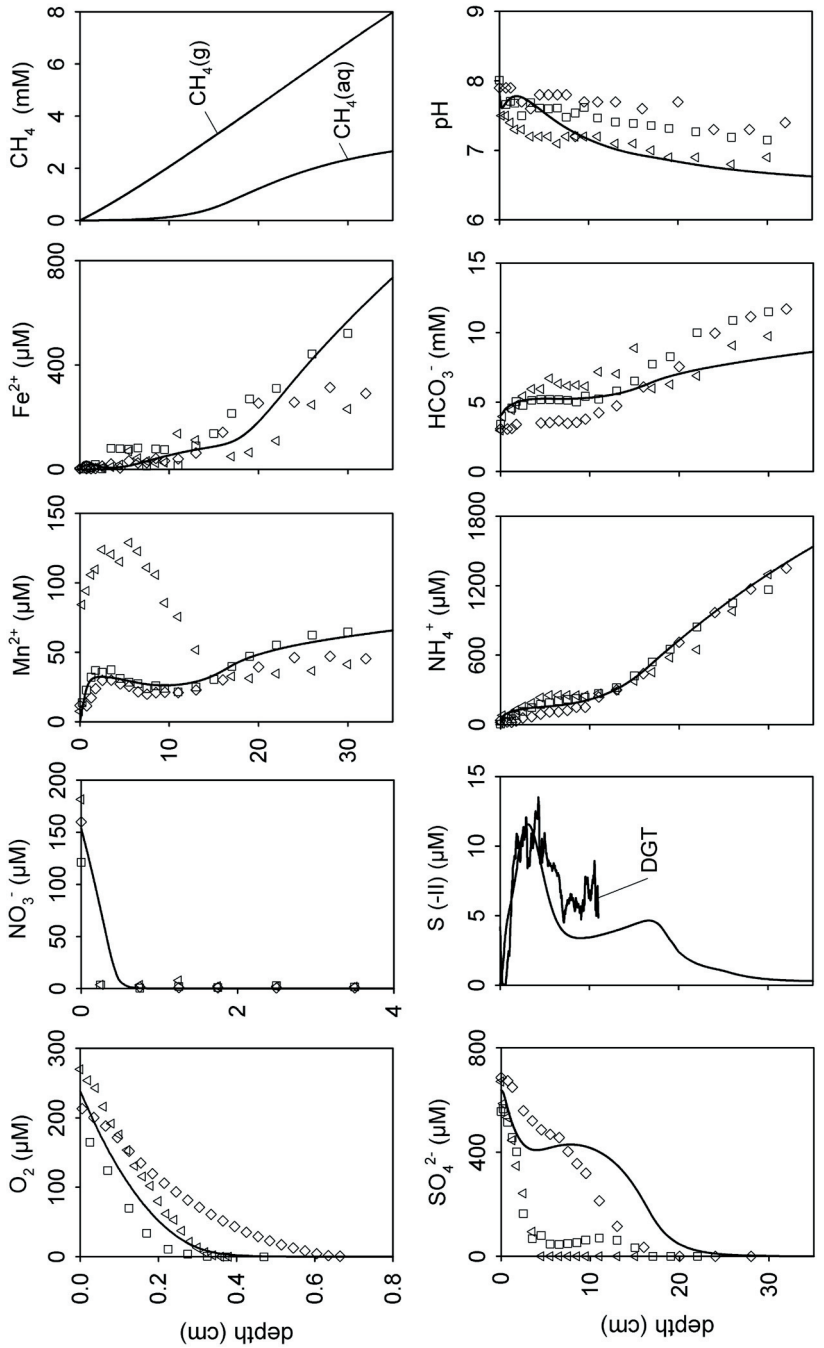

Figure 2.8 Pore water profiles for fall (◊), late-summer (□), and spring (△) of dissolved species; solid lines are modeled profiles. The line marked DGT in the S(-II) plot is the AgI DGT derived sulfide profile measured in the upper 10 cm of the sediment. In the HCO_3^- plot, model results correspond to HCO_3^- concentrations, while the data points correspond to measurements of DIC (fall) or alkalinity (late-summer and spring). Note different depth scales in the O_2 and NO_3^- plots.

Experimentally determined rates of carbon mineralization in oxic slurries were systematically higher than those of anoxic slurries (Table 2.5). The average rate of CO_2 production observed in anoxic slurries was 17 times less than that found in oxic slurries. Potential rates of denitrification were approximately 34 times greater than potential rates of sulfate reduction measured with FTRs from the upper 4 cm of sediment. All methods yielded rates that varied with the sampling date, and depth, but also between duplicates. Despite the observed variability (Table 2.5), the data implied that aerobic respiration and denitrification produced much higher rates of carbon mineralization than other, anoxic degradation pathways.

Table 2.5 Comparison of maximum model derived rates and experimental rates.

model derived maximum rates		*experimental rates*					
			mean	sd[a]	number[b]	depth range	date[c]
pathway	(μmol cm^{-3} yr^{-1})	method	(μmol cm^{-3} yr^{-1})			(cm)	
oxic respiration	1492	oxic slurry	1426	704	9	0-20	LS
denitrification	713	denitrification FTR	783	547	12	0-4	S,LS,F
sulfate reduction	25	sulfate red. FTR	23	16	8	2-4, 8-10	LS
anoxic pathways[d]	220	anoxic slurry	85	86	19	0-20	LS,F

(a) standard deviation; (b) number of experimental replicates; (c) S=spring, LS=late-summer, F=fall; (d) anoxic sediment simulated by setting the upper boundary concentration of O_2 and NO_3^- to zero.

2.6. DISCUSSION

A fully transient simulation of the seasonal variations in sediment biogeochemistry proved unfeasible, primarily because the temporal evolution of the boundary conditions at the SWI could not be accurately constrained. This particularly holds for the input fluxes of reactive organic matter (OM1, OM2) and reactive Fe and Mn phases. In addition, with the notable exceptions of Mn^{2+} and SO_4^{2-}, the overall trends of the pore water profiles did not vary greatly among the sampling times (Fig. 2.8). Therefore, we opted for a modeling strategy aimed at reproducing the general features of the solid-phase and pore water distributions.

The solid curves in Figs. 2.5-2.8 represent the output of a steady-state solution of the model fitted to match the entire set of chemical data collected. As can be seen, the model is able to simultaneously reproduce the majority of observed trends in the concentration profiles. It is important to note that in the model calculations, the transport rates are obtained independently from the fitted data set in Figs. 2.5-2.8 (section 2.4.2). Taken together, the model appears to

provide a reasonable, time-averaged representation of the important biogeochemical processes taking place in the sediment.

Discrepancies between model calculated and measured concentration profiles may arise from the fact that the system is not at steady state. Especially for the solid-phase constituents (Figs. 2.5-2.7), some of the variability in the concentrations reflects historical fluctuations in deposition fluxes. Discrepancies may also result from processes that are not included in the reaction network of the model. For example, the model systematically under-predicts pore water pH and alkalinity at depth in the sediment (Fig. 2.8). This can be explained by additional buffering by carbonate mineral dissolution, a process which is not included in the model version used here (Jourabchi et al., 2005).

In contrast to the other pore water species, large differences in the depth profiles of dissolved Mn^{2+} and SO_4^{2-} are observed between the individual sampling times (Fig. 2.8). The elevated pore water Mn^{2+} values in spring could be the result of a temporarily increased input of reactive Mn oxides at the SWI. The model simulation likely under-predicts the rate of manganese reduction for the spring sampling time. The highly variable shape of the SO_4^{2-} profiles also makes it difficult to define an average pore water profile that can be compared to the model calculated depth distribution. Possible reasons for the observed SO_4^{2-} profile shapes are explored in section 2.6.4.

High rates of organic matter degradation in the upper millimeters of sediment are needed to reproduce the observed O_2 and NO_3^- profiles (Fig. 2.8). This is achieved by including a highly reactive fraction (OM1) in the deposited organic matter, but also by explicitly accounting for the enhanced efficiency of O_2 and NO_3^- as TEAs of organic carbon oxidation. Together aerobic respiration and denitrification are responsible for about 90% of OM1 degradation (Table 2.6). In contrast, the most important decomposition pathways for the less reactive organic matter pool, OM2, are sulfate reduction, methanogenesis and, to a lesser extent, denitrification. The OM1 pool is nearly completely degraded (99%) in the upper 2 cm of the sediment, while only 39% of OM2 is degraded within the upper 30 cm. Dissimilatory Fe and Mn-oxide reduction do not contribute significantly to total C_{org} mineralization. Limited methane gas formation is predicted to occur in the upper 30 cm of sediment (Table 2.6).

The total depth-integrated carbon mineralization rate (764 μmol cm^{-2} yr^{-1}) is at the high end of the range derived by den Heyer and Kalff (1998) from DIC and CH_4 accumulation rates in sediment core incubations of nine lakes in Québec (maximum value for profundal cores: 876 μmol cm^{-2} yr^{-1}). The relatively high rates at our site reflect the large input of degradable organic matter from the water column, but also the high concentrations of oxygen and nitrate in the bottom waters. Both the modeling results and the direct rate measurements imply

order-of-magnitude higher rates of organic carbon degradation by aerobic respiration and denitrification than by the other pathways, in particular sulfate reduction (Table 2.5). The large contributions of aerobic respiration (55%) and denitrification (21%) to total organic carbon oxidation limit the transfer of potentially degradable organic matter to the deeper sediment. Combined with the relatively high concentration of sulfate in the overlying water, this explains why methanogenesis is not a major pathway of organic matter breakdown at the site studied.

Table 2.6 Depth integrated rates of carbon mineralization and secondary redox reactions in the upper 30 cm of sediment. Primary reaction rates are given in units of carbon equivalents, secondary reaction rates refer to the reaction formulas in Table 2.2. For secondary oxygenation reactions, rates are also expressed as O_2 consumption rates.

Primary redox reactions		OM1	OM2	
Reaction	TEA	μmol cm^{-2} yr^{-1}		% total
R1, R7	O_2	422	1.2	55 %
R2, R8	NO_3	149	15	21 %
R3, R9	Mn(IV)	1.4	0.2	0.2 %
R4, R10	Fe(III)	5.1	1.3	0.8 %
R5. R11	SO_4	57	74	17 %
R6, R12	OM[a]	0.0	34	4.4 %
R13	OM[a]	-	4.3	0.6 %
total		634	130	
Secondary redox reactions				
Reaction	code	μmol cm^{-2} yr^{-1}	μmol O_2 cm^{-2} yr^{-1}	
R14	nh4ox	19	39	
R15	tsox	1.5	3.1	
R16	fesox	26	51	
R17	mnox	0.1	0.05	
R18	feox	9.3	2.3	
R19	ch4ox	12	12	
R20	femnox	1.1		
R21	ch4so4ox	0.1		
R22, R23	tsmnox	0.5		
R24, R25	tsfeox	2.5		

(a) methanogenesis

The inferred fraction of total organic carbon oxidation that is due to aerobic respiration (55%) is much larger than found in the model studies by Van Cappellen and Wang (1995)

and van den Berg et al. (2000) of freshwater sediments deposited under oxygenated waters. These authors report contributions in the range 3-12%. In these studies, however, only a single degradable organic carbon pool is included (the so-called 1-G model), hence limiting how accurately carbon mineralization with depth can be described. In particular, the 1-G model approach poorly reproduces the presence of a thin surface layer exhibiting much higher rates of carbon mineralization than the underlying sediment. Additionally, van den Berg et al. (2000) note that their modeled CH_4 concentrations exceed saturation values, which may have caused an over-estimation of methane oxidation by O_2. Using the STEADYQL model Furrer and Wehrli (1996) estimate that 65% of total organic carbon mineralization in sediment of eutrophic Lake Sempach (Switzerland) occurs via aerobic respiration. While this estimate is similar to that obtained here, it should be noted that STEADYQL does not account for secondary oxygenation reactions, and thus overestimates the contribution of oxic respiration.

In Fig. 2.9, the model predicted depth distribution of the rate of sulfate reduction is compared to rates measured with FTRs and a depth distribution derived from an inverse model optimization (Meile et al., 2001). FTR rate measurements were made with sediment from two different depth intervals (2-4 cm and 8-10 cm) collected in late summer. FTRs yield potential rates, because SO_4^{2-} is the only external TEA supplied to the sediment via the inflow during the experiments (Pallud and Van Cappellen, 2006). Potential rates should therefore provide upper estimates of in situ rates. This can be seen for the 2-4 cm sediment interval, where the lowest potential rates approach the model predicted in situ rates. In the 8-10 cm depth interval, potential rates from FTR experiments are close to modeled rates, suggesting that at these depths sulfate reducing activity is mainly limited by the availability of electron donors. This is consistent with the inferred near-complete degradation of the most reactive organic matter (OM1) in the topmost centimeters. Inverse modeling yields the rate of net SO_4^{2-} removal after accounting for diffusion and irrigation. The near-zero values for the net sulfate removal rate in the upper 2 cm reflect the production of sulfate by sulfide oxidation (section 2.6.3) in the top sediment. At greater depths, where sulfide oxidation becomes negligible, the inverse model and the reactive transport model predict similar rates.

The results in Fig. 2.9 suggest that the model-derived sulfate reduction rates are within the correct order of magnitude and approximately reproduce the vertical distribution. Nonetheless, the seasonal variations in the concentration profiles of SO_4^{2-}, but also of other reactive pore water solutes, such as O_2, NH_4^+ and DIC, serve as a reminder that rates of organic matter degradation in the sediment are time-dependent. The observed variations in the concentrations of AVS in the zone of most active sulfate reduction (Fig. 2.7a) further provide evidence that sulfate reduction rates are changing throughout the year (Leonard et al., 1993).

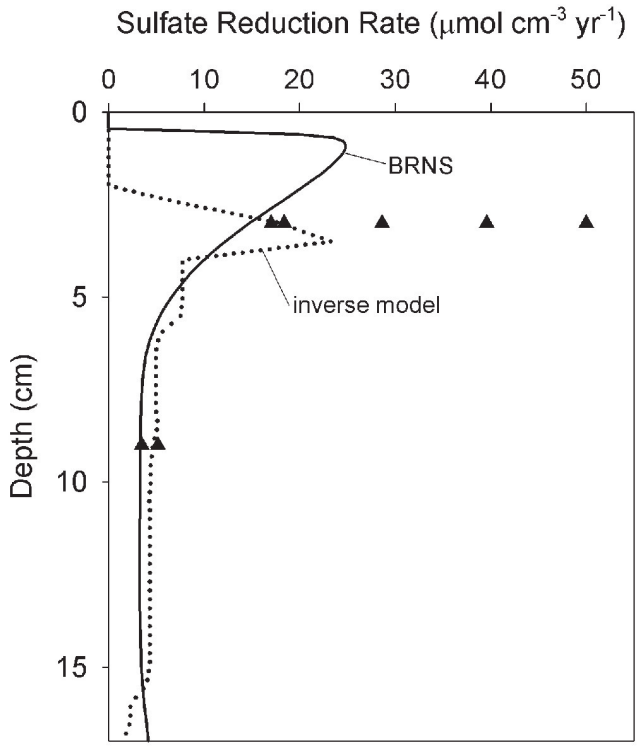

Figure 2.9 Sulfate reduction rates in late-summer. The solid line is the rate distribution obtained with the multi-component reaction-transport model (R5 + R11) and the dotted line corresponds to the rate distribution obtained by inverse modeling of the sulfate concentration distribution (Meile et al., 2003). Potential sulfate reduction rates measured in FTR experiments for depth intervals 2-4 and 8-9 cm are marked with (▲) symbols.

2.6.2 Secondary Reactions

According to the model calculations, secondary oxygenation reactions account for on the order of 20 % of total sediment oxygen consumption, mainly through the oxidation of FeS, NH_4^+, and CH_4(aq) (Table 2.6). The oxidation of NH_4^+ and FeS regenerate NO_3^- and SO_4^{2-}, which in turn help sustain denitrification and sulfate reduction. Abiotic Fe(III) reduction by sulfide (19 μmol Fe cm^{-2} yr^{-1}) and dissimilatory Fe(III) reduction (25 μmol Fe cm^{-2} yr^{-1}) are of comparable magnitude. The oxidation of Fe^{2+} by O_2 (9 μmol Fe cm^{-2} yr^{-1}) exceeds that by MnO_2 (2 μmol Fe cm^{-2} yr^{-1}). Reduction of MnO_2 by Fe^{2+} is responsible for 18% of total manganese reduction. Apart from reaction with Fe^{2+}, the cycling of Mn does not play an important role in the major elemental cycles at the site (Table 2.6).

Methane oxidation is predicted to occur primarily via reaction with O_2 (12 μmol cm^{-2} yr^{-1}), with a negligible contribution of anaerobic methane oxidation (0.1 μmol cm^{-2} yr^{-1}). Because, in the model, CH_4(g) generated in the sediment is assumed to be non-reactive, the calculated rate of methane oxidation represents a conservative estimate. The potential error introduced by neglecting the possible redissolution of gaseous methane in the surface sediment, followed by oxidation, is assessed by running a simulation where all methanogenesis yields CH_4 (aq) production. This nearly doubles the methane oxidation rate, from 12 to 22 μmol cm^{-2} yr^{-1}. The increased methane oxidation rate still has little impact on total oxygen consumption, as the O_2 consumption due to methane oxidation rises from 2 to 4 %.

Iron and sulfur cycling are linked in the reaction network through the formation of FeS and FeS_2, reaction of sulfide with Fe-oxides, and the oxidation of FeS (Fig. 2.10). Most of the Fe^{2+} and S(-II) produced in the sediment forms FeS. Although sulfate reduction is quantitatively a far more important electron sink than iron reduction, the amounts of S (-II) and Fe^{2+} produced are relatively similar due to the 8-fold difference in reaction stoichiometry (Fig. 2.10, Table 2.2). Because of efficient sulfur recycling, the depth-integrated sulfate reduction rate equals nearly twice the SO_4^{2-} influx at the SWI.

Only about 10% of the FeS produced in the sediment is converted into pyrite. According to the model calculations, FeS represents the main burial sink for reactive iron and sulfur (Fig. 2.10). The simulation, however, tends to overestimate the AVS concentrations (Fig. 2.7a), implying that the FeS sink could be somewhat lower than indicated on Fig. 10. Nonetheless, authigenically-formed iron sulfides may account for most solid-phase sulfur in the deeper sediment (Fig. 2.7b). Excess sulfur in the surface sediment may represent particulate sulfur pools not included in the model, such as organically-bound S and elemental S.

Both the chemical extraction data and the model calculations indicate that substantial amounts of reactive Fe(III) are buried below 30 cm (Figs. 2.6 and 2.10). As reported in a number of studies, a fraction of the chemically reducible Fe(III) mineral phases is unavailable for microbial respiration (e.g., Wersin et al., 1991; Berg et al., 2003; Hyacinthe and Van Cappellen, 2004). One important biogeochemical consequence of future seawater intrusion in Haringvliet Lake could be the enhanced reductive dissolution of this Fe(III) pool by sulfide generated by sulfate reduction (section 2.6.5).

Diffusion and non-local transport (bioirrigation) are both important modes of solute transport in the upper 15 cm of sediment. Bioirrigation increases the fluxes of O_2, NO_3^-, and SO_4^{2-} into the sediment (Table 2.7), causing more C_{org} mineralization to be coupled to the soluble TEAs. Overall, increased influx of O_2 and enhanced removal of reduced solutes by bioirrigation (Table 2.7) decreases the fraction of total O_2 consumption due to secondary redox

reactions. In a simulation where all bioirrigation coefficients are set to zero, the contribution of secondary redox reactions to total O_2 consumption increases from 19% to 24%. In the same simulation, methanogenesis increases from 5% to 15% of total C_{org} decomposition.

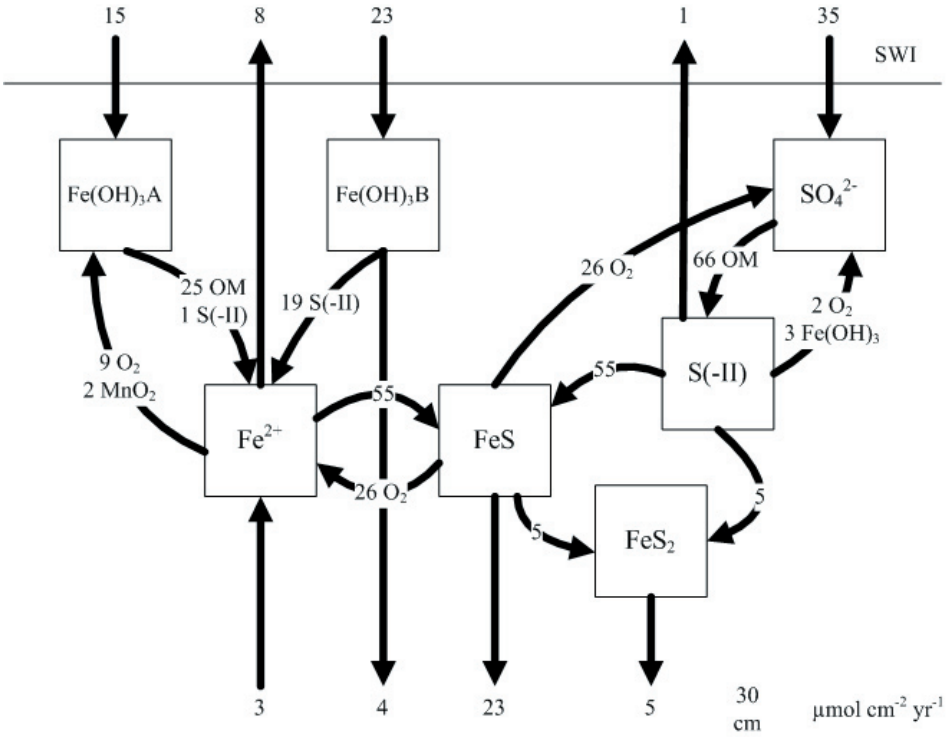

Figure 2.10 The Fe-S cycle as simulated by the multi-component model. All rate and flux values are presented in units of µmol cm^{-2} yr^{-1}, and rounded to the nearest whole number. Rate values are integrated over the upper 30 cm of sediment. Transport fluxes are indicated at the beginning or ends of the arrows. Values on the arrows are reaction rates; for redox reactions the oxidant or reductant is identified to the right of the rate values. Note that rate values are presented for the reaction stoichiometries listed in Table 2. $Fe(OH)_3A$ is the bioavailable Fe-oxide pool, the $Fe(OH)_3B$ pool is only reduced chemically by sulfide.

Recent work has cautioned against the use of a single depth distribution of the irrigation coefficient for all pore water solutes (Aller, 2001; Berg et al., 2003; Grigg et al., 2005; Meile et al., 2005). Following the suggestions of Berg et al. (2003) and Meile et al. (2005), we therefore reduced the α values for Fe^{2+} and Mn^{2+}, relative to those of the conservative ions Na^+ and Cl^- (section 2.4.2). Note that although the model assumes that aqueous Fe^{2+} is not subject to transport by irrigation (α=0), the Fe^{2+} profile is affected by the enhanced pore water mixing

(Fig. 2.8). The lack of significant build-up of pore water Fe^{2+} in the upper 15 cm is due in part to the enhanced downward transport of oxygenated bottom water, fueling oxidation of Fe^{2+} in the irrigated zone.

To some degree, the irrigation coefficients of all reactive solute species should deviate from those of conservative tracers (Meile et al., 2005). This could be particularly important for SO_4^{2-}, whose supply from the water column is strongly affected by irrigation (Table 2.7). According to Meile et al. (2005), SO_4^{2-} exhibits lower than average irrigation coefficients. This could help explain the mismatch between measured and computed SO_4^{2-} profiles. The sensitivity of the SO_4^{2-} pore water distribution to the irrigation intensity is illustrated in Fig. 2.11a. As can be seen, reducing the irrigation coefficient of SO_4^{2-} yields pore water profiles that more closely resemble those observed during spring and late summer. The fall data, however, suggests a possible enhancement of the irrigation intensity. Uncertainties in the transport properties of the pore water solutes directly affect the estimated reaction rates. For instance, reductions of α_0 for SO_4^{2-} by 50 and 100% cause the calculated integrated rate of sulfate reduction to decrease by 6.1 and 32%, respectively.

Table 2.7 Rates of solute exchange by difusion and bioirrigation at the SWI. Negative values denote fluxes into the sediment.

Solute	Diffusion	Bioirrigation	Contribution of Bioirrigation
	(μmol cm^{-2} yr^{-1})		(%)
O_2	-500	-31	6 %
NO_3^-	-92	-20	18 %
Mn^{2+}	4	2	36 %
SO_4^{2-}	-5	-30	86 %
CH_4(aq)	0	19	100 %
NH_4^+	91	27	23 %
HCO_3^-	104	165	62 %

Changes in the particle mixing regime also affect the rates of primary and secondary redox reactions. Some of the effects are examined by changing the value of D_b0 in the equation for the biodiffusion coefficient distribution listed in Table 2.4. The reactive iron and sulfur species are particularly sensitive to the degree of sediment mixing (Figs. 2.11b and c). Increasing D_b0 increases sulfate removal from the pore waters (Fig. 2.11b), as the highly reactive organic matter (OM1) is transported deeper into the sediment where it is utilized by sulfate reduction. Lowering D_b0 has the opposite effects on the SO_4^{2-} concentrations and sulfate reduction rates. In the low mixing simulation (D_b0 = 1 cm^2 yr^{-1}), a significant build-up of reactive

Fe(III) precipitates is observed in the upper 5 cm of the sediment, causing the appearance of a subsurface concentration maximum (Fig. 2.11c). Such an accumulation of Fe(III) oxides at the oxic-suboxic interface has been observed in lake sediments, and may increase the importance of dissimilatory iron reduction (Thomsen et al., 2004).

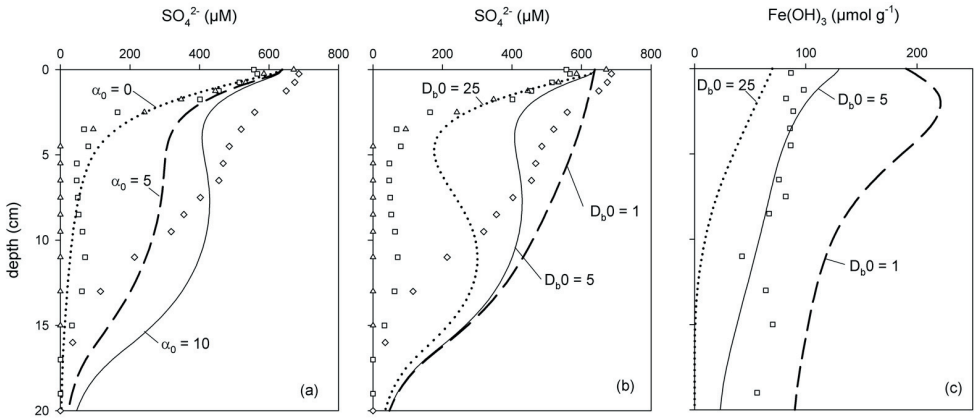

Figure 2.11 Model sensitivity to bioirrigation is shown with the concentration distribution of SO_4^{2-} (a) where the solid line is the baseline simulation (α_0 = 10 yr^{-1}), the dashed line is with α_0 = 5 yr^{-1}, and the dotted line is with α_0 = 0 yr^{-1}. Model sensitivity to the particle mixing intensity (D_b0) is shown using the concentration distributions of SO_4^{2-} (b) and $\Sigma Fe(OH)_3$ (c). The dotted lines correspond to simulations with D_b0 = 25 $cm^2\ yr^{-1}$, the solid lines with D_b0 = 5 $cm^2\ yr^{-1}$ and the dashed lines with D_b0 = 1 $cm^2\ yr^{-1}$. Field data are presented with the following symbols: fall (◇), late-summer (□), and spring (△).

2.6.5 Estuarine Restoration

The model is used to examine potential changes in benthic biogeochemistry that could result from the restoration of estuarine conditions at our study site. In particular, we examine how the primary and secondary redox reaction dynamics would respond to changes in bottom water chemistry, deposition of organic matter and the bioturbation regime. The sensitivity to these changes is initially assessed using steady state solutions of the model (Table 2.8). Then, a transient simulation is performed to illustrate the time scales over which sediment biogeochemistry is expected to respond to a switch from lacustrine to estuarine conditions (Fig. 2.12).

Some of the environmental forcings that will change upon the (regulated) intrusion of seawater in the Haringvliet are predictable, while others are more speculative. For instance, water column salinization will undoubtedly increase the SO_4^{2-} concentration at the SWI.

However, while increased salinity stratification is expected to result in lower bottom water O_2 concentrations, it is not known to what extent O_2 may be depleted. The same is true for the OM deposition fluxes, which are likely to decrease, as increased exchange of water with the adjacent coastal zone will enhance the export of nutrients and particulate matter from the Haringvliet.

Table 2.8 Responses of sediment biogeochemistry to possible changes in site conditions resulting from estuarine restoration. The depth-integrated rates are derived from steady-state model simulations.

Scenario[a]	Oxic respiration	Sulfate Reduction	FeS Oxidation	Fe-oxide reduction by sulfide
	(μmol cm^{-2} yr^{-1})			
existing conditions	423	131	26	2.5
$+SO_4^{2-}$	421	170	32	3.0
$+SO_4^{2-}$, $-O_2$	327	209	26	3.3
$+SO_4^{2-}$, -OM	271	24	1.3	0.2
$+SO_4^{2-}$, $+D_b0$	348	239	43	3.8
$+SO_4^{2-}$, $+\lambda$	414	177	35	3.0
$+SO_4^{2-}$, $-O_2$, -OM, $+D_b0$, $+\lambda$	155	90	25	0.9

(a) + SO_4^{2-}: SWI concentration increased to 10 mM, $-O_2$: SWI concentration decreased to 120 μM, -OM: input flux of OM1 and OM2 reduced by 50%, $+D_b0$: value at SWI increased to 25 cm^2 yr^{-1} (increased mixing intensity), $+\lambda$: value increased to 5 cm (increased mixing depth).

Increasing the sulfate concentration at the SWI to 10 mM from the current 0.6 mM, effectively suppresses methanogenesis in the upper 30 cm of sediment. The increase in sulfate reduction rate with higher SO_4^{2-} availability is further enhanced by lowering the O_2 concentration in the overlying water (Table 2.8). Nevertheless, the relative increases in the rate of sulfate reduction are relatively small, given the large imposed changes in bottom water chemistry. This reflects the overall limitation of sediment respiration by the supply of degradable organic matter. Hence, a reduction of the OM influx by 50% causes a drop in the sulfate reduction rate by nearly an order of magnitude, even when the SO_4^{2-} concentration in the bottom water is maintained at 10 mM (Table 2.8). Under these conditions, the relative contributions of aerobic respiration and denitrification to total C_{org} degradation increase at the expense of that of sulfate reduction. The lower input of OM also results in a reduced redox cycling of Fe and S in the sediment (Wijsman et al., 2002), as illustrated by the much lower rates of FeS oxidation and Fe(III) oxide reduction by sulfide (Table 2.8).

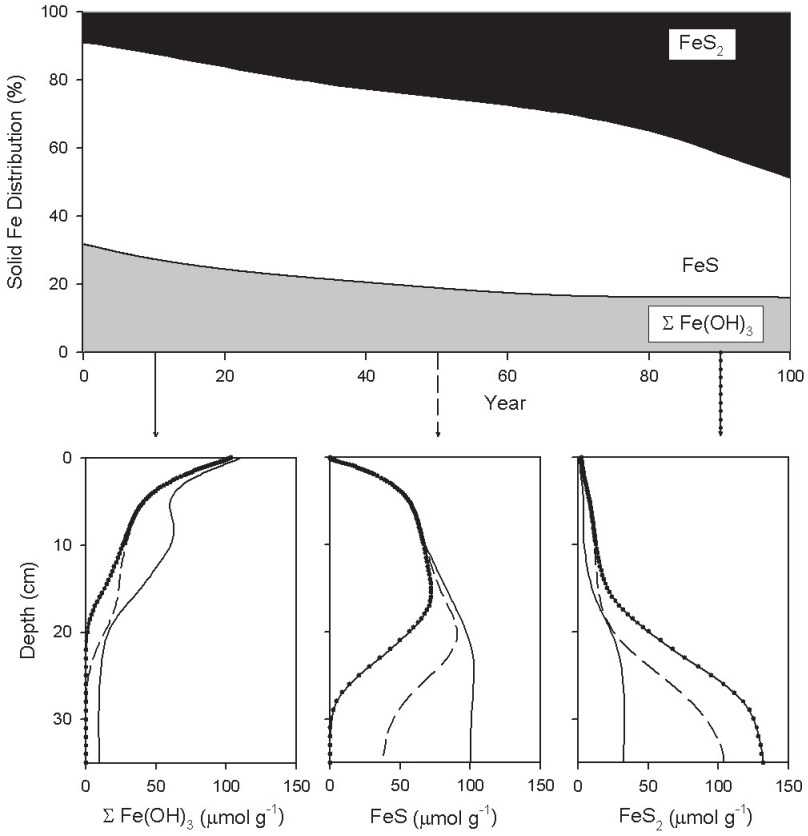

Figure 2.12 Transient simulation of solid-phase iron speciation in the sediment following an increase in the bottom water SO_4^{2-} concentration from 0.6 to 10 mM. The upper plot displays the concentrations of the $\Sigma Fe(OH)_3$, FeS, and FeS_2 pools, integrated over the upper 30 cm of sediment.. The lower plots show the depth profiles of the three solid Fe pools for simulation times of 10 years (solid line), 50 years (dashed line), and 90 years (dotted line).

The current benthic fauna in the Haringvliet can be characterized as poor (Smit et al., 1997). Restoration of estuarine conditions is expected to increase the density and diversity of the macroinvertebrate community in the downstream portion of the Haringvliet. Most likely this will intensify and deepen bioturbation of the sediment. In the model simulations, bioturbation was modified by either increasing the value of D_b0, which controls the intensity of mixing, or by extending the depth of mixing by increasing the depth attenuation parameter, λ. Enhanced mixing promotes sulfate reduction over aerobic degradation (Table 2.8), as reactive

OM is mixed below the oxygen penetration depth (see also section 2.6.4). The rates of FeS oxidation and Fe-oxide reduction by sulfide also increase with greater mixing, as the latter intensifies the exchanges between the oxidized and reduced portions of the sediment. Overall, increasing D_b0 has a greater impact on sediment biogeochemistry than increasing the mixing depth.

The simulation results in Table 2.8 illustrate the broad range of responses that can be expected upon estuarine restoration. To use the model for environmental forecasting thus depends critically on accurately constraining future changes in benthic forcing functions. An important aspect of the model is its ability to simulate the coupled effects of multiple environmental changes. This is illustrated by the last scenario in Table 2.8, which combines the various postulated changes in bottom water chemistry, OM deposition and bioturbation regime. This scenario results in lower mineralization rates, due to the decrease in OM input (Table 2.8). However, the integrated rates of sulfate reduction, FeS oxidation, and sulfide oxidation of Fe-oxides are greater in the combined scenario than expected when only the OM input is reduced, because of the counteracting effect of enhanced mixing.

The results summarized in Table 2.8 provide no information on the time required for the benthic system to adjust to changing environmental conditions. The temporal response of sediment processes to salinization is addressed with a transient simulation using the steady-state model solution for the present conditions as initial condition. As a perturbation, we impose an instantaneous increase of the SO_4^{2-} concentration at the SWI from 0.6 to 10 mM, while all other conditions are kept the same. This perturbation is selected, because estuarine restoration will definitely lead to a significant increase of the SO_4^{2-} levels in the bottom water at the site.

The transient calculations indicate that increased SO_4^{2-} availability at the SWI allows sulfate reduction to immediately suppress methanogenesis in the upper 30 cm of sediment (results not shown). The integrated rates of organic matter degradation by O_2, NO_3^- and SO_4^{2-} adjust to their new steady state values within the first few years. The enhanced production of sulfide by sulfate reduction also leads to further transformation of reactive Fe(III) oxides to iron sulfides. However, the changes in solid-phase Fe speciation require time scales of several decades and more (Fig. 2.12). During the first 50 years of the simulation the reactive Fe-oxide concentrations in the sediment decline, while those of pyrite increase. After the reactive Fe(III) oxide content reaches its new steady state, conversion of FeS to pyrite continues, gradually increasing the amount of pyrite accumulating in the sediment. As shown by Fig. 2.12, the conversion of FeS to FeS_2 is still ongoing 100 years after the imposed increase in SO_4^{2-} concentration at the SWI. Thus, the simulation results imply that the changes in sediment biogeochemistry caused by the planned restoration of estuarine conditions may occur over a wide range of temporal scales. In

particular, the predicted changes in solid-state Fe speciation may have long-term consequences for the biogeochemical cycling of phosphorus (Caraco et al., 1990, Gunnars and Blomqvist, 1997) and trace metals (Huerta-Diaz et al., 1998) in the Haringvliet.

2.7 CONCLUSIONS

Interpretation of chemical sediment and pore water data with a reaction transport model allows us to quantify the rates of primary and secondary redox reactions in sediment of the coastal Haringvliet Lake. The model simultaneously reproduces the depth-dependent trends of multiple constituents, providing strong evidence that it captures the essence of the important reaction and transport processes taking place at the site.

Oxic degradation and denitrification occur at high rates in a shallow zone near the sediment-water interface, and oxidize most (76%) of the degradable organic carbon input. Below this zone, sulfate reduction and methanogenesis are the dominant primary reaction pathways, but proceed at much slower rates due to lower reactivity of C_{org} and less efficient degradation under anoxic conditions. Secondary redox reactions account for only 20% of the total O_2 consumption, which contrasts with many other eutrophic lakes where methanogenesis is the dominant degradation pathway. Dissimilatory Mn(IV) and Fe(III) reduction are not important pathways of C_{org} decomposition, despite the presence of chemically reducible Mn and Fe mineral phases.

Bioirrigation and bioturbation have a major impact on primary and secondary reaction rates and chemical distributions, emphasizing the link between biogeochemical cycling and the activity of benthic fauna. Better representations and parameterizations of biologically-mediated transport processes in reactive transport models remain crucial for improving our quantitative understanding of sediment biogeochemical processes.

Model simulations illustrate the wide range of potential consequences of estuarine restoration for sediment biogeochemistry. The results imply that, as a result of increased concentrations of sulfate in the bottom water, sulfate reduction will rapidly suppress methanogenesis at the site studied. Other changes in benthic biogeochemical dynamics, however, will depend on how the production and deposition of degradable organic matter respond to the restoration of estuarine conditions. In addition, the establishment of a new benthic infaunal community adapted to the increased salinity will most likely modify the transport regime and, hence, the biogeochemical cycling in the sediments.

Acknowledgements We gratefully acknowledge the crew of R.V. Navicula and members of the Utrecht University geochemistry research group for their help in the field and laboratory. We thank Y. van Lith, D. Los, and C. Pallud for sharing their rate measurement data, and A. Dale and C. Meile for assistance with the modeling. The manuscript benefited from discussions with P. Regnier and G. Zwolsman, and the comments of three anonymous reviewers. The Netherlands Institute for Inland Water Management and Waste Water Treatment (RIZA) financially supported the fieldwork and RWC. The Netherlands Organization for Scientific Research (NWO) provided support through the Pioneer (PVC) and VENI (AML) programs. CPS was supported by a fellowship of the Royal Netherlands Academy of Arts and Sciences (KNAW).

REFERENCES

Aguilera D. R., Jourabchi P., Spiteri C., and Regnier P. (2005) A knowledge-based reactive transport approach for the simulation of biogeochemical dynamics in earth systems. *Geochem. Geophy. Geosys.* 6, Q07012.

Aller, R. C. (2001) Transport and reactions in the bioirrigated zone, In *The Benthic Boundary Layer* (eds. B. P. Boudreau and B. B. Jørgensen). Oxford University Press, Oxford. pp. 269-301.

Amberg G., Tonhard R., and Winkler C. (1999) Finite element simulations using symbolic computing. *Math. Comput. Simul.* 49, 257-274.

Anonymous (1998) *MER beheer Haringvlietsluizen report (Environmental Impact Report- Haringvliet dam management).* Rijkswaterstaat directie Zuid-Holland, APV 98.186. (in Dutch).

APHA (1985) Standard methods for the examination of water and wastewater. American Public Health Association, Washington D.C.

Bastviken D., Olsson M., and Tranvik L. (2003) Simultaneous measurements of organic carbon mineralization and bacterial production in oxic and anoxic lake sediments. *Microb. Ecol.* 46, 73-82.

Bastviken D., Persson L., Odham G., and Tranvik L. (2004) Degradation of dissolved organic matter in oxic and anoxic lake water. *Limnol. Oceanogr.* 49, 109-116.

Berg P., Rysgaard S., and Thamdrup B. (2003) Dynamic modeling of early diagenesis and nutrient cycling. A case study in an Arctic marine sediment. *Amer. J. Sci.* 303, 905-955.

Berner R. A. (1980) *Early diagenesis. A theoretical approach*. Princeton University Press, Princeton NJ.

Boudreau B. P. (1996) The diffusive tortuosity of fine-grained unlithified sediments. *Geochim. Cosmochim. Acta* 60, 3139-3142.

Boon, A.R., Duineveld, G.C.A. (1998) Chlorophyll *a* as a marker for bioturbation and carbon flux in southern and central North Sea sediments. *Mar. Ecol. Prog. Ser.* 162, 33-43.

Cai W. J. and Wang Y. (1998) The chemistry, fluxes and sources of carbon dioxide in the estuarine waters of the Satila and Altamaha Rivers, Georgia. *Limnol. Oceanogr.* 43, 657-668.

Canfield D. E., Thamdrup B., and Hansen J. W. (1993) The anaerobic degradation of organic-matter in Danish coastal sediments - iron reduction, manganese reduction, and sulfate reduction. *Geochim. Cosmochim. Acta* 57, 3867-3883.

Capone D. G. and Kiene R. P. (1988) Comparison of microbial dynamics in marine and fresh-water sediments - contrasts in anaerobic carbon catabolism. *Limnol. Oceanogr.* 33, 725-749.

Caraco N., Cole J., and Likens G. E. (1990) A Comparison of Phosphorus Immobilization in Sediments of Fresh-Water and Coastal Marine Systems. *Biogeochemistry* 9, 277-290.

Chilakapati A. (1995) *RAFT: A Simulator for Reactive Flow and Transport of Groundwater Contaminants*. Pacific Northwest Laboratory, Internal Report 10636.

Cline J. D. (1969) Spectrophotometric determination of hydrogen sulfide in natural waters. *Limnol. Oceanogr.* 14, 454-458.

Dauwe B., Middelburg J. J., and Herman P. M. J. (2001) Effect of oxygen on the degradability of organic matter in subtidal and intertidal sediments of the North Sea area. *Mar. Ecol. Prog. Ser.* 215, 13-22.

Davison W., Phillips N., and Tabner B. J. (1999) Soluble iron sulfide species in natural waters: Reappraisal of their stoichiometry and stability constants. *Aquat. Sci.* 61, 23-43.

de Jonge V. N. and de Jong D. J. (2002) Ecological restoration in coastal areas in the Netherlands: concepts, dilemmas and some examples. *Hydrobiologia* 478, 7-28.

den Heyer C. and Kalff J. (1998) Organic matter mineralization rates in sediments: A within- and among-lake study. *Limnol. Oceanogr.* 43, 695-705.

Elsgaard L. and Jørgensen B. B. (1992) Anoxic transformations of radiolabeled hydrogen-sulfide in marine and freshwater sediments. *Geochim. Cosmochim. Acta* 56, 2425-2435.

Ferguson H. A. and Wolff W. J. (1984) The Haringvliet-Project: The development of the Rhine-Meuse Estuary from tidal inlet to stagnant freshwater lake. *Water Sci. Technol.* 16, 11-26.

Fossing H., Berg P., Thamdrup B., Rysgaard S., Sorensen H. M., and Nielsen K. (2004) *A model set-up for an oxygen and nutrient flux model for Aarhus Bay (Denmark)*. National Environmental Research Institute, Denmark, NERI Technical Report No. 483.

Froelich P. N., Klinkhammer G. P., Bender M. L., Luedtke N. A., Heath G. R., Cullen D., Dauphin P., Hammond D., Hartman B., and Maynard V. (1979) Early oxidation of organic matter in pelagic sediments of the eastern equatorial Atlantic: Suboxic diagenesis. *Geochim. Cosmochim. Acta* 43, 1075-1090.

Furrer G. and Wehrli B. (1996) Microbial reactions, chemical speciation, and multicomponent diffusion in porewaters of a eutrophic lake. *Geochim. Cosmochim. Acta* 60, 2333-2346.

Gallon C., Tessier A., Gobeil C., and Alfaro-De La Torre M. C. (2004) Modeling diagenesis of lead in sediments of a Canadian Shield lake. *Geochim. Cosmochim. Acta* 68, 3531-3545.

Grigg N. J., Boudreau B. P., Webster I. T., and Ford P. W. (2005) The nonlocal model of porewater irrigation: Limits to its equivalence with a cylinder diffusion model. *J. Mar. Res.* 63, 437-455.

Gunnars A. and Blomqvist S. (1997) Phosphate exchange across the sediment-water interface when shifting from anoxic to oxic conditions - an experimental comparison of freshwater and brackish-marine systems. *Biogeochemistry* 37, 203-226.

Hamilton-Taylor J., Davison W., and Morfett K. (1996) The biogeochemical cycling of Zn, Cu, Fe, Mn, and dissolved organic C in a seasonally anoxic lake. *Limnol. Oceanogr.* 41, 408-418.

Hedges J. I. and Keil R. G. (1995) Sedimentary organic matter preservation: an assessment and speculative synthesis. *Mar. Chem.* 49, 81-115.

Holmer M. and Storkholm P. (2001) Sulphate reduction and sulphur cycling in lake sediments: a review. *Freshw. Biol.* 46, 431-451.

Huerta-Diaz M. A., Tessier A., and Carignan R. (1998) Geochemistry of trace metals associated with reduced sulfur in freshwater sediments. *Appl. Geochem.* 13, 213-233.

Hunter K. S., Wang Y. F., and Van Cappellen P. (1998) Kinetic modeling of microbially-driven redox chemistry of subsurface environments: coupling transport, microbial metabolism and geochemistry. *J. Hydrol.* 209, 53-80.

Hyacinthe C. and Van Cappellen P. (2004) An authigenic iron phosphate phase in estuarine sediments: composition, formation and chemical reactivity. *Mar. Chem.* 91, 227-251.

Jourabchi P., Van Cappellen P., and Regnier P. (2005) Quantitative interpretation of pH distributions in aquatic sediments: A reaction-transport modeling approach. *Amer. J. Sci.* 305, 919-956.

Koelmans A. A. (1998) Geochemistry of suspended and settling solids in two freshwater lakes. *Hydrobiologia* 364, 15-29.

Kostka J. E. and Luther G. W. (1994) Partitioning and speciation of solid-phase iron in salt-marsh sediments. *Geochim. Cosmochim. Acta* 58, 1701-1710.

Kristensen E. (2000) Organic matter diagenesis at the oxic/anoxic interface in coastal marine sediments, with emphasis on the role of burrowing animals. *Hydrobiologia* 426, 1-24.

Laverman A. M., Van Cappellen P., van Rotterdam-Los, D., Pallud, C. and Abell, J. (2006) Potential rates and pathways of microbial nitrate reduction in coastal sediments. *FEMS Microbiol Ecol* in press.

Leonard E. N., Mattson V. R., Benoit D. A., Hoke R. A., and Ankley G. T. (1993) Seasonal variation of acid volatile sulfide concentration in sediment cores from three Minnesota lakes. *Hydrobiologia* 371, 87-95.

Martens C. S., Albert D. B., and Alperin M. J. (1998) Biogeochemical processes controlling methane in gassy coastal sediments - Part 1. A model coupling organic matter flux to gas production, oxidation and transport. *Cont. Shelf Res.* 18, 1741-1770.

Meile C., Berg P., Van Cappellen P., and Tuncay K. (2005) Solute-specific pore water irrigation: Implications for chemical cycling in early diagenesis. *J. Mar. Res.* 63, 601-621.

Meile C., Koretsky C. M., and Van Cappellen P. (2001) Quantifying bioirrigation in aquatic sediments: An inverse modeling approach. *Limnol. Oceanogr.* 46, 164-177.

Meile C., and Van Cappellen P. (2005) Particle age distributions and O_2 exposure times: Timescales in bioturbated sediments. *Global Biogeochem. Cycles* 19, GB3013.

Naylor C., Davison W., Motelica-Heino M., Van Den Berg G. A., and Van Der Heijdt L. M. (2004) Simultaneous release of sulfide with Fe, Mn, Ni and Zn in marine harbour sediment measured using a combined metal/sulfide DGT probe. *Sci. Total Environ.* 328, 275-286.

Pallud C. and Van Cappellen P. (2006) Kinetics of microbial sulfate reduction in estuarine sediments. *Geochim. Cosmochim. Acta* 70, 1148-1162.

Peretyazhko T., Van Cappellen P., Meile C., Coquery M., Musso M., Regnier P., and Charlet L. (2005) Biogeochemistry of major redox elements and mercury in a tropical reservoir lake (Petit Saut, French Guiana). *Aquat. Geochem.* 11, 33-55.

Pilson M. E. Q. (1998) *An introduction to the chemistry of the sea*. Prentice Hall, Upper Saddle River, New Jersey.

Poulton S. W., Krom M. D., and Raiswell R. (2004) A revised scheme for the reactivity of iron (oxyhydr)oxide minerals towards dissolved sulfide. *Geochim. Cosmochim. Acta* 68, 3703-3715.

Regnier P., Jourabchi P., and Slomp C. P. (2003) Reactive-transport modeling as a technique for understanding coupled biogeochemical processes in surface and subsurface environments. *Geol. Mijnbouw* 82, 5-18.

Regnier P., O'Kane J. P., Steefel C. I., and Vanderborght P. (2002) Modeling complex multi-component reactive-transport systems: towards a simulation environment based on the concept of a Knowledge Base. *Appl. Math. Model.* 26, 913-927.

Reinhold-Dudok van Heel H. C. and den Besten P. J. (1999) The relation between macroinvertebrate assemblages in the Rhine-Meuse delta (The Netherlands) and sediment quality. *Aquat. Ecosyst. Health Manag.* 2, 19-38.

Revsbech N. P. (1989) Diffusion characteristics of microbial communities determined by use of oxygen microsensors. *J. Microbiol. Methods* 9, 111-122.

Rickard D. (1997) Kinetics of pyrite formation by the H2S oxidation of iron (II) monosulfide in aqueous solutions between 25 and 125 degrees C: The rate equation. *Geochim. Cosmochim. Acta* 61, 115-134.

Roychoudhury A. N., Van Cappellen P., Kostka J. E., and Viollier E. (2003) Kinetics of microbially mediated reactions: dissimilatory sulfate reduction in saltmarsh sediments (Sapelo Island, Georgia, USA). *Estuar. Coast. Shelf Sci.* 56, 1001-1010.

Sarazin G., Michard G., and Prevot F. (1999) A rapid and accurate spectroscopic method for alkalinity measurements in sea water samples. *Water Res.* 33, 290-294.

Smit H., Reinhold-Dudok van Heel H. C., and Wiersma S. M. (1995) Sublittoral macrozoobenthic assemblages in the enclosed sediment-polluted Rhine-Meuse Delta; their relationship to environmental conditions. *Neth. J. Aquat. Ecol.* 29, 31-47.

Smit H., Smits R., van der Velde G., and Coops H. (1997) Ecosystem responses in the Rhine-Meuse delta during two decades after enclosure and steps toward estuary restoration. *Estuaries* 20, 504-520.

Stephens M. P., Kadko D. C., Smith C. R., and Latasa M. (1997) Chlorophyll-a and pheopigments as tracers of labile organic carbon at the central equatorial Pacific seafloor. *Geochim. Cosmochim. Acta* 61, 4605-4619.

Sun M., Aller R. C., and Lee C. (1991) Early diagenesis of chlorophyll-a in Long Island Sound sediments: A measure of carbon flux and particle reworking. *J. Mar. Res.* 49, 379-401.

Sun M., Aller R. C., and Lee C. (1994) Spatial and temporal distributions of sedimentary chloropigments as indicators of benthic processes in Long Island Sound. *J. Mar. Res.* 52, 149-176.

Sweerts J.-P. R. A., Bar-Gilissen M.-J., Cornelese A. A., and Cappenberg T. E. (1991) Oxygen-consuming processes at the profundal and littoral sediment-water interface of a small meso-eutrophic lake (Lake Vechten, The Netherlands). *Limnol. Oceanogr.* 36, 1124-1133.

Teasdale P. R., Hayward S., and Davison W. (1999) In situ, high-resolution measurement of dissolved sulfide using diffusive gradients in thin films with computer-imaging densitometry. *Anal. Chem.* 71, 2186-2191.

Thomsen U., Thamdrup B., Stahl D. A., and Canfield D. E. (2004) Pathways of organic carbon oxidation in a deep lacustrine sediment, Lake Michigan. *Limnol. Oceanogr.* 49(6), 2046-2057.

Tromp, T.K., Van Cappellen, P., and Key, R.M. (1995) A global model for the early diagenesis of organic carbon and organic phosphorus in marine sediments. *Geochim. Cosomchim. Acta.* 59 1259-1284.

Urban N. R., Brezonik P. L., Baker L. A., and Sherman L. A. (1994) Sulfate reduction and diffusion in sediments of Little Rock Lake, Wisconsin. *Limnol. Oceanogr.* 39(4), 797-815.

Van Cappellen P. and Wang Y. (1995) Metal Cycling in surface sediments: Modeling the interplay of transport and reaction. In *Metal Contaminated Sediments* (ed. H. E. Allen), Ann Arbor Press, Chelsea, MI. pp. 21-64.

Van Cappellen P. and Wang Y. F. (1996) Cycling of iron and manganese in surface sediments: A general theory for the coupled transport and reaction of carbon, oxygen, nitrogen, sulfur, iron, and manganese. *Amer. J. Sci.* 296, 197-243.

van den Berg G. A., Buykx S. E. J., van den Hoop M., and van der Heijdt L. M. (2001) Vertical profiles of trace metals and acid-volatile sulphide in a dynamic sedimentary environment: Lake Ketel, The Netherlands. *Appl. Geochem.* 16, 781-791.

van den Berg G. A., Loch J. P. G., van der Heijdt L. M., and Zwolsman J. J. G. (1998) Vertical distribution of acid-volatile sulfide and simultaneously extracted metals in a recent sedimentation area of the river meuse in The Netherlands. *Environ. Toxicol. Chem.* 17, 758-763.

van den Berg G. A., Loch J. P. G., van der Heijdt L. M., and Zwolsman J. J. G. (1999) Mobilisation of heavy metals in contaminated sediments in the river Meuse, The Netherlands. *Water Air Soil Pollut.* 116, 567-586.

van den Berg G. A., Loch J. P. G., van der Heijdt L. M., and Zwolsman J. J. G. (2000) Redox processes in recent sediments of the river Meuse, The Netherlands. *Biogeochemistry* 48, 217-235.

van Wijngaarden M., Venema L. B., De Meijer R. J., Zwolsman J. J. G., Van Os B., and Gieske J. M. J. (2002) Radiometric sand-mud characterisation in the Rhine-Meuse estuary part A. Fingerprinting. *Geomorphology* 43, 87-101.

Wang X. S. and Matisoff G. (1997) Solute transport in sediments by a large freshwater oligochaete, Branchiura sowerbyi. *Environ. Sci. Technol.* 31, 1926-1933.

Wersin P., Hohener P., Giovanoli R., and Stumm W. (1991) Early Diagenetic Influences on Iron Transformations in a Fresh-Water Lake Sediment. *Chem. Geol.* 90, 233-252.

Westrich J. T. and Berner R. A. (1984) The role of sedimentary organic matter in bacterial sulfate reduction: the G-model tested. *Limnol. Oceanogr.* 29, 236-249.

Wetzel R. G. (2001) *Limnology: lake and river ecosystems.* Academic Press, San Diego.

Wijsman J. W. M., Herman P. M. J., Middelburg J. J., and Soetaert K. (2002) A model for early diagenetic processes in sediments of the continental shelf of the Black Sea. *Estuar. Coast. Shelf Sci.* 54, 403-421.

Chapter 3

Nitrate removal in sediment of a coastal freshwater lake (Haringvliet Lake, The Netherlands) and response to salinization

image: a flow through reactor experiment in progress

A.M. Laverman, R.W. Canavan, C.P. Slomp, and P. Van Cappellen
submitted

ABSTRACT

Porewater NO_3^- profiles in sediment of the coastal freshwater Haringvliet Lake (The Netherlands) show complete nitrate removal within the uppermost centimeter. Rapid NO_3^- consumption is consistent with the results of sediment flow-through reactor (FTR) experiments, which reveal high potential rates of nitrate reduction in the 0-4 cm depth interval. The observed seasonal variations of the potential rates are explained in part by seasonal fluctuations in bottom water temperature and possibly by changes in organic matter deposition. Acetylene-block FTR experiments indicate that only about half of the nitrate reducing activity is accounted for by complete denitrification to N_2. The remaining NO_3^- reduction is due to incomplete denitrification and alternative reaction pathways, most likely dissimilatory nitrate reduction to ammonium (DNRA). Increasing the salinity of the inflow solution in FTR experiments increases the release of ammonium and dissolved organic carbon from the sediment. It also enhances the rates of nitrate reduction and nitrite production, but not that of denitrification.

3.1 INTRODUCTION

Nearshore sediments often exhibit high rates of organic carbon (C_{org}) mineralization and intense cycling of nitrogen (N). Up to 40% of C_{org} mineralization in coastal sediments may be coupled to denitrification (Soetaert and Herman, 1995), which converts dissolved nitrate to gaseous N products, principally N_2, that are released to the atmosphere (Seitzinger, 1988). This makes denitrification a crucial removal pathway of bioavailable N from aquatic ecosystems.

Denitrification is widely viewed as the dominant process of nitrate reduction in coastal sediments (Herbert, 1999), although alternative pathways such as dissimilatory reduction of nitrate to ammonium (DNRA) may be an important N transformation process in sediments with high inputs of labile organic substrates and limited nitrate availability (Megonigal et al., 2003). Unlike denitrification, DNRA does not remove bioavailable N from the aquatic ecosystem. Nitrate reduction can also occur via processes not directly coupled to organic matter oxidation, for instance through anaerobic ammonium oxidation, or anammox (Strous et al., 1999).

The pathways and rates of nitrate reduction depend on environmental factors such as temperature and salinity. Increased salinity displaces NH_4^+ from cation exchange sites of the sediment, thereby reducing the pool of NH_4^+ available for nitrifying bacteria, which, in turn, decreases denitrifying activity fueled by nitrification (Seitzinger et al., 1991). Salinization may further stress freshwater nitrifiers and denitrifiers and lower their activities (Rysgaard et al., 1999). Decreased denitrification rates and accumulation of nitrite in response to increasing salinity have also been reported for waste water sludge (Glass and Silverstein, 1999, Park et al., 2001).

The aim of this study was to quantify nitrate reduction in, and release of dissolved inorganic nitrogen species from, a coastal freshwater sediment. Haringvliet Lake (The Netherlands) was chosen as a study site because this freshwater lake is currently targeted for a possible restoration of estuarine conditions. This would increase the salinity of the bottom waters, thereby modifying benthic nutrient cycling.

3.2 MATERIALS AND METHODS

3.2.1 Field Sampling

Haringvliet Lake is a coastal freshwater lake located in a heavily populated area in the southwest of the Netherlands (Canavan et al., 2006). To increase the ecological diversity of the Haringvliet, a partial restoration of estuarine conditions has been proposed. This would be accomplished by changing the management of the sluices of the storm-surge dam, which separates the lake from the North Sea. The sampling site is located near the dam at a water depth of approximately 7.5 m, within the area that would be affected by salinization.

Sediment was sampled in fall (November 2001), late-summer (September 2002), and spring (April 2003), using a cylindrical box corer. Each box core contained approximately 40 cm of surface sediment and 30 cm of overlying water. Box cores were sub-sampled immediately with polycarbonate tubes (10 cm i.d.) for pore water analysis. Sediment sub-cores for pore water analysis processed under N_2 atmosphere, inside a shipboard, temperature-controlled laboratory as described in Canavan et al. (2006). Filtered pore water sub-samples for NO_3^-, NO_2^- and NH_4^+ were stored frozen until analysis. Additional sub-cores (perspex, 4.2 cm i.d.) were used for oxygen microprofiling.

Sediment for the flow-through reactor (FTR) experiments was collected using a specially designed shuttle corer (Fig. 3.1a; Laverman et al. 2006). The shuttle corer was comprised of reactor cells that are stacked and fixed in position within a stainless steel sleeve. The shuttle corer was pushed by hand into a box core on board the ship. The reactor cells were separated from one another with a Teflon knife. Both end of the reactor cell were immediately covered with 0.2 mm pore size nitrocellulose filters and glass fiber filters (1.2mm thick, 47mm diameter), and capped (Fig. 3.1b). Input/output channels open at the center of the caps, in direct contact with the glass fiber filters. The glass fiber filters ensure radially homogeneous flow through the reactors.

3.2.2. Rate measurements

Nitrogen transformation kinetics were determined on one-centimeter thick, undisturbed sediment slices in flow-through reactors subjected to various conditions (Table 3.1). The

sediment FTR approach was used to measure potential rates of nitrate reduction, denitrification, ammonium production, and nitrite production. Rates were calculated from measured concentration differences between inflow and outflow (ΔC in nmol cm^{-3}), the flow rate (Q in cm h^{-1}) and the volume of sediment inside the reactor (V in cm^3), according to:

$$rate = (\Delta C \star Q) / V \quad (1)$$

where the rate is expressed per unit total (or wet) sediment volume, and C is the concentration of a reactant or (by-)product of the reaction process of interest.

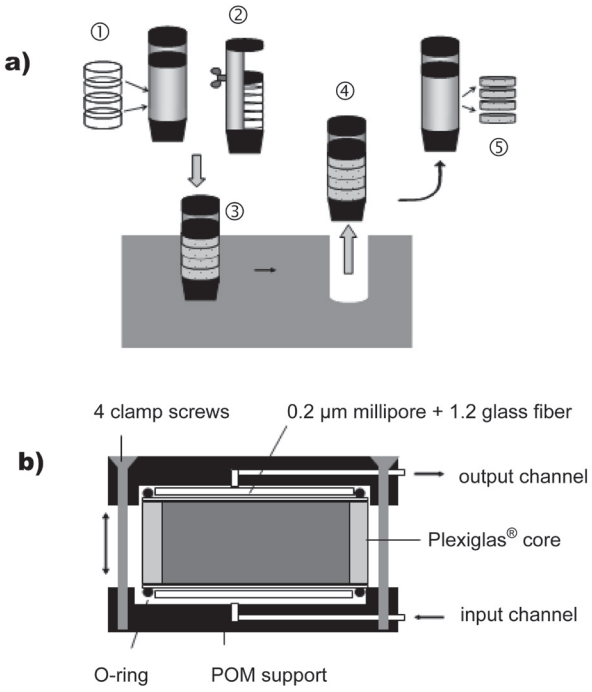

Figure 3.1 (a) Shuttle corer for sampling undisturbed sediment slices. (1) Empty reactor cells are stacked inside the corer. (2) Side view: the reactor cells form the core liner and are kept in place by a movable cover plate. (3) The shuttle corer is manually pushed into the sediment, then closed at the top and bottom. Once taken out of the sediment, (4) the cover plate is loosened and removed. (5) The reactor cells are then separated with a Teflon® knife and enclosed by two caps. (b) Cross sectional view of a flow-through reactor. The length of the reactor cells (L) are 1 cm and the inner diameter is 4.2 cm. The caps are constructed from poly-oxy methylene (POM) Delrin®.

Table 3.1 Overview of potential rate measurements in flow through reactor (FTR) experiments. DNR stands for denitrification rate, NRR for nitrate reduction rate.

	experimental conditions			*sample period*		
	$[NO_3^-]$ (mM)	depth intervals (cm)	treatments	fall	late-summer	spring
NRR	2.5	0-1, 1-2, 2-3, 3-4	-	x	x	x
NRR and DNR	2.5	0-1	8, 12, 18 °C	-	-	x
NRR and DNR	0.5-5	0-1	0; 10‰ NaCl	-	-	x

A peristaltic pump was used to continuously pump water through the sediment containing reactor cells (Fig. 3.1b). The inflow solutions contained KNO_3 (0.5-5 mM), NO_3^- was the only external electron acceptor supplied to the reactors. In a number of experiments, the inflow solution was amended with acetylene (10% v/v), which inhibits the conversion of N_2O to N_2 (Sørensen, 1978). The inflow solutions were vigorously bubbled with N_2 to remove any traces of O_2. Outflow samples were collected at regular (0.5, 1 or 2 h) intervals for chemical analyses. The flow rate (Q) through the reactors was monitored by weighing the outflow samples. At the end of each experiment, the water content and the concentrations of C_{org} and N of the sediment in the reactor were determined.

Seasonal variations and depth distributions of potential nitrate reduction rates were determined with FTR experiments run at *in situ* sediment temperature (Table 3.1). Each FTR experiment ran for 20-24 hours. The effects of temperature and increased salinity on potential nitrate reduction and denitrification rates were investigated using the 0-1 cm depth interval of sediment collected in April 2003 (spring). One FTR was subjected successively to three temperatures (8, 12 and 18 °C), covering the annual temperature range of the bottom waters at the sampling site. Eight reactors containing the topmost cm of sediment were supplied with inflow solutions containing NO_3^- (0.5- 5 mM) and either no added NaCl (-NaCl) or 10 ‰ NaCl (+NaCl). The reactors were run for 50 hours. In addition to nitrogen species, the concentration of dissolved organic carbon (DOC) was measured in the outflow solutions.

3.2.3 Analyses

Nitrate, nitrite and ammonium concentrations were determined colorimetrically with a Nutrient Autoanalyzer 3 (Bran and Luebbe). Porosity was derived from the weight loss of a known volume of wet sediment upon oven-drying at 60ºC. Sediment C and N contents were determined on a Carlo Erba CN analyzer. Dissolved organic carbon (DOC) was measured with

a Shimadzu TOC-5050A analyzer. Oxygen microprofiles were recorded on intact sediment subcores, using a miniaturized Clark-type oxygen sensor mounted on a micromanipulator (Revsbech, 1989). Nitrous oxide concentrations in the outflow of acetylene-block FTR experiments were monitored with a miniaturized Clark-type N_2O sensor (Unisense; Århus, Denmark). The most-probable-numbers (MPN) of denitrifying organisms were obtained as described in Laverman et al. (2006).

3.3 RESULTS

3.3.1 Sediment properties and pore water profiles

The sediment is highly porous and organic-rich (Table 3.2). Bulk sediment C:N ratios are greater than Redfield values (~16 > 6.6). The overlying water remains fully oxygenated year-round, although a somewhat lower O_2 concentration was observed in late summer. Bottom water nitrate concentrations varied between 120 and 180 μM. Oxygen penetration depths were shallower in late summer and spring (3.5 mm) than in fall (6.5 mm; Fig. 3.2). Pore water NO_3^- concentrations were always below the detection limit (1 mM), even in the 0-0.5 cm depth interval (Fig. 3.2). Pore water NH_4^+ concentrations increased with depth, with the highest values recorded in spring (Fig. 3.2).

Table 3.2 Bottom water O_2 and NO_3^- concentrations, and sediment properties.

	bottom water		sediment (0-4 cm)				
	O_2	NO_3^-	Temp.	Porosity	C_{org}	N	C_{org}:N
sample period	(μM)		(°C)	(vol%)	(%)	(%)	(mol/mol)
Fall (November 2001)	225	160	8	87	3.5	0.27	15.1
Late-summer (September 2002)	218	120	18	88	4.3	0.31	16.1
Spring (April 2003)	274	180	12	89	-	-	-

3.3.2 Rates

Potential nitrate reduction rates measured in FTRs at *in situ* temperatures were systematically higher in late-summer than in spring and fall, with maximum values up to 200 nmol cm^{-3} h^{-1} (Fig. 3.3). Nitrate reduction activity was detected at all depths sampled, but the potential rates showed no clear trends with depth. Denitrifiers were abundant in all sediment intervals studied (Fig. 3.3); MPNs, however, did not correlate with depth, sampling time or potential nitrate reduction activity. Rates of ammonium export from FTRs with NO_3^--containing inflow

solutions were also highest in late summer (Fig. 3.3). For both late summer and fall, the rates tended to increase somewhat with depth.

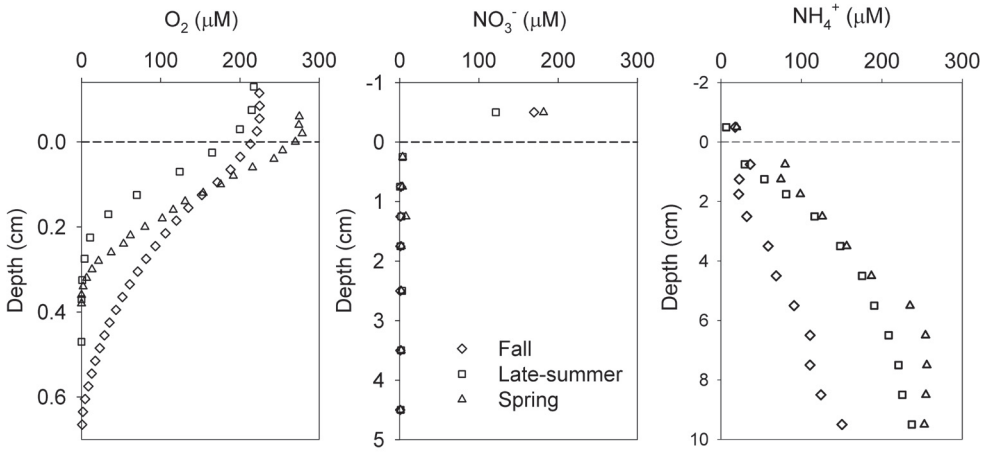

Figure 3.2 Pore water profiles of O_2, NO_3^- and NH_4^+: om fall (◇), late-summer (□), and spring (△). Note the differences in depth scales between the panels. The broken horizontal line corresponds to the sediment-water interface.

At *in situ* temperature (12°C), the average N_2O production rate in C_2H_2-amended FTR experiments with the 0-1 cm depth interval of the spring sediment was 35 nmol cm^{-3} h^{-1}. Denitrification to N_2 therefore only explained 47% of total nitrate reduction measured during the same experiments (Fig. 3.4). Nitrite was also detected in the outflow solutions of the FTR reactors, with NO_2^- production accounting for 17% of NO_3^- reduction.

Potential nitrate reduction and denitrification rates increased near-linearly from 8 to 18°C (results not shown), yielding Q_{10} temperature coefficients (Winkler et al., 1996) of 2.5 and 3.6 for NO_3^-consumption and N_2O production, respectively. In the C_2H_2-amended FTR experiments run at 8 and 18°C, 54 and 34% of total NO_3^- reduction was recovered as N_2O, respectively.

3.3.3 Effect of salinity

Addition of 10 ‰ NaCl to the inflow enhanced potential NO_3^- reduction and NO_2^- production rates in the 0-1 cm of spring sediment (Fig. 3.4). After reaching steady state outflow concentrations (between 20 and 50 hours), the average NO_3^- reduction rates were on the order of 115 nmol cm^{-3} h^{-1} in NaCl amended FTRs, compared to approximately 80 nmol cm^{-3} h^{-1} in

control FTRs. Nitrite production rates were about three times higher in the NaCl-amended FTR experiments (Fig. 3). In contrast, N_2O production in acetylene-amended FTRs did not change significantly upon addition of NaCl (Fig. 3.4).

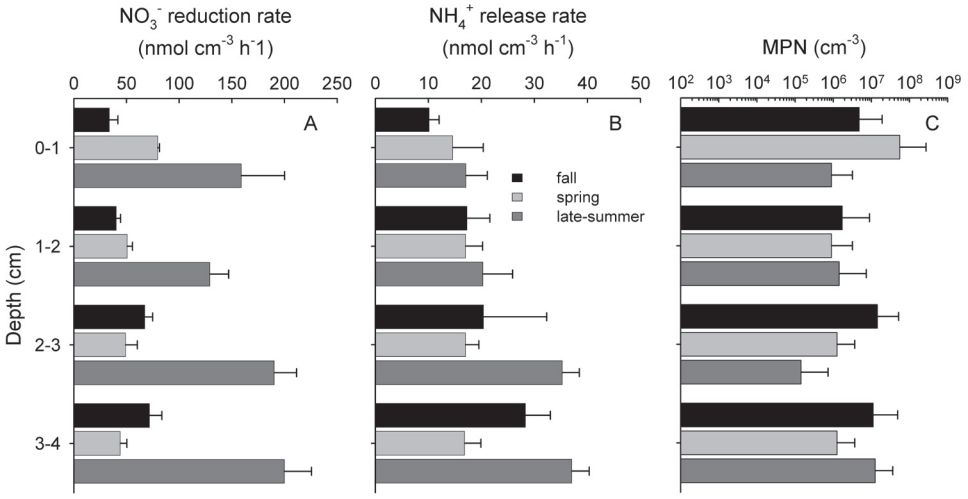

Figure 3.3 Nitrate reduction rates (A), ammonium production rates (B) and Most Probable Numbers of denitrifiers (C) in four depth intervals collected in fall, late-summer and spring. The rates were obtained in FTR experiments incubated at *in situ* temperatures (see Table 3.1). For the rates, error bars indicate the standard deviations of the rates calculated between 14 to 24 hours of the experiments. For the Most Probable Numbers of denitrifiers error bars indicate 95% confidence intervals.

The fraction of NO_3^- reduction resulting in NO_2^- production increased from 17% to 31% when NaCl-amended solution was supplied, while the fraction of NO_3^- reduction attributed to denitrification to N_2 dropped from 47 to 27%. No systematic differences in the abundances of denitrifiers, as determined by the MPN method, were observed in media with or without added NaCl (data not shown).

NaCl addition to the inflow also had pronounced effects on the ammonium and dissolved organic carbon (DOC) concentrations measured in the outflow. The average rate of NH_4^+ release during the first 30 hours of the experiments more than doubled when NaCl was added (Fig. 3.5). Although the NH_4^+ release rates decreased with time, they remained systematically higher in the NaCl-amended experiments. The release of DOC also increased significantly when NaCl-amended inflow was supplied to the sediment (Fig. 3.5).

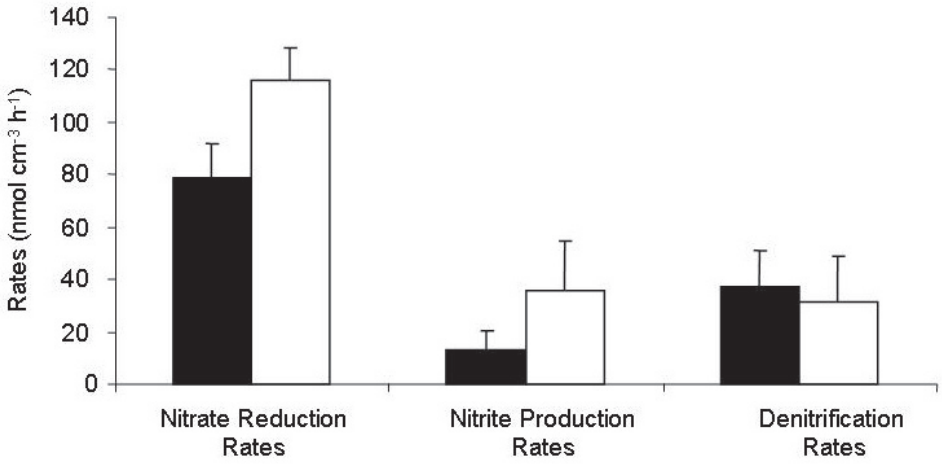

Figure 3.4 Effects of NaCl amendments on nitrate consumption, NO_2^- production and N_2O production rates in the 0-1 cm depth interval of sediment collected in April 2003 (spring). FTRs were supplied with NO_3^--containing inflow solutions without (filled bars) or with added NaCl (10‰, open bars). Values are the average of four reactors supplied with different NO_3^- concentrations (0.5-5 mM) between 30 – 55 hours, error bars correspond to standard deviations. The reactors were run at *in situ* temperature (12°C) and a flow rate of 6 ml h^{-1}.

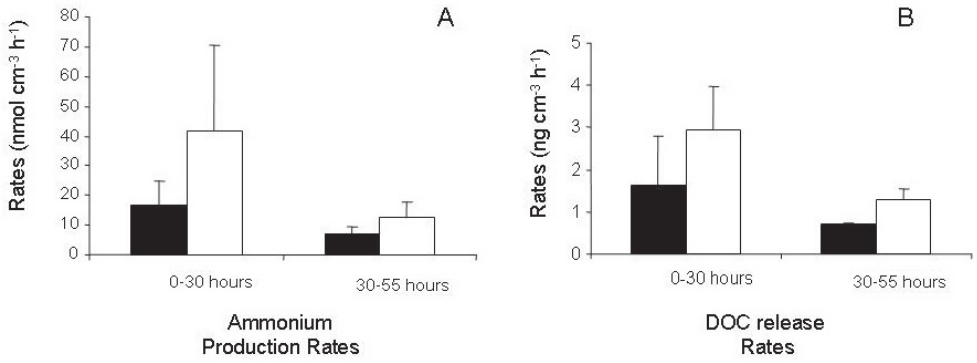

Figure 3.5 Effects of NaCl amendment on ammonium (A) and dissolved organic carbon (B) release, from the 0-1 cm depth interval of sediment collected in April 2003 (spring). FTRs were supplied with NO_3^--containing inflow solutions without (filled bars) or with added NaCl (10‰, open bars). Error bars indicate standard deviations on rates obtained from 4 reactors supplied with different NO_3^- concentrations (0.5-5 mM), between 0 and 30 hours and 30 and 55 hours. The reactors were run at *in situ* temperature (12 °C) and a flow rate of 6 ml h^{-1}.

3.4 DISCUSSION

Based on reactive transport model calculations, Canavan et al. (2006) estimate that the average depth-integrated of organic carbon mineralization in the sediment studied is on the order of 764 μmol cm^{-2} yr^{-1}, of which approximately 21% may be coupled to nitrate reduction. Intense sediment metabolism, which is also reflected in the limited penetration depths of O_2 and NO_3^- in the sediment (Fig. 3.2), implies a key role of benthic processes in the biogeochemical functioning of the shallow, eutrophic Haringvliet Lake. In particular, the sediments represent an important sink for nitrate.

Seasonal temperature changes only explain part of the observed variations in nitrate reducing activity. Based on the measured Q_{10} value, the 10°C difference between late-summer and fall sampling times accounts for about half (55%) of the 4-fold difference in potential nitrate reduction rates. Most likely, the rates also reflect seasonal fluctuations in the deposition of labile organic substrates from the water column. The abundance of denitrifying organisms and high potential NO_3^- reduction rates well below the depth of NO_3^- penetration (Figs. 3.3-4) indicate that benthic nitrate reduction is limited by the supply of NO_3^- from the overlying bottom water. In addition to molecular diffusion, pore water irrigation by benthic infauna is a major mechanism for transferring NO_3^- from the water column to the sediment (Canavan et al., 2006).

Two immediate effects of a future salinization of the Haringvliet would be the release of sediment-bound $NH_4^+$and organic matter (Fig. 3.5). While the mobilization of ammonium due to cation exchange by Na^+ is well-established (Rysgaard et al., 1999, Seitzinger et al., 1991), DOC release upon salinization is poorly understood. It probably involves changes in the macromolecular structure of the organic matter with increased ionic strength (Tombacz and Meleg, 1990), which may enhance its bioavailability (Nyvang, 2003, Weston et al., 2006). DOC mobilization following saltwater intrusion has been invoked to explain increased microbial respiration in a Danish coastal aquifer (Nyvang, 2003). A similar effect may explain the increase in NO_3^- reduction rate observed in the NaCl-amended FTR experiments (Fig. 3.4).

Salt addition to the inflow solutions also increases the production of NO_2^- (Fig. 3.4), suggesting that salinity stress may favor incomplete denitrification. A negative impact of increased salt concentrations on NO_2^- reductase has been previously documented (Glass and Silverstein, 1999). Both NO_2^- and N_2O reductases are periplasmatic enzymes and, hence, more sensitive to environmental stress than NO_3^- reductase, which is membrane-bound (Zumft, 1997).

An unexpected finding is that (complete) denitrification to N_2 only accounts for about 50% of NO_3^- reduction in the FTR experiments. Addition of NaCl even further decreases the

relative contribution of denitrification (Fig. 3.4). A decoupling between NO_3^- reduction and denitrification is consistent with their different temperature dependencies. An experimental artifact due to incomplete blockage by acetylene of N_2O reductase as a result of nitrate limitation (Oremland et al., 1984) is unlikely, given the high NO_3^- concentrations of the inflow solutions. Similarly, an interference by sulfide (Dalsgaard and Bak, 1992) is not expected, as no sulfate is supplied to the reactors. Furthermore, for other freshwater sediments the exact same experimental approach yields N_2O recoveries approaching 100% (Laverman et al., 2006).

Incomplete N_2O recovery in the acetylene-amended FTR experiments implies pathways of nitrate removal other than denitrification to N_2. The estimated contributions of denitrification to N_2 (47%) plus incomplete denitrification to nitrite (17%) leave 36% of nitrate removal unaccounted for. DNRA and anammox are commonly invoked as additional NO_3^- removal processes in sediments. Although both pathways consume NO_3^-, DNRA produces NH_4^+ while anammox consumes NH_4^+. Ratios of net ammonium production (APR) and net NO_3^- removal (NRR) in the FTR experiments should therefore help to further constrain the pathways of nitrate removal.

The expected range of APR:NRR ratios for denitrification to N_2 is shown on Fig. 3.6. The values of APR:NRR observed for the late-summer FTR experiments (0.09-0.19) fall within the range for denitrification (Fig. 3.6). Most of the FTR experiments run with sediments collected in fall and spring, however, yield higher values, indicating excess NH_4^+ production. The latter supports DNRA as a pathway for nitrate reduction in Haringvliet Lake sediments, in line with the high abundance of degradable organic matter, relative to the limited supply of NO_3^- from the water column (Herbert, 1999).

For the relative distribution of nitrate reduction inferred from the FTR experiments with the 0-1 cm depth interval collected in spring (denitrification = 47%, incomplete denitrification = 17%, DNRA = 36 %), net APR:NRR should be on the order of 0.5. The observed values mostly fall below 0.5, suggesting consumption of NH_4^+. In FTR experiments with coastal sediments exhibiting a wider range of potential nitrate reduction rates, NH_4^+ removal was attributed to uptake by nitrate reducing microorganisms, although some contribution from anammox could not be excluded (Laverman et al., 2006). The continuous supply of electron acceptor via the inflow probably triggers nitrate reducers to assimilate NH_4^+ for protein synthesis.

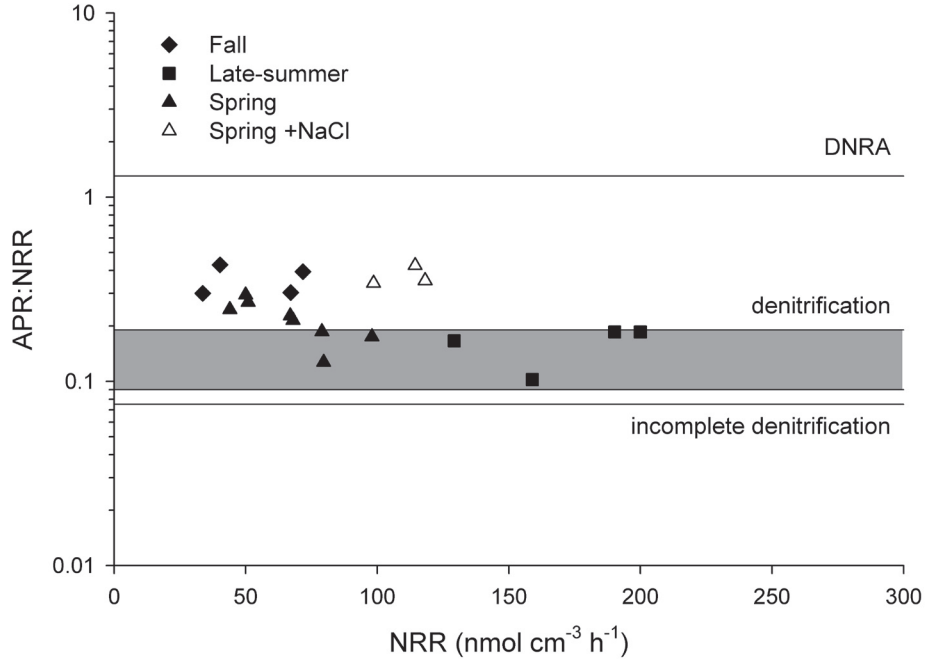

Figure 3.6 Ratio of net ammonium production rate (APR) and nitrate reduction rate (NRR) in FTR experiments with Haringvliet sediments, plotted as a function of NRR. The shaded area corresponds to the APR:NRR ratios expected for denitrification to N_2, assuming an idealized stoichiometry of the decomposing organic matter of $(CH_2O)_x(NH_3)_y$ and end-member molar C:N ratios equal to the measured bulk C_{org}:N ratio in the sediments (16, Table 3.2) and the Redfield C:N ratio for fresh phytoplankton (6.6). Also shown as horizontal lines are the theoretical APR:NRR ratios for DNRA and incomplete denitrification to NO_2^-, assuming the Redfield C:N ratio for the decomposing organic matter.

3.5 CONCLUSIONS

Sediments of the Haringvliet exhibit a high potential for nitrate removal. *In situ* benthic nitrate reduction is controlled by bottom water temperature, the deposition of organic substrates, and the transfer of nitrate from the water column by diffusion and pore water irrigation. Acetylene-block FTR experiments and ammonium production rates indicate that, in addition to denitrification, incomplete denitrification and dissimilatory nitrate reduction to ammonium (DNRA) are significant pathways of nitrate reduction. In contrast to denitrification, the other pathways regenerate bioavailable forms of nitrogen (nitrite and ammonium).

Salinity increase enhances nitrate consumption, possibly as a result of a salinity-induced mobilization of sediment-bound organic matter. The higher nitrate reducing activity, however, is mainly due to increased rates of incomplete denitrification and DNRA. Combined with the displacement of ammonium from cation exchange sites, the immediate impact of salinization of the Haringvliet is therefore expected to be an increased efflux of bioavailable inorganic nitrogen from the sediments.

The salinity effects observed in the FTR experiments may be relatively short-lived as the microbial populations adapt to new bottom water conditions. Longer-term experiments, for example with large sediment mesocosms, are needed to delineate the changes in benthic nitrogen cycling following prolonged exposure to saline bottom waters. Furthermore, direct salinity effects on microbial activity are only one aspect of the changes that will affect benthic-pelagic coupling upon restoration of estuarine conditions. The latter will also modify organic matter deposition, bottom water oxygenation and benthic infaunal activity, all of which influence nitrogen removal and regeneration in sediments.

Acknowledgments We thank the crew of the R.V. Navicula for their expert help during the cruises. Debby Los and Dineke van de Meent assisted with the experiments and analyses. Financial support was provided by the Netherlands Organisation for Scientific Research, NWO (Veni Grant to AML, Pioneer Grant to PVC), the Royal Netherlands Academy of Arts and Sciences, KNAW (Fellowship to CPS), and the Netherlands Institute for Inland Water Management and Waste Water Treatment, RIZA (Fellowship to RWC).

References

Canavan, R.W., Jourabchi, P., Slomp, C.P., Van Cappellen, P., Laverman, A.M. and van den Berg, G.A. (2006) Organic matter mineralization in sediment of a coastal freshwater lake and response to salinization. Geochimica et Cosmochimica Acta 70 (11), 2836-2855.

Dalsgaard, T. and Bak, F. (1992) Effect of acetylene on nitrous-oxide reduction and sulfide oxidation in batch and gradient cultures of *Thiobacillus denitrificans*. Applied and Environmental Microbiology 58 (5), 1601-1608.

Glass, C. and Silverstein, J. (1999) Denitrification of high-nitrate, high-salinity wastewater. Water Research 33 (1), 223-229.

Herbert, R.A. (1999) Nitrogen cycling in coastal marine ecosystems. FEMS Microbiology Reviews 23 (5), 563-590.

Laverman, A.M., Los, D., Pallud, C., Abel, J. and Van Cappellen, P. (2006) Potential rates and pathways of microbial nitrate reduction in coastal sediments. FEMS Microbiology Ecology, in press.

Megonigal, J.P., Hines, M.E. and Visscher, P.T. (2003) Anaerobic Metabolism: Linkages to Trace Gases and Aerobic Processes. pp. 317-424. In W. H. Schlesinger (ed.), Biogeochemistry Vol. 8 *Treatise on Geochemistry* (eds. H.D. Hollands and K.K. Turekian), Elsevier-Pergamon, Oxford.

Nyvang, V. (2003) Redox processes at the salt-/freshwater interface in an anaerobic aquifer, Ph.D. Thesis, Technical University of Denmark.

Oremland, R.S., Umberger, C., Culbertsen, C.W. and Smith, R.L. (1984) Denitrification in san francisco bay intertidal sediments. Applied and Environmental Microbiology 47 (5), 1106-1112.

Park, E.J., Seo, J.K., Kim, M.R., Jung, I.H., Kim, J.Y. and Kim, S.K. (2001) Salinity acclimation of immobilized freshwater denitrifier. Aquacultural Engineering 24 (3), 169-180.

Revsbech, N.P. (1989) Diffusion characteristics of microbial communities determined by use of oxygen microsensors. Journal of Microbiological Methods 9, 111-122.

Rysgaard, S., Thastum, P., Dalsgaard, T., Christensen, P.B. and Sloth, N.P. (1999) Effects of salinity on NH_4^+ adsorption capacity, nitrification, and denitrification in Danish estuarine sediments. Estuaries 22 (1), 21-30.

Seitzinger, S.P. (1988) Denitrification in freshwater and coastal marine ecosystems: Ecological and geochemical significance. Limnology and Oceanography 33 (4 part 2), 702-724.

Seitzinger, S.P., Gardner, W.S. and Spratt, A.K. (1991) The effect of salinity on ammonium sorption in aquatic sediments - implications for benthic nutrient recycling. Estuaries 14 (2), 167-174.

Soetaert, K. and Herman, P.M.J. (1995) Nitrogen dynamics in the Westerschelde estuary (SW Netherlands) estimated by means of the ecosystem model moses. Hydrobiologia 311 (1-3), 225-246.

Sørensen, J. (1978) Denitrification rates in a marine sediment as measured by the acetylene inhibition technique. Applied and Environmental Microbiology 36 (1), 139-143.

Strous, M., Kuenen, J.G. and Jetten, M.S.M. (1999) Key physiology of anaerobic ammonium oxidation. Applied and Environmental Microbiology 65 (7), 3248-3250.

Tombacz, E. and Meleg, E. (1990) A theoretical explanation of the aggregation of humic substances as a function of pH and electrolyte concentration. Organic Geochemistry 15 (4), 375-381.

Weston, N.B., Dixon, R.E. and Joye, S.B. (2006) Ramifications of increased salinity in tidal freshwater sediments: Geochemistry and microbial pathways of organic matter mineralization. Journal of Geophysical Research 111, G01009.

Winkler, J.P., Cherry, R.S. and Schlesinger, W.H. (1996) The Q_{10} relationship of microbial respiration in a temperate forest soil. Soil Biology and Biochemistry 28 (8), 1067-1072.

Zumft, W.G. (1997) Cell biology and molecular basis of denitrification. Microbiology and Molecular Biology Reviews 61 (4), 533-616.

Chapter 4

Modeling nitrogen cycling in a coastal freshwater sediment

image: sub-sampling a boxcore

R.W. Canavan, A.M. Laverman, and C.P. Slomp
submitted

ABSTRACT

Increased nitrogen (N) loading to coastal marine and freshwater systems is occurring worldwide as a result of human activities. Diagenetic processes in sediments can change the N availability in these systems, by supporting removal through denitrification and burial of organic N (N_{org}) or by enhancing N recycling. In this study, we use a reactive transport model (RTM) to examine N transformations in a coastal fresh water sediment and quantify N removal rates. We also assess the response of the sediment N cycle to environmental changes that may result from increased salinity which is planned to occur at the site as a result of an estuarine restoration project. Field results show that much of the N_{org} deposited on the sediment is currently remineralized to ammonium. A rapid removal of nitrate is observed in the sediment pore water, with the resulting nitrate reduction rate estimated to be 130 μmol N cm^{-2} yr^{-1}. A model sensitivity study was conducted altering the distribution of nitrate reduction between dissimilatory nitrate reduction to ammonium (DNRA) and denitrification. These results show a 40% decline in sediment N removal as NO_3^- reduction shifts from denitrification to DNRA. This decreased N removal leads to a shift in sediment-water exchange flux of dissolved inorganic nitrogen (DIN) from near zero with denitrification to 133 μmol N cm^{-2} yr^{-1} if DNRA is the dominant pathway. The response to salinization includes a short-term release of adsorbed ammonium. Additional changes expected to result from the estuarine restoration include: lower NO_3^- concentrations and greater SO_4^{2-} concentrations in the bottom water, decreased nitrification rates, and increased sediment mixing. The effect of these changes on net DIN flux and N removal vary based on the distribution of DNRA versus denitrification, illustrating the need for a better understanding of factors controlling this competition.

4.1 INTRODUCTION

Nitrogen inputs to freshwater and near shore marine systems have increased strongly due to human activities, leading to eutrophication (Cloern, 2001; de Jonge et al., 2002). A significant fraction of this excess N may be removed in the sediment through denitrification or burial of organic N (N_{org}). This nitrogen removal has been shown to correlate to N input loads and discharge rates of water (Windolf et al., 1996; Saunders & Kalff, 2001). Aquatic systems with high discharge rates have lower removal rates as sediment-water interactions are limited.

Removal through denitrification may also be limited by competition with an alternative sediment pathway, dissimilatory nitrate reduction to ammonium (DNRA). DNRA has been found to be a significant pathway of nitrate reduction in a variety of sediments and saturated soils (Gilbert et al., 1997; Ogilvie et al., 1997; Revsbech et al., 2005). It is thought that an abundance of organic carbon relative to NO_3^- favors DNRA over denitrification, but little is known

about the competition between the organisms responsible for the two pathways (Megonigal et al., 2003). The difference between these two pathways is significant for water quality as denitrification produces a form of gaseous N that is generally unavailable to primary producers, while the NH_4^+ produced through DNRA is readily bioavailable (Fig. 4.1). In addition to diffusion from the overlying water, nitrification of NH_4^+ in the oxic surface sediment can also be an important source of NO_3^- for reduction (Seitzinger, 1988).

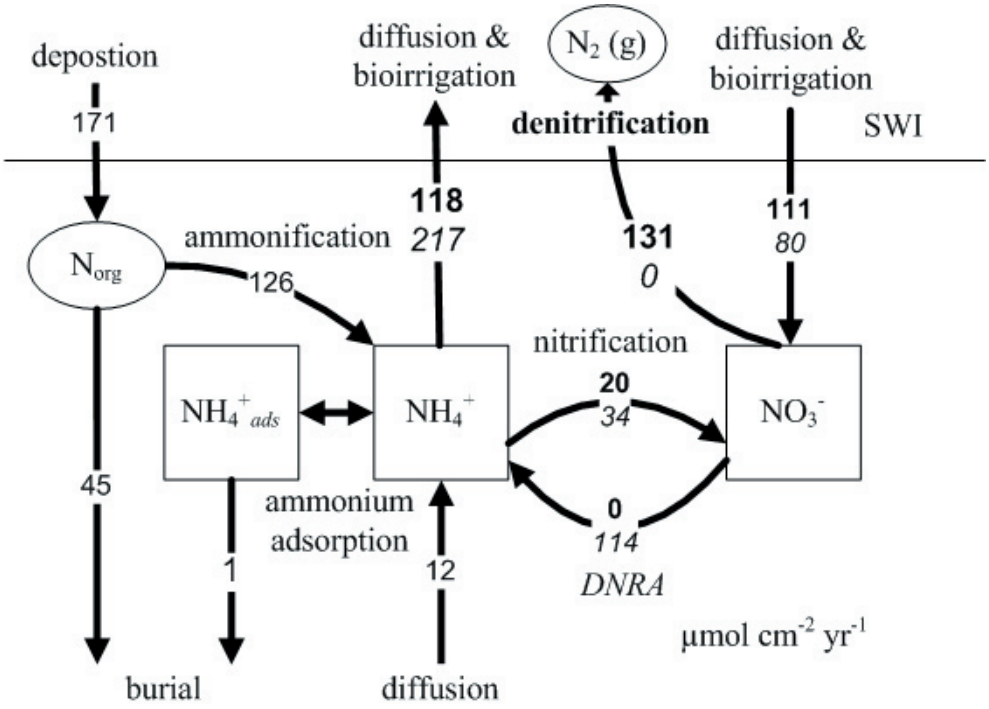

Figure 4.1 A schematic diagram of the sedimentary N cycle with both reaction and transport processes labeled. Model derived values of rates and fluxes for the upper 30 cm of sediment are presented on the arrows in μmol N cm^{-2} yr^{-1}. Results of two steady-state simulations are shown, in one simulation all nitrate reduction occurs via denitrification (bold), in the other via DNRA (italics). The influx of organic matter and mineralization rates were kept constant.

Ammonium can be retained in sediment due to adsorption at cation exchange sites, which are present on the surface of organic matter and clay minerals (Berner, 1980). Salinization of fresh water sediments can cause the desorption of NH_4^+ from cation exchange sites as a result

of competition with Na^+ ions (Seitzinger et al., 1991). Lower nitrification rates (Gardner et al., 1991; Rysgaard et al., 1999), increased NO_2^- production, and increased rates of organic matter mineralization (Nyvang, 2003) have also been associated with increased salinity. Salinization of fresh waters, and the associated changes in N cycling, may occur in the coastal zone due to rising sea level, dam construction, and ground water withdrawal.

Our study site is currently a freshwater lake that will become brackish from 2008 onwards as a result of an ecological restoration project. In this study we adapt a previously developed reactive transport model (Canavan et al., 2006), to examine the response of the sediment N-cycle to changes that may result from salinization of this fresh water lake. Possible changes in site conditions are represented by changing parameters in steady-state and transient simulations. To allow for a more detailed model representation of the sediment N processes the existing model was adapted to include DNRA, in addition to denitrification, as experimental results suggest a possible role for DNRA at the site (Laverman et al., 2006). In this model sensitivity study, we specifically focus on the consequences for net sediment dissolved inorganic nitrogen (DIN) efflux rates.

4.2 METHODS

4.2.1 Study site

Haringvliet Lake (The Netherlands) is a eutrophic freshwater lake in the southwestern Netherlands. The lake was created as a result of damming of the mouth of a tidal estuary in 1970. Prior to dam construction, the Haringvliet was an outlet of the Meuse-Rhine River system to the North Sea. The closure of the Haringvliet caused physical and chemical changes in the water body, including the disappearance of the salinity gradient and the accumulation of river derived suspended matter (Smit et al., 1997). The lake is relatively shallow; the water depth at the sample site was 7.5m. The lake retains some fluvial characteristics, such as high flow rates. The residence time of water in Haringvliet Lake is typically on the order of several days (Smit et al., 1997), however periods of increased residence time occur when river levels are low and discharge through the dam is stopped. Thermal stratification and bottom water anoxia are not observed. A partial restoration of estuarine conditions in Haringvliet Lake is proposed to increase the diversity and availability of estuarine habitat in the area (Anonymous, 1998). Restoration would be achieved by changing the opening and closing of gates in the dam that separates the lake from the North Sea. Our sample location was located near the dam in an area that would be affected by the restoration (51.50.080 N, 51.48.245 E). The sediment at the site was fine-grained and highly porous. A previous study at this site indicates organic matter mineralization rates on the order of 764 μmol cm^{-2} yr^{-1} where oxic degradation (55%),

nitrate reduction (21%) and sulfate reduction (17%) are the important degradation pathways (Canavan et al., 2006).

4.2.2 Sample collection and analysis

Field sampling was carried out in November 2001, September 2002, and April 2003. These sampling times are referred to in the text as fall, late-summer, and spring, respectively. Sediment was collected using a cylindrical box corer (31 cm i.d.) deployed from RV Navicula. Sub-cores were taken with polycarbonate tubes (10 cm i.d.) and immediately sectioned in a N_2 purged glove box on board the ship. Sediment was centrifuged at 2500 g for 10 to 30 minutes in polyethylene tubes to collect pore water. After centrifugation, tubes were transferred to a N_2 purged glove box, and the pore water was filtered through 0.2 or 0.45 μm pore size filters. Pore water was then sub-divided and preserved for the different analyses. Sub-samples for NO_3^- and NH_4^+ were stored frozen until analysis at the laboratory and were determined colorimetrically on a nutrient auto-analyzer (Bran and Luebbe). Dissolved oxygen microprofiles were determined on-board the sampling ship with a Clark-type oxygen sensor as described in Canavan et al. (2006). Sediment C and N contents were determined on freeze dried sediments using a Carlo Erba CN analyzer and a LECO CS analyzer.

4.2.3 Model development

RTM calculations of 1-D sediment profiles were carried out with the Biogeochemical Reaction Network Simulator (BRNS; Aguilera et al., 2005; Jourabchi et al., 2005). The development and calibration of the model, which includes a reaction network of 24 chemical species and 32 reactions, is presented in detail in Canavan et al. (2006). The current study focuses solely on the sediment N-cycle, therefore the model description and results are limited to N transformation processes. The RTM includes 6 N-species: NH_4, NO_3^-, adsorbed NH_4^+ ($NH_{4\ ads}^+$), and three pools of N_{org} (Table 4.1), which are linked to the organic carbon pools through C:N ratios. The different organic matter pools are abbreviated as OM1, a highly reactive pool, OM2, a less reactive pool, and OM3, a refractory (non-reactive) pool (Westrich & Berner, 1984). Upper boundary conditions for the N-species are given in Table 4.1. All lower boundaries are set to no-flux conditions, where the lower boundary of the simulation was 100 cm.

The decomposition of organic matter, which is modeled as a first order process defined by a rate constant kOM (yr^{-1}), results in the mineralization of N_{org} (Table 4.2). Organic matter mineralization occurs with a series of terminal electron acceptors: O_2, NO_3^-, Mn-oxides, Fe-oxides, SO_4^{2-}, and organic carbon. The distribution of the total organic matter

decomposition rate over the different terminal electron acceptor pathways follows the approach of Van Cappellen & Wang, (1996). The model reaction network, which initially included only denitrification, was adapted to include both nitrate reduction pathways. The DNRA reactions were added to the reaction network (Table 4.2) and a term *f*DNRA was included to distribute the total nitrate reduction between the two pathways. This *f*DNRA term is set empirically and equals the fraction of total nitrate reduction occurring via DNRA. The fraction of total nitrate reduction occurring by denitrification is defined as 1-*f*DNRA. Because this study uses the boundary conditions calibrated in Canavan et al. (2006) the initial value of *f*DNRA is set to zero. Sensitivity of sediment processes to changes in the distribution of nitrate reduction pathways is examined by varying the *f*DNRA term. With the exception of Kelly-Gerreyn et al. (2001), existing sediment diagenetic models ignore DNRA and assume all nitrate reduction to occur via denitrification.

Table 4.1 Model nitrogen species and upper boundary conditions

solute	μM	*solid*	(μmol cm^{-2} yr^{-1})	C:N ratio
NO_3^-	154	N_{org}-OM1	113	5.6
NH_4^+	14.5	N_{org}-OM2	32	10
		N_{org}-OM3	27	20
		$NH_{4\ ads}^+$	0	-

NO_3^- and NH_4^+ upper boundary concentrations are mean values of overlying water from the three sampling events. Input fluxes of N_{org} were calculated from the input fluxes for the three organic matter pools and C:N ratios that were defined for those pools.

The oxidation of NH_4^+ with O_2 (nitrification) is described with a bimolecular rate law (Table 4.2; Van Cappellen & Wang, 1996). Adsorption of NH_4^+ to cation exchange sites is represented by a linear equilibrium isotherm, with a constant adsorption coefficient, K_N (Berner, 1980; Van Cappellen & Wang, 1996). K_N is a dimensionless adsorption coefficient:

$$K_N = \frac{1-\varphi}{\varphi}\rho K^* \qquad (1)$$

where φ is porosity (vol. % porewater), ρ is sediment density (g cm^{-3}), and $K^\star$ (cm^3 g dw^{-1}) is the ratio of $NH_{4\ ads}^+$ (μmol g dw^{-1}) to NH_4^+ (mM). The concentration of $NH_{4\ ads}^+$ is estimated to be 3 μmol g dw^{-1} based on the release of NH_4^+ from sediment flow through reactors exposed to increased salinity (Laverman, unpublished results). Using this estimate and the corresponding pore water NH_4^+ concentration of 0.077 mM, gives a value of 39 (cm^3 g dw^{-1})

for $K^{\star}$ and of 10 for K_N. Both values fall within the range reported for fresh water sediments by Seitzinger et al. (1991).

Table 4.2 Nitrogen containing reactions in the model

Reactions	Kinetic or equilibrium formulation
Ammonification[a,b]	
$[(CH_2O)_y(\mathbf{NH_3})_z] + yTEA_{ox} \rightarrow z\mathbf{NH_4^+} + yCO_2 + yH_2O + yTEA_{red}$	$k_{OM}[OM]\,f_{TEA}$
Denitrification	
$[(CH_2O)_y(\mathbf{NH_3})_z] + 0.8yNO_3^- \rightarrow z\mathbf{NH_4^+} + 0.4y\mathbf{N_2} + (0.2y\text{-}z)CO_2 + (0.8y+z)HCO_3^- + (0.6y\text{-}z)H_2O$	$k_{OM}[OM]\,f_{NO3}$ $(1\text{-}f\mathrm{DRNA})$
DNRA	
$[(CH_2O)_y(\mathbf{NH_3})_z] + 0.5y\mathbf{NO_3^-} + zCO_2 + (0.5y+z)H_2O \rightarrow (0.5y+z)\mathbf{NH_4^+} + (y+z)HCO_3^-$	$k_{OM}[OM]\,f_{NO3}$ $f\mathrm{DRNA}$
Nitrification	
$\mathbf{NH_4^+} + 2O_2 + 2HCO_3^- \rightarrow \mathbf{NO_3^-} + 2CO_2 + 3H_2O$	$k_{NH4OX}[NH_4^+][O_2]$
Ammonium adsorption[c]	
$\mathbf{NH_{4\ ads}^+} \leftrightarrow \mathbf{NH_4^+}$ $(K_N\,\varphi/\rho(1\text{-}\varphi))$	$K_N[NH_4^+]$

(a) Organic matter is represented by the formula $[(CH_2O)_y(NH_3)_z]$ where y/z is the C:N ratio. (b)A generalized mineralization reaction is depicted for ammonification where TEA_{ox} and TEA_{red} represent the oxidized and reduced terminal electron acceptor. The term f_{TEA} defines the fraction of the total carbon mineralization by each TEA pathway (Van Cappellen and Wang, 1996), for example f_{NO3} represents the nitrate reduction pathways.
(c) K_N is the dimensionless adsorption coefficient as defined in eq. 1.

The model includes transport of solutes by molecular diffusion, bioirrigation, bioturbation, and advection (burial). Transport of solids occurs by bioturbation and advection. Molecular diffusion and the associated tortuosity and temperature effects are included as described in Van Cappellen & Wang (1996). Bioirrigation is represented as a non-local exchange with the surface water of which the intensity is controlled by the coefficient, α (Boudreau, 1984); and bioturbation is parameterized using an additional diffusion term, D_b (Berner, 1980). The advective velocity of solids and solutes is determined from the sediment accumulation rate, ω (cm yr^{-1}) and porosity (φ) as described by Berner (1980). Table 4.3 includes a list of parameter values used in the model including the depth distributions of α, D_b, and φ.

Table 4.3 Initial parameter values and distributions

Parameter	Value	Unit	Description
k_{OM1}	25	yr^{-1}	degradation rate constant OM1
k_{OM2}	0.01	yr^{-1}	degradation rate constant OM2
k_{OM3}	0	yr^{-1}	degradation rate constant OM3
K_N	10	-	NH_4^+ adsorption coefficient (eq. 1)
*f*DNRA	0	-	fraction of nitrate reduction occurring as DNRA
k_{NH4OX}	20	$\mu M^{-1}yr^{-1}$	nitrification rate constant
ω	1.0	cm yr^{-1}	sediment accumulation rate
ρ	2.1	g cm^{-3}	sediment density
α_0	10	yr^{-1}	bioirrigation coefficient at surface
D_{b0}	5	cm^2 yr^{-1}	bioturbation coefficient at surface
λ	2.5	cm^{-1}	D_b depth attenuation coefficient
φ_o	0.89	cm^3 cm^{-3}	porosity at surface
φ_∞	0.79	cm^3 cm^{-3}	porosity at depth
τ	0.2	cm^{-1}	φ depth attenuation coefficient
x	0-30	cm	sediment depth
Depth distributions			Description
$\alpha = \begin{cases} \alpha_0 \left(1 - e^{(x-17)}\right) & (x \le 17cm) \\ 0 & (x > 17cm) \end{cases}$			distribution of bioirrigation coefficient α
$D_b = D_b 0\ e^{-(x/\lambda)}$			distribution of bioturbation coefficient D_b
$\varphi(x) = \varphi_\infty + (\varphi_o - \varphi_\infty)e^{-(\tau x)}$			porosity distribution

4.3 RESULTS & DISCUSSION

4.3.1 Existing conditions

The oxygen penetration depth was between 0.3 to 0.6 cm in the sediment. Nitrate concentrations in the overlying water ranged from 120-180 μM, while NO_3^- in pore water from the 0-0.5 cm layer was always below 5 μM (Fig. 4.2). The relatively coarse scale of the pore water sampling (0.5 cm sections in the upper 2 cm) and the rapid reduction of nitrate in the samples, limits the resolution of measured pore water NO_3^-. Typically the NO_3^- penetration should extend below that of O_2 (Stief et al., 2003). The resolution of the O_2 profiles is improved by the use of the microelectrode. Pore water NH_4^+ concentrations increased with depth, as

a result of ammonification. Seasonal differences in NH_4^+ were observed in the upper 17 cm with highest concentrations in spring and lowest in fall, where high NH_4^+ corresponded with shallower O_2 penetration. The NH_4^+ profiles exhibit evidence of bioirrigation in the upper 17 cm with somewhat homogeneous concentrations, while below this depth upward diffusion is evident. Sediment N_{org} concentrations decline with depth due to organic matter decomposition. The model derived profiles of O_2, NO_3^-, NH_4^+, and N_{org} capture the vertical trends observed in the measured values (Fig. 4.2). The modeled NH_4^+ concentrations are greater when *f*DNRA is 1. The model was calibrated for the condition *f*DRNA = 0 (Canavan et al, 2006). It is not possible to estimate a possible value of *f*DNRA directly from the NH_4^+ profiles given the uncertainty in the input fluxes of organic matter.

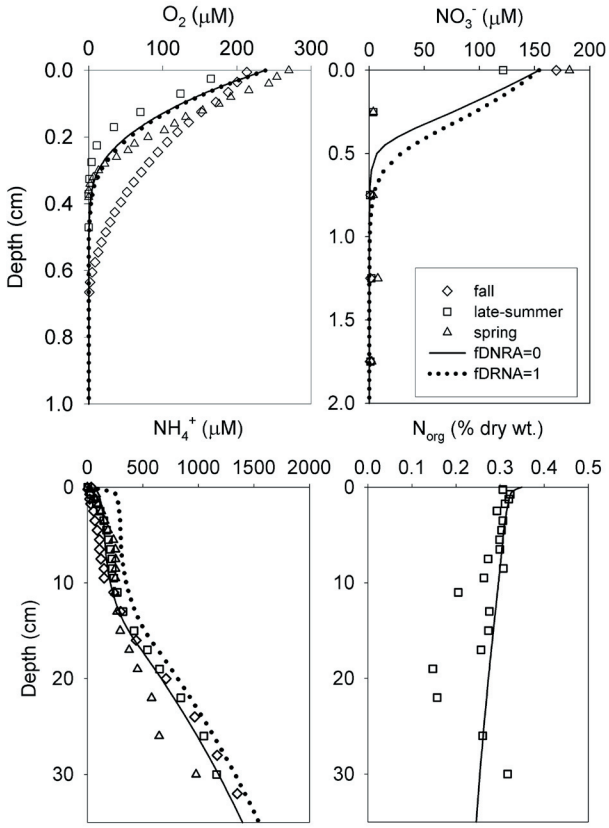

Figure 4.2 Sediment pore water O_2, NO_3^-, and NH_4^+ concentrations and sediment organic nitrogen (N_{org}) concentrations from fall (◇), late-summer (□), and spring (△). Steady-state model derived profiles for porewater species are plotted for *f*DNRA = 0 (solid line) and for *f*DNRA = 1 (dotted line). The modeled N_{org} profile is not sensitive to changes in *f*DNRA which is depicted with a solid line.

Model-derived rates of transport and reaction in the sediment are presented in the schematic representation of N-cycling (Fig. 4.1) including results of two examples where all nitrate reduction occurs either by denitrification (in bold) or DNRA (in italics). The decomposition of organic matter releases 73% of the deposited N_{org} as NH_4^+ in the upper 30 cm of sediment. Much of the remaining N_{org} is buried in the sediment, however, decomposition does continue deeper in the sediment resulting in the upward diffusion of NH_4^+ in the pore water. The major part of the NH_4^+ generated by ammonification is transported to the overlying water, while approximately 15-26% is oxidized to NO_3^- (nitrification). Limitation of nitrification in the sediment may be due to the shallow O_2 penetration depth (Fig. 4.2), and competition from other processes such as oxic organic matter decomposition, and the oxidation of sulfides and methane (Canavan et al., 2006). Low rates of nitrification have been observed in coastal sediment with significant DNRA activity (Gilbert et al., 1997, shellfish farm site; An & Gardner, 2002; Magalhães et al., 2005, muddy sediment site). Conditions favoring DNRA over denitrification, such as highly reduced sediments, and low NO_3^- concentrations relative to organic substrate availability, may also contribute to low nitrification rates (Megonigal et al., 2003).

4.3.2 Role of Denitrification versus DNRA

Experimental results from flow through reactor (FTR) experiments show that potential rates of denitrification were approximately 50% less than those of NO_3^- reduction at our site (Laverman et al., 2006). Conditions in the FTR experiments favor denitrification over DNRA when compared to the in-situ conditions as NO_3^- concentrations in the FTRs were greater (Sørensen, 1987). Initial experimental evidence from the site (Laverman et al. 2006; unpublished results of N_2O microprofiling) suggests that a significant portion of the nitrate reduction in the sediment occurs by processes other than denitrification. To examine how the competition between DNRA and denitrification affects the N-cycle at our site we conducted several steady state simulations while varying *f*DNRA from 0 (all denitrification) to 1 (all DNRA).

The removal of N entering the sediment (NO_3^- influx and N_{org} deposition) ranges from 63% to 18%, with maximum removal occurring at *f*DNRA=0 (Fig. 4.3a). The decreased N removal with increasing prevalence of DNRA leads to a shift from a situation where sediment is essentially neutral with respect to DIN efflux to one there the sediment is a net source with an efflux rate of 133 μmol cm^{-2} yr^{-1}. The NH_4^+ efflux ranged from 115 to 213 μmol cm^{-2} yr^{-1}. Such high NH_4^+ efflux rates have been found in other freshwater sediments (65-307 μmol cm^{-2} yr^{-1}; Gardner et al., 2001). However, in sediments with a greater rate of coupled nitrification-denitrification, the NH_4^+ efflux is typically lower as more N is released as N_2 (Seitzinger, 1988).

Nitrate influx decreased with increasing values of *f*DNRA (Fig. 4.3b), due to an accompanying increase in nitrification rate. In our simulations, much of the NO_3^- reduced in the sediment is transported from the overlying water, while only 15-30% of reduced NO_3^- is produced by nitrification (Fig. 4.1).

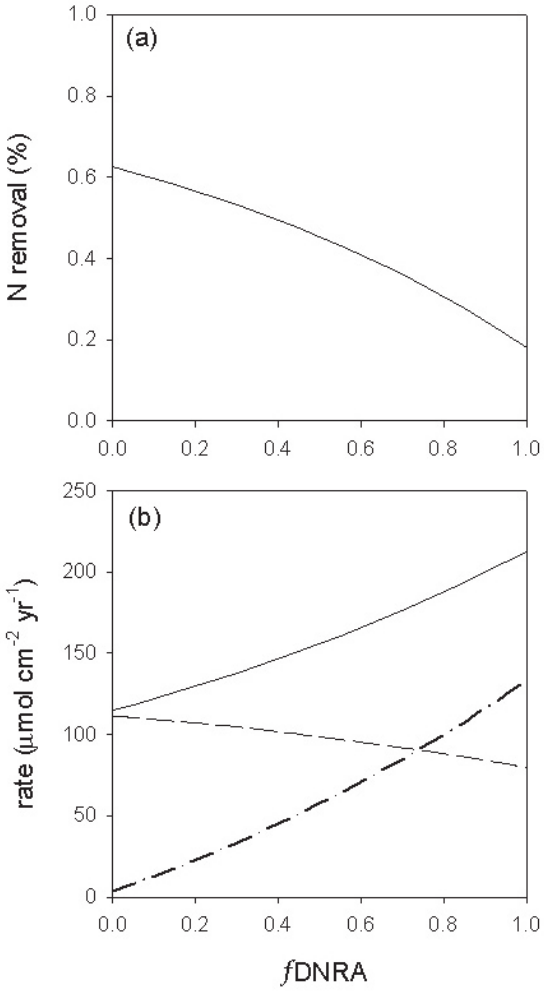

Figure 4.3 The N removal as a percentage of the total N influx to the sediment for steady-state simulations where *f*DNRA was varied from 0-1 (a). N removal is calculated from denitrification and burial (at 30 cm) and sediment input is N_{org} deposition and NO_3^- influx. The rates of sediment ammonium efflux (solid line), nitrate influx (dashed line), and net DIN efflux (dash dot line) versus *f*DNRA are presented in plot (b).

4.3.3 Ammonium adsorption response to salinization

The release of $NH_4^+{}_{ads}$ in response to increasing salinity was examined with a transient model simulation. Results from the steady-state simulation using the parameter values listed in Table 4.3 were used as the initial conditions in a simulation where the value of K_N was reduced from 10 to 1.3 based on an estimate for marine sediments (Mackin & Aller, 1984). The response of the sediment is very rapid. Over the first day, the NH_4^+ efflux was approximately 2.5 times greater than was observed for the initial conditions, primarily driven by the diffusive efflux (Fig. 4.4). Ammonium released to the pore water at depth is transported to the overlying water via bioirrigation, which responds more slowly. Ammonium efflux declines to rates that are 15% greater than found for the initial conditions after a 6-month simulation period (not shown).

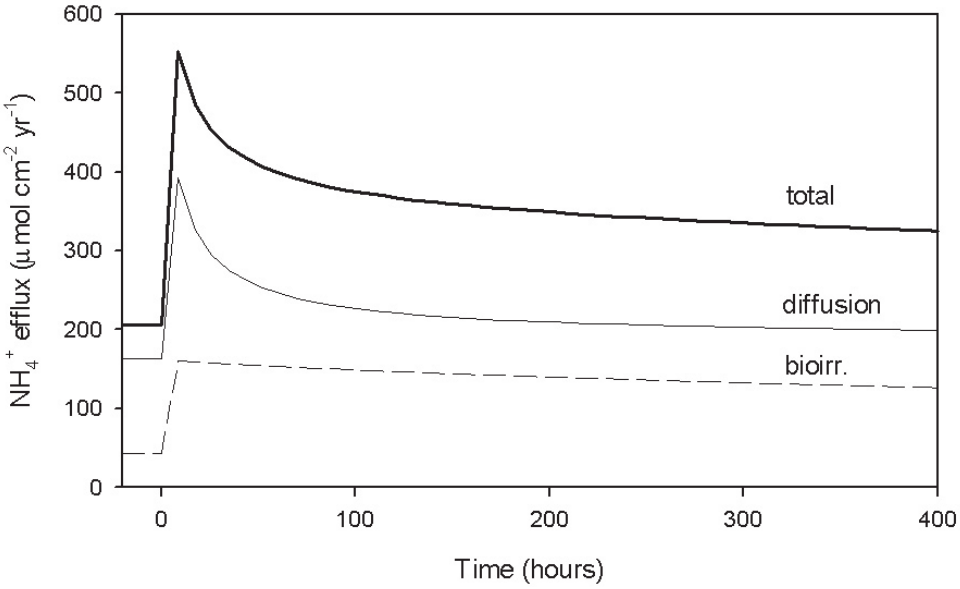

Figure 4.4 Ammonium efflux from freshwater sediment subject to salinization. Results determined in a transient simulation where K_N was initially 10 and reduced to 1.3 at the start of the simulation (time =0). Efflux by diffusion is the thin solid line, efflux via bioirrigation is the dashed line and the sum of the two processes is the thick solid line.

4.3.4 Estuarine Restoration

Restoration of the estuary will result in changes to the bottom water chemistry and sediment pore water. In addition to greater Na^+ and Cl^- concentrations, the coastal water adjacent to the dam contains less NO_3^- and more SO_4^{2-}. Salinity stratification in the water column is expected and this could further affect the chemistry of the bottom water, for example, by resulting in lower oxygen concentrations. Additionally, changes in the microbial population and benthic fauna are expected, which will affect rates of reaction and transport in the sediment. To examine the sediment response to these possible changes, steady-state simulations were run where parameters were changed to represent the new conditions. Many of the salinity-related changes result in small changes to the net DIN flux (positive values are efflux to overlying water) and sediment N removal (Table 4.4). All simulations conducted with *f*DNRA equal to zero showed greater N removal rates than those with *f*DNRA equal to 0.95. When denitrification dominated, DIN flux was sensitive to O_2 and NO_3^- concentrations. Lower O_2 concentration in the overlying water led to increased NO_3^- influx as demand for other terminal electron acceptors increased, while lower NO_3^- concentration in the overlying water limited its transport into the sediment. In the DRNA dominated simulations, net DIN efflux was lowered by decreasing the input flux of highly reactive organic matter (OM1) and by increasing the amount of bioturbative mixing (D_{b0}). Both of these processes reduce the rate of ammonification in the upper most part of the sediment, which in turn, lowers the diffusive efflux of NH_4^+ to the overlying water. The response of N removal to environmental changes is generally greater in the denitrification dominated sediment, since in the sediment where DNRA is most important, removal is controlled mainly by burial.

4.4 CONCLUSIONS

Competition between denitrification and DNRA has a significant impact on N removal in aquatic sediments as only denitrification removes N from the system. Salinization results in a rapid and transient release of adsorbed NH_4^+. When DNRA is a key pathway at our site, changes in the chemistry of the overlying water and in reaction and transport parameters expected upon salinization do not significantly change the N removal rates. The ratio of DNRA to denitrification and the rates of N_{org} input and ammonification are the most sensitive sediment processes for N removal in this study. Our results show that DNRA needs to be included in diagenetic models of the sediment N-cycle. Additionally, a better understanding of the controls on the interaction between DNRA and denitrification is needed before such models can be used as predictive tools.

Table 4.4 Sediment DIN flux (NH_4^+ efflux – NO_3^- influx) and N removal (denitrification + N_{org} burial) from steady-state simulations made to approximate possible changes resulting from estuarine restoration. Simulations were made with the initial conditions of only denitrification (*f*DNRA = 0) and where DNRA accounted for 95% of nitrate reduction (*f*DNRA = 0.95). Additional simulations where the input flux of labile organic matter (OM1) was decreased are also presented.

			*f*DNRA = 0		*f*DNRA = 0.95	
	initial	new	DIN flux	N removal	DIN flux	N removal
Parameter[a]	value	value	($\mu mol\ cm^{-2}\ yr^{-1}$)			
initial conditions		-	3	177	124	55
NO_3^- (μM)	154	90	39	141	126	53
SO_4^{2-} (mM)	0.64	10	3	177	124	55
O_2 (μM)	238	120	-42	222	121	57
K_N	10	1.3	7	177	129	55
D_{b0} ($cm^2\ yr^{-1}$)	5	25	-2	178	110	55
k_{NH4OX} ($\mu M^{-1} yr^{-1}$)	20	10	7	173	124	54
kOM1&2 (yr^{-1})	25, 0.01	50, 0.02	14	164	130	46
All of the above changes			7	165	127	47
input flux OM1 ($\mu mol\ cm^{-2}\ yr^{-1}$)	630	420	6	177	90	52

(a) see table 3 for a description of parameters

Acknowledgements We gratefully acknowledge the crew of the RV Navicula and members of the Utrecht University geochemistry research group for their help in the field. We thank Debby Los and Dineke van de Meent for analysis, and Parisa Jourabchi for the use of the reaction transport model. Philippe Van Cappellen, Gerard van den Berg, and Gertjan Zwolsman are acknowledged for their contributions to this project. The Netherlands Institute for Inland Water Management and Waste Water Treatment (RIZA) supported the fieldwork and RWC (contract no. RI-3494). AML was supported by a VENI fellowship of the Netherlands Organization for Scientific Research (NWO). CPS was supported by a fellowship of the Royal Netherlands Academy of Arts and Sciences (KNAW).

References

Aguilera, D. R., P. Jourabchi, C. Spiteri & P. Regnier, 2005. A knowledge-based reactive transport approach for the simulation of biogeochemical dynamics in earth systems. Geochemistry, Geophysics, Geosystems 6: Q07012.

An, S. M. & W. S. Gardner, 2002. Dissimilatory nitrate reduction to ammonium (DNRA) as a nitrogen link, versus denitrification as a sink in a shallow estuary (Laguna Madre/Baffin Bay, Texas). Marine Ecology-Progress Series 237: 41-50.

Anonymous, 1998. MER beheer Haringvlietsluizen report (Environmental Impact Report- Haringvliet dam management). Rijkswaterstaat directie Zuid-Holland, APV 98.186. (in Dutch).

Berner, R. A., 1980. Early diagenesis. A theoretical approach. Princeton University Press, Princeton NJ.

Boudreau, B. P., 1984. On the equivalence of nonlocal and radial-diffusion model for porewater irrigation. Journal of Marine Research 42: 731-735.

Canavan, R. W., C. P. Slomp, P. Jourabchi, P. Van Cappellen, A. M. Laverman & G. A. van den Berg, 2006. Organic matter mineralization in sediment of a coastal freshwater lake and response to salinization. Geochimica et Cosmochimica Acta 70: 2836-2855.

Cloern, J. E., 2001. Our evolving conceptual model of the coastal eutrophication problem. Marine Ecology-Progress Series 210: 223-253.

de Jonge, V. N., M. Elliott & E. Orive, 2002. Causes, historical development, effects and future challenges of a common environmental problem: eutrophication. Hydrobiologia 475: 1-19.

Gardner, W. S., S. P. Seitzinger & J. M. Malczyk, 1991. The effects of sea salts on the forms of nitrogen released from estuarine and freshwater sediments: Does ion pairing affect ammonium flux. Estuaries 14: 157-166.

Gardner, W. S., L. Y. Yang, J. B. Cotner, T. H. Johengen & P. J. Lavrentyev, 2001. Nitrogen dynamics in sandy freshwater sediments (Saginaw Bay, Lake Huron). Journal of Great Lakes Research 27: 84-97.

Gilbert, F., P. Souchu, M. Bianchi & P. Bonin, 1997. Influence of shellfish farming activities on nitrification, nitrate reduction to ammonium, and denitrification at the water-sediment interface of Thau lagoon, France. Marine Ecology Progress Series 151: 143-153.

Jourabchi, P., P. Van Cappellen & P. Regnier, 2005. Quantitative interpretation of pH distributions in aquatic sediments: A reaction-transport modeling approach. American Journal of Science 305: 919-956.

Kelly-Gerreyn, B. A., M. Trimmer & D. J. Hydes, 2001. A diagenetic model discriminating denitrification and dissimilatory nitrate reduction to ammonium in a temperate estuarine sediment. Marine Ecology-Progress Series 220: 33-46.

Laverman, A. M., P. Van Cappellen, D. van Rotterdam-Los, C. Pallud & J. Abell, 2006. Potential rates and pathways of microbial nitrate reduction in coastal sediments. FEMS Microbiology Ecology. in press.

Mackin, J. E. & R. C. Aller, 1984. Ammonia adsorption in marine sediments. Limnology and Oceanography 29: 250-257.

Magalhães, C. M., W. J. Wiebe, S. B. Joye & A. A. Bordalo, 2005. Inorganic nitrogen dynamics in intertidal rocky biofilms and sediments of the Douro River Estuary (Portugal). Estuaries 28: 592-607.

Megonigal, J. P., M. E. Hines & P. T. Visscher, 2003. Anaerobic metabolism: Linkages to trace gases and aerobic processes. In W. H. Schlesinger (ed.), Biogeochemistry. 8, Treatise on Geochemistry. H. D. Hollands and K. K. Turekian (eds.). Elsevier-Pergamon, Oxford: 317-424.

Ogilvie, B., D. B. Nedwell, R. M. Harrison, A. Robinson & A. Sage, 1997. High nitrate, muddy estuaries as nitrogen sinks: The nitrogen budget of the River Colne estuary (United Kingdom). Marine Ecology-Progress Series 150: 217-228.

Revsbech, N. P., J. P. Jacobsen & L. P. Nielsen, 2005. Nitrogen transformations in microenvironments of river beds and riparian zones. Ecological Engineering 24: 447-455.

Rysgaard, S., P. Thastum, T. Dalsgaard, P. B. Christensen & N. P. Sloth, 1999. Effects of Salinity on NH_4^+ Adsorption Capacity, Nitrification, and Denitrification in Danish Estuarine Sediments. Estuaries 22(1): 21-30.

Saunders, D. L. & J. Kalff, 2001. Nitrogen retention in wetlands, lakes and rivers. Hydrobiologia 443: 205-212.

Seitzinger, S. P., 1988. Denitrification in freshwater and coastal marine ecosystems: Ecological and geochemical significance. Limnology and Oceanography 33: 702-724.

Seitzinger, S. P., W. S. Gardner & A. K. Spratt, 1991. The effect of salinity on ammonium sorption in aquatic sediments: Implications for benthic nutrient recycling. Estuaries 14: 167-174.

Smit, H., R. Smits, G. van der Velde & H. Coops, 1997. Ecosystem responses in the Rhine-Meuse delta during two decades after enclosure and steps toward estuary restoration. Estuaries 20: 504-520.

Sørensen, J., 1987. Nitrate reduction in marine sediment: pathways and interactions with iron and sulfur cycling. Geomicrobiology Journal 5: 401-421.

Stief, P., A. Schramm, D. Altmann & D. de Beer, 2003. Temporal variation of nitrification rates in experimental freshwater sediments enriched with ammonia or nitrite. FEMS Microbiology Ecology 46: 63-71.

Van Cappellen, P. & Y. F. Wang, 1996. Cycling of iron and manganese in surface sediments: A general theory for the coupled transport and reaction of carbon, oxygen, nitrogen, sulfur, iron, and manganese. American Journal of Science 296: 197-243.

Westrich, J. T. & R. A. Berner, 1984. The role of sedimentary organic matter in bacterial sulfate reduction: the G-model tested. Limnology and Oceanography 29: 236-249.

Windolf, J., E. Jeppesen, J. P. Jensen & P. Kristensen, 1996. Modelling of seasonal variation in nitrogen retention and in-lake concentration: A four-year mass balance study in 16 shallow Danish lakes. Biogeochemistry 33: 25-44.

Chapter 5

Phosphorus cycling in the sediment of a coastal freshwater lake and response to salinization

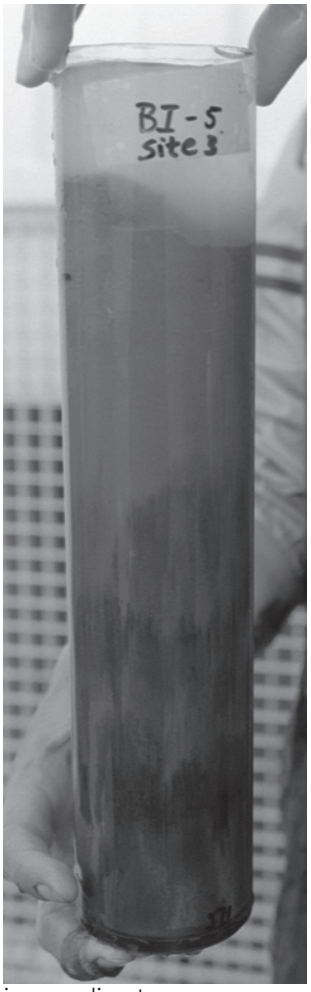

image: sediment core

R.W. Canavan and C.P. Slomp
in preparation

ABSTRACT

Pore water and solid phase data for sediments from Haringvliet Lake (The Netherlands) are used to investigate the coupling between the sedimentary cycles of iron (Fe), sulfur (S) and phosphorus (P). The data are interpreted with an existing multi-component reaction transport model, which is expanded to include P diagenesis. Extraction data provide evidence for the abundant presence of a reducible Fe-P mineral (P-Fe(III)) in the surface sediment with an average molar Fe:P ratio of 2.6. Model results indicate that release of P from this phase through reductive dissolution dominates the input of PO_4 to the pore water in the upper 20 cm of the sediment. Furthermore, the results suggest that ~56% of the total P deposited on the sediment is returned to the overlying water through diffusion and bioirrigation. The remaining P is buried in the form of organic P (P-org), P-Fe(III) and another inorganic P mineral phase (P-min). P-min accounts for 50% of total P burial and may be actively forming in the sediment. Additional model simulations are performed to predict possible changes in P-cycling that may result from estuarine restoration of the site. These simulations predict a lower preservation of P-Fe(III) as a result of increased sulfate reduction and reduction of the Fe(III) by sulfide. The results also show that benthic P release is more sensitive to changes in the sediment mixing regime than to bottom water sulfate concentrations.

5.1 INTRODUCTION

Benthic phosphorus (P) release is important in determining the water quality in many shallow aquatic systems. This internal source of P typically explains the slow response of many lakes to reduced external P inputs (Sondergaard et al. 2003). Benthic P release is particularly apparent in lakes where periodic bottom water anoxia leads to enhanced release of P from Fe-oxyhydroxides from previously oxic surface sediments (Einsele 1936; Mortimer 1941). Significant benthic release of P may also occur from oxic sediments without such temporal redox changes, however. This release is driven by organic matter degradation at the sediment-water interface (e.g. Martens et al. 1978) and biologically enhanced transport of dissolved or adsorbed PO_4 from greater sediment depths (Aller 1980; Matisoff and Wang 1998; Meile and Van Cappellen 2003; Schink and Guinasso 1978; Slomp et al. 1998). Thus, long-term trends in benthic release of P from oxic surface sediments are often strongly determined by the retention of P in the underlying anoxic sediment (Gächter and Müller 2003; Moosmann et al. 2006).

The major burial forms of P in anoxic freshwater sediments are organic-P, P associated with Fe(III) oxyhydroxides, Fe(II) phosphate minerals (e.g. vivianite, $Fe_3(PO_4)_2 \cdot 8H_2O$) and calcium phosphates; House, 2003). The burial of Fe(III) bound P and the formation of ferrous phosphate minerals are both limited when sulfate reduction rates in the sediment are high. Dissimilatory

Fe(III) reduction is typically limited in freshwater environments, making chemical reduction of Fe(III) bound P by sulfides a major removal process (Canavan et al. 2006; Roden and Edmonds 1997; Wersin et al. 1991). Thus, in freshwater sediments where sulfate reduction rates are low, Fe(III)-oxyhydroxides may be an important sink for P. This has been observed, for example, in sediments of the freshwater part of the western Scheldt estuary where Fe(III)-bound P accounts for up to 70% of total P burial (Hyacinthe and Van Cappellen 2004). Ferrous phosphate minerals such as vivianite are also most important as a sink for P when rates of sulfate reduction are low because the Fe^{2+} required for their formation is otherwise removed to FeS and FeS_2 (Gächter and Müller 2003).

Coastal freshwater systems worldwide are expected to be increasingly encroached by saline waters due to sea level rise and greater demands for fresh water. By increasing sulfate availability, salinization of freshwater sediment may stimulate sulfate reduction rates and the release of dissolved P (Blomqvist et al. 2004; Caraco et al. 1990; 1989). Sulfate reduction rates are also very sensitive to other factors, such as bottom water oxygen concentrations and organic matter availability (Canavan et al. 2006). We expect that in particular changes in benthic macrofaunal communities (Nixon 1988) and associated increased downward bioturbative transport of organic matter could play a major role in reducing P preservation upon salinization.

In this study, we quantitatively describe the sedimentary P cycle and its coupling to the carbon, iron and sulfur cycles in a sediment of a coastal freshwater lake (Haringvliet Lake, The Netherlands) and assess the response to salinization. We use a 1D reactive transport model (RTM) for organic matter mineralization (Canavan et al. 2006) expanded with P diagenesis. Part of the lake will become brackish from 2008 onwards as part of an ecological restoration project. This makes it a suitable site to evaluate the expected response of the sedimentary P cycle to increased seawater input.

5.2 MATERIALS AND METHODS

5.2.1 Site description

The Haringvliet is a eutrophic freshwater lake located in the southwest of the Netherlands (Fig. 5.1). It was created as a result of the damming of the mouth of an estuary in 1970, as part of the Dutch Delta Project. Prior to dam construction, the Haringvliet was a tidal estuary and an outlet of the Meuse-Rhine river system to the North Sea (Ferguson and Wolff 1984; Smit et al. 1997). The lake still maintains a riverine quality, with highly variable flow conditions (Smit et al. 1997). Phosphorus levels in the lake closely follow those of the river input and declined substantially in response to improved waste-water treatment in the river watershed over the past decades (de Wit 1999). Thus, water column dissolved inorganic P concentrations in the

Haringvliet, which were on average 8 μM in 1977 (van Eck 1982) are now down to 2.4 μM (2001-2003; Rijkswaterstaat, www.waterbase.nl). The present study is part of a larger effort to assess how benthic biogeochemistry may respond to seawater intrusion in the lake (Canavan et al. 2006; Laverman et al. 2006; Chapter 3). Our study site is located near the dam, within the area that will be most impacted by salinization (Fig. 5.1). The sediment at the site is highly porous and fine-grained (Canavan et al. 2006).

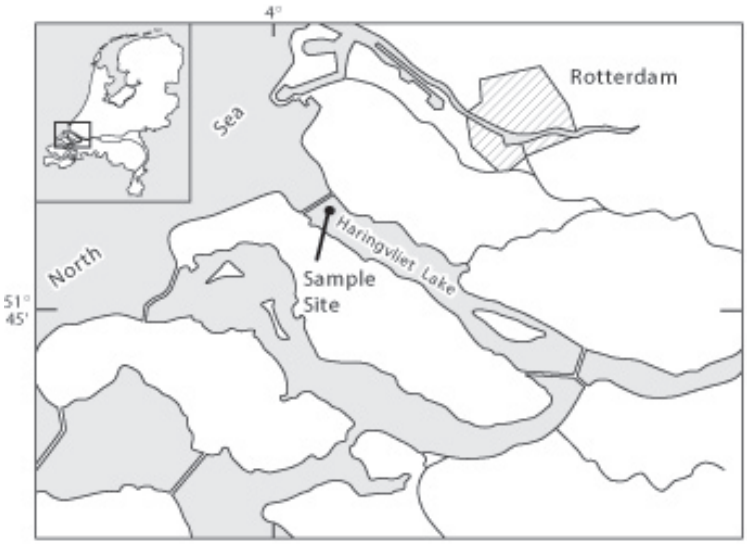

Figure 5.1 The sampling location in Haringvliet Lake. The inset map shows the Netherlands with a box denoting the location of the detail section. The Rhine-Meuse river complex flows into the lake in the east and the lake discharges through the dam at the western limit of the lake.

5.2.2 Sample collection

The site was sampled in fall (November 2001), late-summer (September 2002), and spring (April 2003). Sediment was collected using a cylindrical box corer (31 cm i.d.) deployed from RV Navicula. Each box core contained approximately 40 cm of surface sediment and 30 cm of overlying water. Sub-cores for pore water and sediment analyses were taken from a single box core (10 cm i.d.). The sub-cores were immediately sectioned in a N_2 purged glove box on board the ship in a temperature-controlled laboratory. Sediment was centrifuged at 2500 *g* for 10 to 30 minutes in polyethylene tubes to collect pore water.

5.2.3 Pore water analyses

After centrifugation, the pore water was filtered through 0.2 μm (fall and late-summer) or 0.45 μm (spring) pore size filters in a N_2 purged glove tent. Sub-samples for total dissolved metals (e.g. Fe) were acidified with suprapur HNO_3 (10 μl conc. HNO_3 per ml pore water) and analyzed by ICP-MS. Sub-samples for total phosphate analysis were acidified with HCl (10 μl conc. HCl per ml pore water) and determined colorimetrically on a nutrient auto-analyzer (Bran and Luebbe). Nitrate and ammonium concentrations were determined with the auto-analyzer using an additional un-acidified sub-sample. Sulfate determination was made by ion chromatography (Dionex DX-120). Samples for metal and phosphate analysis were stored at 4 °C prior to analysis, and samples for nitrate, ammonium, and sulfate were stored frozen.

Dissolved oxygen microprofiles were obtained on board using a Clark-type oxygen sensor with an internal reference and a guard cathode (Revsbech 1989) attached to a micromanipulator. Perspex cores (4.2 cm i.d.) with 10 cm sediment and 5 cm overlying water were collected from a box core. The surface of each core was sparged with air and profiling was completed within 30 minutes of core retrieval (Canavan et al. 2006). Pore water thermodynamic speciation modeling was conducted using Visual MINTEQ (Version 2.4, this program is an adaptation of MINTEQA2; Allison et al. 1991). Calculations included the following constituents: Na^+, Ca^{2+}, Mg^{2+}, K^+, NH_4^+, SO_4^{2-}, Cl^-, PO_4^{3-}, HS^-, Alkalinity, pH, Fe^{2+}, Mn^{2+}, Co^{2+}, Ni^{2+}, Zn^{2+}, Pb^{2+}.

5.2.4 Solid phase extraction and analysis

The water content and density of the sediment were determined from the weight loss upon freeze-drying. Total organic carbon (following carbonate removal with 1 M HCl) was determined on freeze-dried sediment using an elemental analyzer (LECO SC-1440H). Total Fe and P were determined by ICP-MS after HF-$HClO_4$-HNO_3 digestion of freeze dried sediment as described in Hyacinthe and Van Cappellen (2004). Extractions with buffered ascorbic acid (Hyacinthe and Van Cappellen 2004; Kostka and Luther 1994), with citrate-dithionite-bicarbonate (CDB; Ruttenberg 1992), and 1M HCl were conducted with wet sediment in an Ar purged glove tent with subsequent Fe and P analysis (ascorbate and 1M HCl by ICP-MS, CDB by ICP-OES). An additional kinetic ascorbate extraction was conducted on a freeze-dried sample (0-0.5 cm depth interval; Hyacinthe and Van Cappellen, 2004). Extractant sub-samples were collected throughout a 25-hour extraction period with Fe and P analysis by ICP-OES. Organic P was estimated from the difference between total and HCl-extractable P (Aspila 1976). Ascorbate and CDB-extactable P are assumed to represent P bound to more easily reducible Fe-phases (Hyacinthe and Van Cappellen 2004) and total Fe(III)-bound P, respectively (Ruttenberg 1992). The difference between 1 M HCl and CDB-extractable P is

used as a measure of additional inorganic P phases not associated with reducible Fe-phases.

5.2.5 Reactive-transport modeling

A multi-component reactive transport model (RTM) was developed to quantitatively describe organic carbon decomposition in 1-D sediment profiles at our study site. This model includes a reaction network of 24 chemical species and 32 reactions, and is described in detail in Canavan et al. (2006). Here, the RTM is extended to include P diagenesis. Five pools of P are considered: dissolved inorganic P (PO_4), adsorbed P (P-ads), sediment organic P (P-org), Fe(III)- bound P (P-Fe(III)), and an additional inorganic solid phase (P-min; Table 5.1).

Table 5.1 Species and reactions of P in the model

Species	*Boundary condition*[a]	*notes*
PO_4	4.0 μmol l^{-1}	Measured in bottom water
P-org	9.0 μmol cm^{-2} yr^{-1}	Linked to the influx of OM through C:P ratios
P-Fe(III)	14.6 μmol cm^{-2} yr^{-1}	Linked to the influx of Fe-oxides through a Fe:P ratio
P-min	3.2 μmol cm^{-2} yr^{-1}	Influx is used to fit the measured profile
P-ads	1.5 μmol g^{-1}	Determined from equilibrium conditions

Reactions	*Rate law*
Organic P mineralization[b]	
$[(CH_2O)_x(\mathbf{PO_4})_z] + TEA_{ox} \rightarrow z\mathbf{PO_4} + xCO_2 + xH_2O + TEA_{red}$	$k_{OM}\,[OM]\,f_{TEA}$
Reductive dissolution of P-Fe	
$4\mathbf{Fe(OH)_3A\text{-}P} + [(CH_2O)_x(\mathbf{PO_4})_z] \rightarrow 4\mathbf{PO_4}$ /FeP ratio $+ z\mathbf{PO_4} + 4Fe^{2+} + xCO_2 + xH_2O$	$k_{OM}\,[OM]\,f_{Fe(OH)3A}$
$8\mathbf{Fe(OH)_3A,\ B\text{-}P} + HS^- \rightarrow 8\mathbf{PO_4}$ /FeP ratio $+ 8Fe^{2+} + SO_4^{2-}$	$k_{HSFe}\,[HS^-]\,[Fe(OH)_3]$
P-Fe precipitation	
$\mathbf{PO_4}$ /FeP ratio $+ Fe^{2+} + ¼O_2 + 2HCO_3^- + ½\,H_2O \rightarrow \mathbf{Fe(OH)_3A\text{-}P} + 2\,CO_2$	$k_{FeOx}\,[O_2]\,[Fe^{2+}]$
$2\mathbf{PO_4}$ /FeP ratio $+ 2Fe^{2+} + MnO_2 + 2\,HCO_3^- + 2H_2O \rightarrow 2\mathbf{Fe(OH)_3A\text{-}P} + Mn^{2+} + 2\,CO_2$	$k_{FeMn}\,[MnO_2]\,[Fe^{2+}]$
P-mineral precipitation	
$\mathbf{PO_4} \leftrightarrow \mathbf{P\text{-}min}$	$k_{min}\,(PO_4 - P_{eq})$
Phosphate adsorption	
$\mathbf{PO_4} \leftrightarrow \mathbf{PO_4\text{-}ads}$	$K_P\,[PO_4]$

(a) Lower boundary conditions for all species is zero flux, where the lower boundary is at 100 cm
(b) Organic matter is represented by the formula $[(CH_2O)_x(PO_4)_z]$ where x/z is the C/P ratio. A generalized mineralization reaction is depicted where TEA_{ox} and TEA_{red} represent the oxidized and reduced terminal electron acceptor. The fraction of total OM degradation by each TEA is abbreviated as fTEA. The production and consumption of H^+ in the reactions is linked to carbonate equilibrium: $H^+ + HCO_3^- \leftrightarrow CO_2 + H_2O$.

Reactions include organic P mineralization, reductive dissolution and precipitation of P-Fe(III), precipitation of another P-mineral phase and equilibrium sorption of P (Table 5.1). Rate laws and parameter values used to describe the reaction and transport of P are given in Tables 5.1 and 5.2, respectively. Three pools of organic matter are included in the model: a highly reactive pool (OM1), a less reactive pool (OM2), and a non-reactive pool (OM3). The decomposition of the organic matter of each pool is modeled as a first order process defined by a rate constant kOM (yr^{-1}). The distribution of the total organic matter decomposition rate over the different terminal electron acceptor (TEA) pathways follows the approach of Van Cappellen and Wang, (1996). In this approach a limiting concentration (Km) is assigned to each TEA. When the TEA concentration exceeds Km, the corresponding degradation pathway is not limited by the TEA availability. When the TEA concentration drops below Km, the corresponding primary redox pathway is limited by the concentration of the TEA, and energetically less favorable TEAs are allowed to compete for the organic substrates, in the prescribed order: O_2, NO_3^-, Mn-oxides, Fe-oxides, SO_4^{2-}, and finally organic matter (methanogenesis).

The release of PO_4 is related to the rate of carbon mineralization through the C:P ratio assigned to each fraction (Table 5.2). The reductive dissolution of Fe-oxides leads to the release of associated PO_4 (Table 5.1). The model includes two Fe-oxide pools: pool A is available as a terminal electron acceptor for carbon mineral and for the oxidation of sulfide, and pool B is only reactive with sulfide (Berg et al. 2003). Conversely, the oxidation of Fe^{2+} results in the precipitation of P-Fe(III) ($Fe(OH)_3A$-P). The amount of P release and removal is related to reactions of Fe by a Fe:P ratio (Table 5.2). An additional mineral precipitation reaction is included in the model where PO_4 removal occurs when the pore water concentration, $[PO_4]$, exceed an equilibrium value, P_{eq}, and the rate of reaction is determined by the rate constant k_{min} (Slomp et al. 1996):

$$R = k_{min} ([PO_4] - P_{eq}) \quad (1)$$

The equilibrium adsorption of PO_4 is included in the model as a linear isotherm:

$$P\text{-}ads = K_p [PO_4] \quad (2)$$

where K_p is the equilibrium constant ($cm^3\ g^{-1}$) and is dependent on the concentration of $FeOH_3A$ (Table 5.2).

Table 5.2 Initial parameter values and distributions[a]

Parameter	Value	Unit	Description
k_{OM1}	25-1	yr^{-1}	degradation rate constant OM1
k_{OM2}	0.01	yr^{-1}	degradation rate constant OM2
k_{OM3}	0	yr^{-1}	degradation rate constant OM3
$C:P_{OM1}$	112	mol:mol	C:P ratio OM1; estimated from Koelmans (1998)
$C:P_{OM2}$	200	mol:mol	C:P ratio OM2; estimated from SPM data
$C:P_{OM3}$	300	mol:mol	C:P ratio OM3; model fitting
FePratio	2.6	mol:mol	Fe:P ratio; estimated from reactive extractions
k_{HSFe}	2.5×10^{-3}	$\mu M^{-1}\ yr^{-1}$	rate constant for sulfide reduction of Fe-oxides
k_{FeOx}	5×10^{1}	$\mu M^{-1}\ yr^{-1}$	rate constant for Fe^{2+} oxidation by O_2
k_{FeMn}	1×10^{-1}	$\mu M^{-1}\ yr^{-1}$	rate constant for Fe^{2+} oxidation by Mn-oxides
k_{min}	3	yr^{-1}	rate constant for the precipitation of P-min; model fitting
P_{eq}	4.0	$\mu mol\ l^{-1}$	equilibrium concentration of PO_4 (eq. 1); set to the overlying water concentration of PO_4
K_P	960 x $Fe(OH)_3A$	$cm^3\ g^{-1}$	PO_4 adsorption coefficient (eq. 2); K_P = 38 $cm^3\ g^{-1}$ at x=0 (Krom and Berner 1980)
ω	1.0	$cm\ yr^{-1}$	sediment accumulation rate
ρ	2.1	$g\ cm^{-3}$	sediment density
α_0	10	yr^{-1}	bioirrigation coefficient at surface
D_{b0}	5	$cm^2\ yr^{-1}$	bioturbation coefficient at surface
λ	2.5	cm^{-1}	D_b depth attenuation coefficient
φ_o	0.89	$cm^3\ cm^{-3}$	porosity at surface
φ_∞	0.79	$cm^3\ cm^{-3}$	porosity at depth
τ	0.2	cm^{-1}	φ depth attenuation coefficient
x	0-30	cm	sediment depth
Depth distributions			Description
$\alpha = \begin{cases} \alpha_0 \left(1 - e^{(x-17)}\right) & (x \le 17\,cm) \\ 0 & (x > 17\,cm) \end{cases}$			distribution of bioirrigation coefficient α
$D_b = D_b0\ e^{-(x/\lambda)}$			distribution of bioturbation coefficient D_b
$\varphi(x) = \varphi_\infty + (\varphi_o - \varphi_\infty)e^{-(\tau x)}$			porosity distribution

(a) See (Canavan et al. 2006) for further information about the source or derivation of reaction rate constants, and transport parameters.

The model includes transport of solutes by molecular diffusion, bioirrigation, bioturbation, and advection (burial). Transport of solids occurs by bioturbation and advection. Molecular diffusion and the associated tortuosity and temperature effects are included as described in Van Cappellen and Wang (1996). Bioirrigation is represented as a non-local exchange with the surface water of which the intensity is controlled by the coefficient, α (Boudreau 1984); and bioturbation is parameterized using an additional diffusion term, D_b (Berner 1980). The advective velocity of solids and solutes is determined from the sediment accumulation rate, ω (cm yr^{-1}) and porosity (φ) as described by Berner (1980). Table 5.2 includes a list of parameter values used in the model including the depth distributions of α, D_b, and φ.

5.3 RESULTS

5.3.1 Pore water

Oxygen and nitrate are depleted within the uppermost centimeter of the sediment, implying high rates of oxygen respiration and nitrate reduction (Fig. 5.2). Dissolved Fe pore water concentrations are low in the upper 4 cm and then increase with depth, particularly below 13 cm depth. Sulfate concentrations in pore water decline with increasing depth. The sulfate pore water profile in fall displays a gradual removal over the upper 20 cm, while in spring sulfate penetrates to 5 cm depth. In late-summer, a relatively constant concentration of approximately 50 μM is found in the depth range of 5-15cm. The pore water profiles for NH_4^+ increase with depth particularly below the zone of bioirrigation (>17 cm). Pore water phosphate concentrations are highly variable but generally show a maximum between 5 and 20 cm depth and then decline, suggesting removal at depth. Pore water PO_4 concentrations were greater in late-summer than during the other sample periods.

5.3.2 Solid phase

Organic C and P concentrations (Fig. 5.3) decrease only gradually with depth in the sediment, suggesting that the major part of the organic matter is refractory. Profiles of ascorbate- and CDB-extractable Fe and P also decrease with depth. Ascorbate-extractable P comprised approximately 40% of total P with an average Fe:P ratio of 2.6. A kinetic ascorbate extraction of surface sediment gave approximately the same Fe:P ratio (Fig. 5.4). Extraction of the sediment with CDB led to dissolution of significant additional Fe but only little P. This suggests that most of the P-Fe(III) in the sediment is associated with easily reducible Fe-phases. Increased concentrations of another mineral P phase (P-min) with depth suggest possible authigenic P mineral formation. Saturation index values determined for several P containing minerals show super-saturation of the sediment pore water with respect to various minerals, including vivianite ($Fe_3(PO_4)_2 8H_2O$), ($MnHPO_4$) and hydroxyapatite ($Ca_5(PO_4{:}H_2O)$) (Table 5.3).

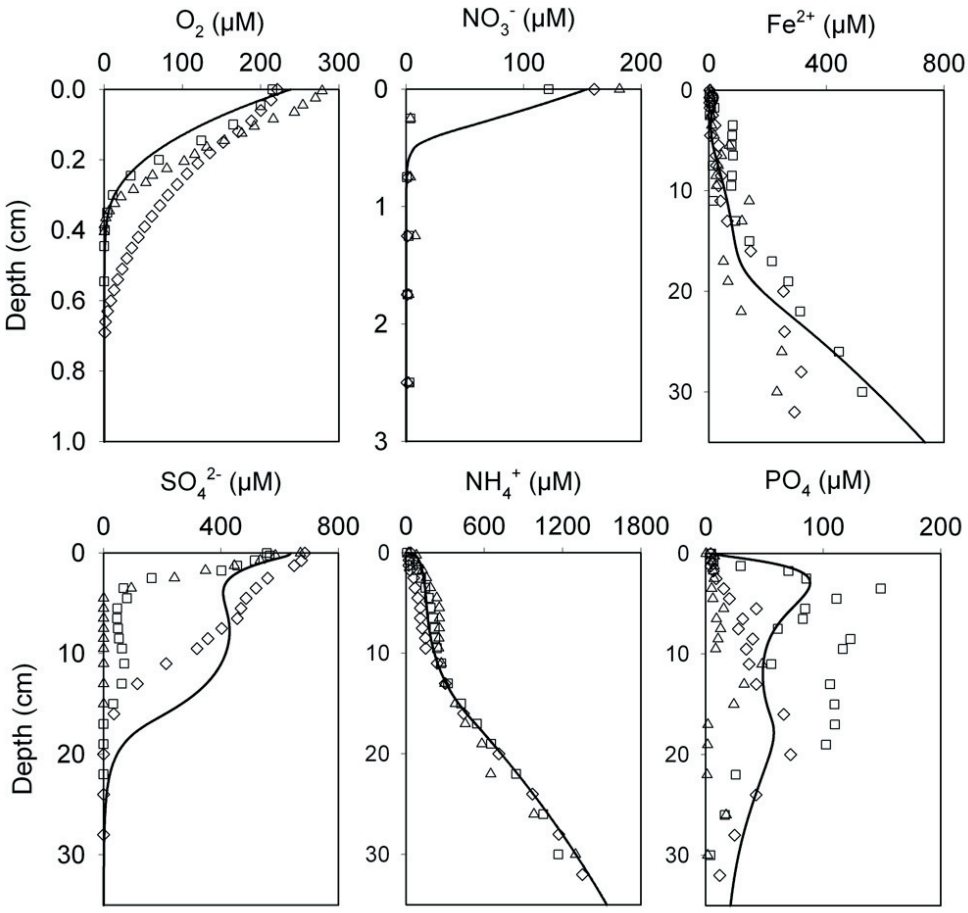

Figure 5.2 Porewater profiles of O_2, NO_3^-, Fe^{2+}, SO_4^{2-}, NH_4^+ and PO_4 from fall (◇), late-summer (□), and spring (△). Model fits are plotted as continuous lines in the plots. Note the change in depth scale for O_2 and NO_3^-.

5.4 DISCUSSION

5.4.1 Present-day sedimentary P cycle

The solid curves in Figures 5.2 and 5.3 represent the output of the steady state solution of the model fitted to the full data set. For the model calculations, a steady state approach was used since a fully transient simulation of the seasonal variations in sediment biogeochemistry proved unfeasible, primarily because the temporal evolution of the boundary conditions at the sediment-water interface could not be constrained. A detailed description of the estimation of parameters and boundary conditions is given by Canavan et al. (2006). Two additional

parameters were adjusted for the fitting of P output to experimental results: the rate constant for P-min precipitation and the C:P_{OM3} ratio.

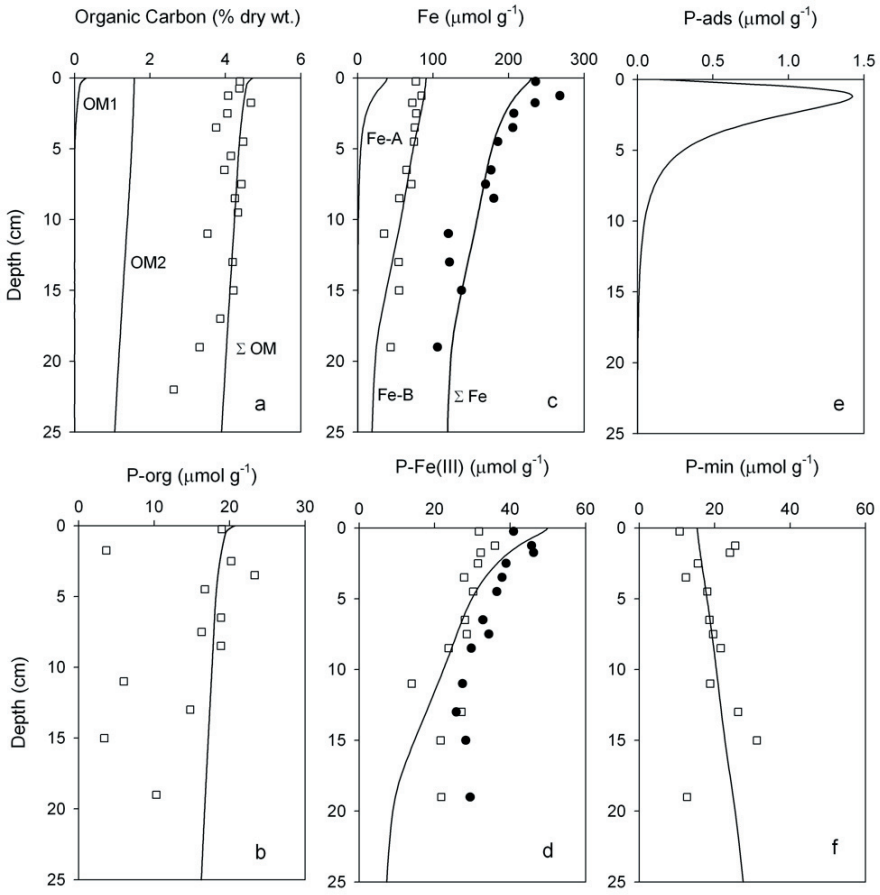

Figure 5.3 Sediment solid phase distributions where model results are given as solid lines. (a) Depth distribution of the measured total organic carbon (□) and model distributions of the reactive organic carbon pools OM1, OM2, and the sum of the three OM pools (Σ OM). Extraction estimates of the P-org pool (□) as determined by the difference of the total and HCl extractions (b). Sediment distributions of ascorbate (□) and CDB (•) extractable Fe and model distributions of $Fe(OH)_3A$, $Fe(OH)_3B$, and total Fe-oxides where an additional non-reactive pool is added (c). Sediment distributions of ascorbate (□) and CDB (•) extractable P(d)and modeled P-Fe(III) pool. The model distribution of P-ads is depicted in plot (e). The difference P concentrations obtained from the HCl and CDB extractions is included in plot f (□) and represents P-min, additional mineral pool(s). All sediment sample results are obtained from sediment collected in late-summer.

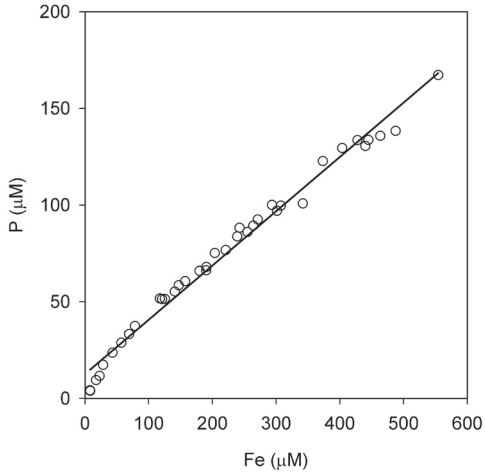

Figure 5.4 Extraction solution concentrations of P versus Fe in μmol l^{-1} from the kinetic ascorbate extraction. Samples were collected periodically over a 25-hour extraction conducted on a freeze-dried sediment sample from 0-0.5 cm depth collected in late-summer.

Table 5.3 Saturation Index (SI) values for selected P-containing minerals determined from pore water solute concentrations collected in September, 2002 (late-summer) and April, 2003 (spring). The SI values were determined using visual MINTEQ v2.32, where SI is determined as the difference of the Log Ion Activity Product (Log IAP) and the Log solubility product of the mineral (Log K_{sp}).

depth range	vivianite		$MnHPO_4$		hydroxyapatite		$CaPO_4$	
(cm)	Sept.	April	Sept.	April	Sept.	April	Sept.	April
1.0 - 1.5	1.74	0.45	3.17	3.06	8.24	6.77	-0.88	-1.44
2 - 3	1.05	-0.06	3.62	3.08	8.91	4.81	-0.42	-1.54
4 -5	6.13	0.82	3.70	2.96	9.62	4.29	-0.32	-1.60
6 - 7	6.00	2.00	3.54	3.12	9.28	4.34	-0.43	-1.46
9-10	6.16	1.43	3.60	2.95	9.90	4.70	-0.26	-1.46
10-12	3.00	5.10	3.25	3.61	8.34	7.00	-0.59	-0.72

As can be seen from the profiles (Figs. 5.2 and 5.3), the model is able to simultaneously reproduce the majority of the observed trends in the concentration profiles. Results suggest that oxic degradation (55%), denitrification (21%) and sulfate reduction (17%) are currently the main organic carbon degradation pathways in the upper 30 cm of the sediment at this site (Canavan et al. 2006). Most organic matter degradation occurs in the upper 2 cm of the sediment. The more rapid removal of SO_4^{2-} in spring may represent a reduction in bioirrigative transport rather than an increased sulfate reduction rate (Canavan et al. 2006).

The sedimentary P cycle as calculated with the model is presented in Figure 5.5. The results show that release from P-Fe(III) is the dominant source of dissolved P in the sediment accounting for 75% of the total PO_4 released over the upper 20 cm of the sediment. Model calculations suggest that 58% of the Fe-oxide reduction is coupled to organic matter mineralization, with the remaining being accounted for by reaction with sulfide. The relatively low (~2.6) and constant molar Fe:P ratio with depth and nearly-identical dissolution kinetics of P and Fe in ascorbate solution (Fig. 5.4) suggest the presence of a relatively stable hydrous ferric phosphate mineral. Evidence for a discrete Fe-P phase was previously reported for suspended matter in Haringvliet Lake (van Eck 1982) and for sediments in the Scheldt estuary (Hyacinthe and Van Cappellen 2004). The P-Fe(III) phase is responsible for 17% of the total P burial below 20 cm depth. P-org is the other major source of pore water PO_4 and accounts for 33% of the total burial at 20 cm (Fig. 5.5).

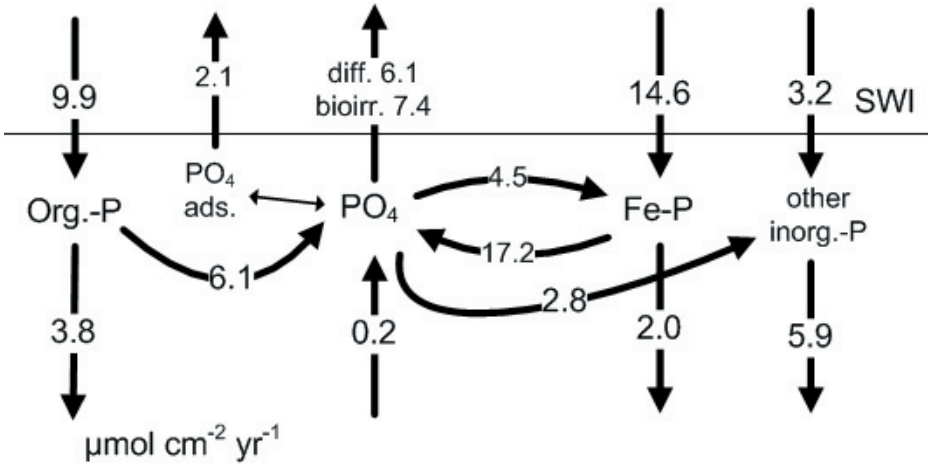

Figure 5.5 Schematic representation of the modeled sediment P cycle. All rates and fluxes are presented in units of μmol cm^{-2} yr^{-1}. The upper boundary of the calculation is the sediment water interface (SWI) the lower boundary is 20 cm depth..

Approximately 64% of the P-org and P-Fe(III) deposited on the sediment is released to the overlying water through bioirrigation (47%) and diffusion (53%). Reversible sorption in combination with bioturbation enhances the upward diffusive flux of dissolved P (Schink and Guinasso 1978; Slomp et al. 1998) and accounts for 25% of the total diffusive release at the sediment-water interface.

Currently unidentified authigenic P mineral phases are responsible for 50% of the total P burial below 20 cm depth (Fig. 5.5). Our thermodynamic calculations suggest that vivianite, $MnHPO_4$, and/or hydroxyapatite could be forming in the sediment (Table 5.3).

5.4.2 Response to Estuarine Restoration

The model is used to examine potential changes in P release from the sediments that could result from the restoration of estuarine conditions at our study site. We focus on two expected changes in detail: increased sulfate concentrations and increased sediment mixing by bioturbation. The sensitivity of sulfate reduction rates and benthic P release to changes in these parameters is examined using steady-state simulations.

Bottom water sulfate was varied through a range of 0.1 to 20 mM where the current concentration is approximately 0.64 mM in the lake and 10 mM in the water adjacent to the lake outside of the dam. Maximum P release was found at bottom water concentrations in the range of 0.64-3.0 mM (Fig. 5.6). The rate sulfate reduction was significantly limited by sulfate availability at 0.1 mM, allowing for increased P-Fe(III) burial. The rate of sulfate reduction remains relatively constant at bottom water concentrations above 1.5 mM, where the rate of sulfate reduction is limited by the availability of organic matter substrate. A decline in the rate of P release is observed as sulfate concentrations are increased from 3 to 5 mM (Fig. 5.6a). This result is caused by increased pyrite precipitation, which is a terminal sink for sulfide in the model, and therefore limits sulfide reaction with Fe-oxides. An additional simulation where the rate constant for pyrite formation was reduced by a factor 100 resulted in an increase in the rate of P release from the initial condition of 15.6 to 18.0 $\mu mol\ cm^{-2}\ yr^{-1}$, but did not change the sulfate reduction rate (Fig. 5.6a-b). In reality, the reduction of P-Fe(III) may outcompete pyrite formation for reaction with sulfide in the sediment.

Additional changes examined included a 50% reduction in bottom water oxygen concentration and the elimination of the mineral precipitation reaction. Bottom water oxygen levels may decrease if salinity stratification limits the mixing of the bottom waters. Lower O_2 concentrations increased the availability of organic matter for sulfate reduction, which lead to both higher sulfate reduction rates and P release rates (19.0 $\mu mol\ cm^{-2}\ yr^{-1}$). Salinization will affect the solubility of P minerals. The formation of vivianite may be limited under high sulfide conditions. Eliminating the formation of the P-mineral pool increases the P release to (16.6 $\mu mol\ cm^{-2}\ yr^{-1}$) but does not influence the rate of sulfate reduction.

The bioturbation coefficient, D_b, was varied from 1.25 to 12.5 ($cm^2\ yr^{-1}$; 0.25-2.5 times the initial value). The release of P from the sediment increases with increasing values of D_b throughout the range of values tested (Fig. 5.6). The burial of P-Fe(III) below 20 cm depth

declined to nearly zero at the highest values of D_b. Sulfate reduction was favored by increasing mixing rates because more highly reactive organic matter was mixed deeper in the sediment below the penetration depth of O_2 and NO_3^-, and FeS was mixed to the surface increasing oxygen consumption. An increase in sulfate concentration from the existing 0.64 mM to 10 mM has little effect on the distribution of P release and sulfate reduction in the bioturbation sensitivity analysis (Fig. 5.6c,d) as sulfate reduction rates are near the maximum rate at existing concentrations (not shown). These results show that the rates of sulfate reduction and sediment P release are sensitive to changes in the vertical distribution of redox processes which result from sediment mixing.

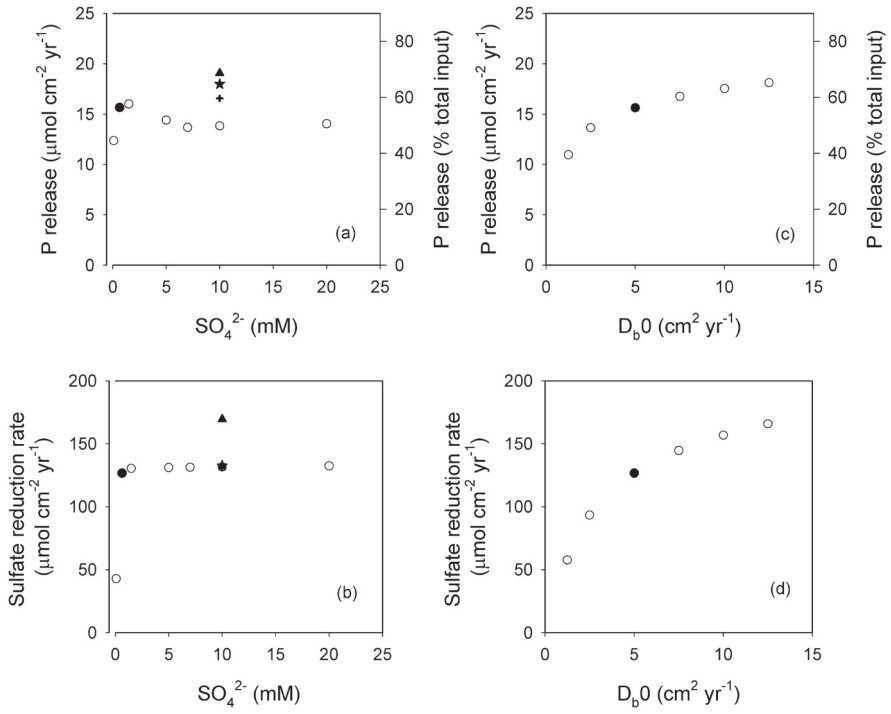

Figure 5.6 The rate of P release (a) and rate of sulfate reduction (b) determined in several steady-state simulations where the concentration of SO_4^{2-} at the upper boundary was changed (o). Values of the initial conditions are marked with a filled symbol. Results of additional simulations at 10 mM SO_4^{2-} are contained in plots a & b $^-$: a factor 100 reduction in the rate constant for pyrite precipitation (★), reduction of the bottom water oxygen concentration from 238 to 120 μM (▲), and elimination of P-min formation (+). The rate of P release (c) and sulfate reduction (d) determined in steady-state simulations where the value of the bioturbation coefficient (D_b0) was varied (o). The initial conditions are marked with a filled symbol.

A comparison of steady-state profiles from the existing conditions and a simulation with increased SO_4^{2-} (10 mM) and D_b0 (10 cm^2yr^{-1}) illustrates that a significant portion of the existing P stored in the sediment may be released as a result of estuarine restoration (Fig. 5.7). Phosphorus efflux will be greater than the steady-state efflux (17.6 μmol cm^{-2} yr^{-1}) initially following restoration as the existing P-Fe(III) pool is reduced.

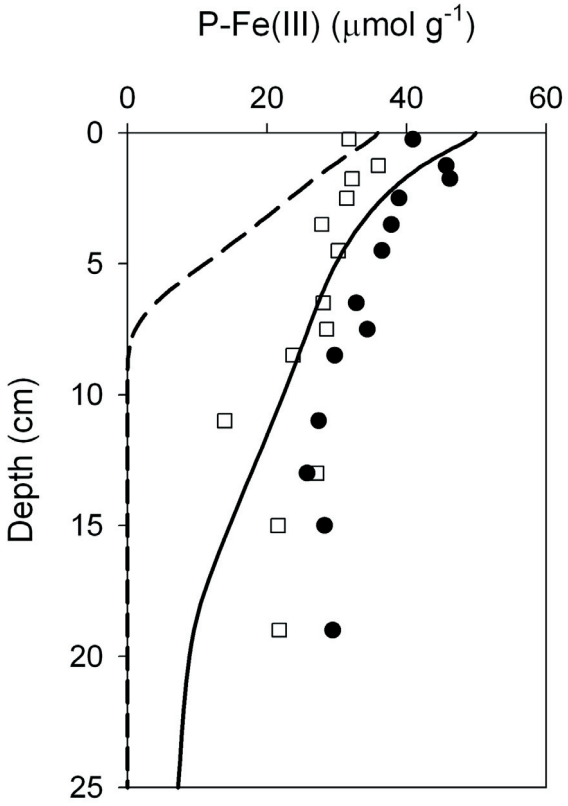

Figure 5.7 Sediment distributions of ascorbate (▫) and CDB (•) extractable P with the results of the P-Fe(III) pool simulated by the model for existing conditions (bottom water SO_4^{2-} 0.64 mM, D_b0 5 cm^2yr^{-1}; solid line) and for estuarine conditions (bottom water SO_4^{2-} 10 mM, D_b0 10 cm^2yr^{-1}; broken line).

5.5 CONCLUSIONS

Results from ascorbate extractions provide evidence that up to 40% of the total sediment P is present as a reducible P-Fe(III) mineral. The biogeochemical processes determining the coupled cycling of Fe, S and P are effectively described using a multi-component reaction transport model. Results from the model show that P-Fe(III) and P-org are the major sources of sediment pore water phosphate. Approximately 50% of the deposited P is transported back to the overlying water as dissolved PO_4. Estuarine restoration is expected to lower sediment P retention. This is expected as a result of increased sulfate reduction and subsequent P-Fe(III) reduction by sulfide. Increased sediment mixing upon estuarine restoration may be more important in enhancing this benthic P release than increased availability of sulfate.

Acknowledgements We gratefully acknowledge the crew of RV Navicula and members of the Utrecht University geochemistry research group for their help in the field and laboratory. We thank Parisa Jourabchi for the use of the steady state version of the code and modeling assistance. The Netherlands Institute for Inland Water Management and Waste Water Treatment (RIZA) financially supported the fieldwork and RWC. CPS was supported by a fellowship of the Royal Netherlands Academy of Arts and Sciences (KNAW) and by the Netherlands Organization for Scientific Research (NWO;VIDI-grant).

References

Aller, R. C. 1980. Diagenetic processes near the sediment-water interface of Long Island Sound I. Decomposition and nutrient element geochemistry (S,N,P). Advances in Geophysics 22**:** 237-350.

Allison, J. D., D. S. Brown, and K. J. Novo-Gradac. 1991. MINTEQA2/PRODEFA2, a geochemical assessment model for environmental systems: Version 3.0 Users Manual. U.S. Environmental Protection Agency,

Aspila, K. I. 1976. Semiautomated method for determination of inorganic, organic and total phosphate in sediments. Analyst 101**:** 187-197.

Berg, P., S. Rysgaard, and B. Thamdrup. 2003. Dynamic modeling of early diagenesis and nutrient cycling. A case study in an Arctic marine sediment. American Journal of Science 303**:** 905-955.

Berner, R. A. 1980. Early diagenesis. A theoretical approach. Princeton University Press.

Blomqvist, S., A. Gunnars, and R. Elmgren. 2004. Why the limiting nutrient differs between temperate coastal seas and freshwater lakes: A matter of salt. Limnology and Oceanography 49**:** 2236-2241.

Boudreau, B. P. 1984. On the equivalence of nonlocal and radial-diffusion model for porewater irrigation. Journal of Marine Research 42**:** 731-735.

Canavan, R. W., C. P. Slomp, P. Jourabchi, P. Van Cappellen, A. M. Laverman, and G. A. Van Den Berg. 2006. Organic matter mineralization in sediment of a coastal freshwater lake and response to salinization. Geochimica Et Cosmochimica Acta 70**:** 2836-2855.

Caraco, N., J. Cole, and G. E. Likens. 1990. A Comparison of Phosphorus Immobilization in Sediments of Fresh-Water and Coastal Marine Systems. Biogeochemistry 9**:** 277-290.

Caraco, N., J. J. Cole, and G. E. Likens. 1989. Evidence for sulphate-controlled phosphorus release from sediments of aquatic systems. Nature 341**:** 316-318.

de Wit, M. 1999. Nutrient fluxes in the Rhine and Elbe basins. PhD thesis. Utrecht University.

Einsele, W. 1936. Uber die Beziehungen des Eisenkreislaufs zum Phsophatkreislauf im eutrophen See. Archiv Fur Hydrobiologie**:** 664-686.

Ferguson, H. A., and W. J. Wolff. 1984. The Haringvliet-Project: The development of the Rhine-Meuse Estuary from tidal inlet to stagnant freshwater lake. Water Science and Technology 16**:** 11-26.

Gächter, R., and B. Müller. 2003. Why the phosphorus retention of lakes does not necessarily depend on the oxygen supply to their sediment surface. Limnology and Oceanography 48**:** 929-933.

House, W. A. 2003. Geochemical cycling of phosphorus in rivers. Applied Geochemistry 18**:** 739.

Hyacinthe, C., and P. Van Cappellen. 2004. An authigenic iron phosphate phase in estuarine sediments: composition, formation and chemical reactivity. Marine Chemistry 91**:** 227-251.

Koelmans, A. A. 1998. Geochemistry of suspended and settling solids in two freshwater lakes. Hydrobiologia 364**:** 15-29.

Kostka, J. E., and G. W. Luther. 1994. Partitioning and speciation of solid-phase iron in salt-marsh sediments. Geochimica et Cosmochimica Acta 58**:** 1701-1710.

Krom, M. D., and R. A. Berner. 1980. Adsorption of phosphate in anoxic marine sediments. Limnology and Oceanography 25**:** 797-806.

Laverman, A. M., P. Van Cappellen, D. Van Rotterdam-Los, C. Pallud, and J. Abell. 2006. Potential rates and pathways of microbial nitrate reduction in coastal sediments. FEMS Microbiology Ecology**:** in press.

Martens, C. S., R. A. Berner, and J. K. Rosenfeld. 1978. Interstitial water chemistry of anoxic Long Island Sound sediments. 2. Nutrient regeneration and phosphate removal. Limnology and Oceanography 23**:** 605-617.

Matisoff, G., and X. S. Wang. 1998. Solute transport in sediments by freshwater infaunal bioirrigators. Limnology and Oceanography 43**:** 1487-1499.

Meile, C., and P. Van Cappellen. 2003. Global estimates of enhanced solute transport in marine sediments. Limnology and Oceanography 48**:** 777-786.

Moosmann, L., R. Gächter, B. Müller, and A. Wüest. 2006. Is phosphorus retention in autochthonous lake sediments controlled by oxygen or phosphorus? Limnology and Oceanography 51**:** 763-771.

Mortimer, C. H. 1941. The exchange of dissolved substances between mud and water in lakes. I. Journal of Ecology 30**:** 280-329.

Nixon, S. W. 1988. Physical energy inputs and the comparative ecology of lake and marine ecosystems. Limnology and Oceanography 33**:** 1005-1025.

Revsbech, N. P. 1989. Diffusion characteristics of microbial communities determined by use of oxygen microsensors. Journal of Microbiological Methods 9**:** 111-122.

Roden, E. E., and J. W. Edmonds. 1997. Phosphate mobilization in iron-rich anaerobic sediments: Microbial Fe(III) oxide reduction versus iron-sulfide formation. Archiv Fur Hydrobiologie 139**:** 347-378.

Ruttenberg, K. C. 1992. Development of a sequential extraction method for different forms of phosphorus in marine sediments. Limnology and Oceanography 37**:** 1460-1482.

Schink, D. R., and N. L. Guinasso. 1978. Redistribution of dissolved and adsorbed materials in abyssal marine sediments undergoing biological stirring. American Journal of Science 278**:** 687-702.

Slomp, C. P., E. H. G. Epping, W. Helder, and W. Vanraaphorst. 1996. A key role for iron-bound phosphorus in authigenic apatite formation in North Atlantic continental platform sediments. Journal of Marine Research 54**:** 1179-1205.

Slomp, C. P., J. F. P. Malschaert, and W. Van Raaphorst. 1998. The role of adsorption in sediment-water exchange of phosphate in North Sea continental margin sediments. Limnology and Oceanography 43**:** 832-846.

Smit, H., R. Smits, G. Van Der Velde, and H. Coops. 1997. Ecosystem responses in the Rhine-Meuse delta during two decades after enclosure and steps toward estuary restoration. Estuaries 20**:** 504-520.

Sondergaard, M., J. P. Jensen, and E. Jeppesen. 2003. Role of sediment and internal loading of phosphorus in shallow lakes. Hydrobiologia 506**:** 135-145.

Van Cappellen, P., and Y. F. Wang. 1996. Cycling of iron and manganese in surface sediments: A general theory for the coupled transport and reaction of carbon, oxygen, nitrogen, sulfur, iron, and manganese. American Journal of Science 296**:** 197-243.

van Eck, G. T. M. 1982. Forms of phosphorus in particulate matter from the Hollands Diep/Haringvliet, The Netherlands. Hydrobiologia 92**:** 665-681.

Wersin, P., P. Hohener, R. Giovanoli, and W. Stumm. 1991. Early Diagenetic Influences on Iron Transformations in a Fresh-Water Lake Sediment. Chemical Geology 90**:** 233-252.

Chapter 6

Trace metal geochemistry in a freshwater sediment: field results and diagenetic modeling

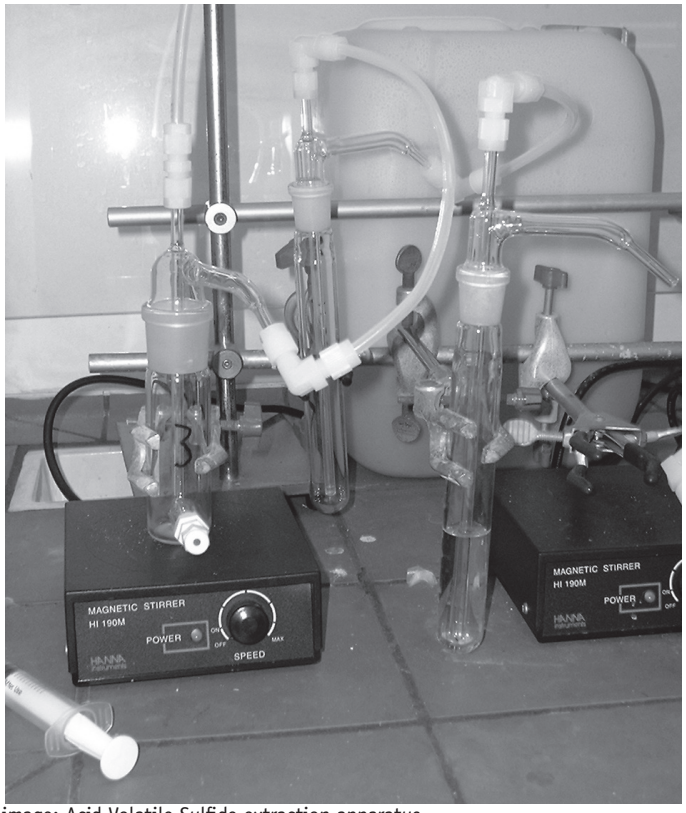

image: Acid Volatile Sulfide extraction apparatus

R.W. Canavan, P. Van Cappellen, C.P. Slomp, J.J.G Zwolsman, and G.A. van den Berg - to be submitted

ABSTRACT

Concentrations of Fe, Mn, Cd, Co, Ni, Pb, and Zn were determined in pore water and sediment of a coastal fresh water lake (Haringvliet Lake, The Netherlands). Elevated sediment trace metal concentrations reflect anthropogenic inputs from the Rhine and Meuse Rivers. Pore water and sediment analyses, together with thermodynamic calculations, indicate a shift in trace metal speciation from oxide-bound to sulfide-bound over the upper 20 cm of the sediment. Concentrations of reducible Fe and Mn decline with increasing depth, but do not reach zero values at 20 cm depth. The reducible phases are relatively more important for the binding of Co, Ni, and Zn than Pb and Cd. Pore waters exhibit supersaturation with respect to Zn, Pb, Co, and Cd monosulfides, while significant fractions of Ni and Co are bound to pyrite. A multi-component, diagenetic model developed for organic matter degradation was expanded to include Zn and Ni dynamics. Pore water transport of trace metals is primarily diffusive, with a lesser contribution of bioirrigation. Reactions affecting trace metal mobility near the sediment-water interface, especially sulfide oxidation and sorption to newly formed oxides, strongly influence the modeled estimates of the diffusive effluxes to the overlying water. Model results imply less efficient sediment retention of Ni than Zn. Sensitivity analyses show that increased bioturbation and sulfate availability, which are expected upon restoration of estuarine conditions in the lake, should increase Zn and Ni retention in the sediments.

6.1 INTRODUCTION

Elevated concentrations of trace metals in sediments pose toxicological risks to biota and may impair water quality (Baird and Cann 2005). Under oxidizing conditions, trace metals bind to organic matter (OM), clays, and Fe plus Mn-oxides (Turner et al. 2004; Young and Harvey 1992). These phases are frequently intimately associated with one another (Perret et al. 2000; Taillefert et al. 2002), making it difficult to separate them by physical and chemical techniques. Decomposition of OM and reductive dissolution of Fe and Mn-oxides, which tend to be highest near the sediment water interface (SWI; Canavan et al. 2006; Douglas and Adeney 2000), may lead to release of trace metals to the pore waters (Zhang et al. 1995).

In reducing sediments, trace metals often associate with insoluble sulfide precipitates (e.g. Huerta-Diaz et al. 1998). Sulfide is produced by bacterial sulfate reduction coupled to OM decomposition (Holmer and Storkholm 2001). In coastal marine sediments and salt marsh soils, abundant sulfate and OM cause high rates of sulfide production, with pyrite (FeS_2) being the most common end-product (Huerta-Diaz and Morse 1990; Kostka and Luther 1994; Otero and Macias 2002). In freshwater sediments, sulfide mineral phases may also immobilize trace metals, despite the lower sulfate concentrations relative to marine systems (Huerta-Diaz et al.

1998; Motelica-Heino et al. 2003). The metals are then buried in the sediment, unless oxidative dissolution of the sulfide mineral phases occurs, upon sediment mixing by resuspension and bioturbation (Cappuyns and Swennen 2005; Carroll et al. 2002).

Reactive transport models (RTMs) are often used to simulate the complex interplay of reaction and transport processes in sediments (Boudreau 1999). However, only few studies have used this approach to quantitatively describe trace metal cycling in freshwater sediments. Recently, Gallon et al. (2004) used an inverse, steady state model to describe Pb diagenesis in sediments of a Canadian shield lake. Others have applied multi-component RTMs to assess metal sulfide oxidation (Carbonaro et al. 2005; Di Toro et al. 1996) and the controls on arsenic mobility in sediments (Smith and Jaffé 1998).

In this study, we present results of pore water analyses and sediment extractions for Fe, Mn, Cd, Co, Ni, Pb and Zn in sediment of a coastal fresh water lake, Haringvliet Lake, which is part of the Rhine-Meuse River Delta and has experienced elevated trace metal inputs from anthropogenic sources. We also include Zn and Ni in an existing multi-component RTM, which accounts for organic matter degradation, secondary redox reactions, mineral precipitation and dissolution, and transport by bioirrigation and bioturbation (Canavan et al. 2006). The analytical results, thermodynamic calculations, and reactive transport modeling are used to examine how trace metal speciation changes with depth in the sediment. A better understanding of trace metal behavior in sediments is needed to guide management efforts to improve water quality and ecosystem health of the lake.

6.2 STUDY SITE AND METHODS

6.2.1 Haringvliet Lake

In 1970, the Haringvliet estuary was converted to a freshwater lake by building a dam at the outlet to the North Sea. This alteration caused the accumulation of metal-polluted sediments in the lake and habitat loss (Ferguson and Wolff 1984; Smit et al. 1997). A partial restoration of estuarine conditions is proposed for Haringvliet Lake, beginning in 2008. Changes in management of the dam will allow water from the adjacent North Sea to enter the lake at low tide (Anonymous 1998). The sampling site lies within the area that will be affected by the estuarine restoration.

Trace metal contamination has adversely affected benthic communities in sediments of the Rhine-Meuse Delta (Reinhold-Dudok van Heel and den Besten 1999; van Griethuysen et al. 2004). Studies of sediment trace metal biogeochemistry, including pore water analysis, have been conducted at other locations within the delta with the aim of describing possible release of trace metals from the sediment to the overlying water (Paalman 1997; van den Berg

et al. 1999). The present work is part of a study of biogeochemical processes and their response to salinization in Haringvliet Lake. Additional studies conducted at the site have examined organic matter mineralization (Canavan et al. 2006), nitrogen cycling (Chapters 3, 4), and phosphorus cycling (Chapter 5).

6.2.2 Sample collection

Sediment and pore water samples were collected in September 2002, and April-May 2003. The sampling periods are referred to as late-summer, and spring, respectively. Sediment was collected using a cylindrical box corer (31 cm i.d.) deployed from RV Navicula. Each box core contained approximately 40 cm of surface sediment and 30 cm of overlying water. Sub-cores were taken with polycarbonate tubes (10 cm i.d.). Sub-cores for pore water and solid phase analysis were taken from a single box core and immediately sectioned in a N_2 purged glove box on board the ship in a temperature-controlled laboratory.

6.2.3 Pore water analyses

Sediment sub-samples for pore water collection were placed in polyethylene centrifuge tubes in a N_2 purged glove box during core sectioning. The tubes were subsequently removed from the glove box and centrifuged at 2500 g for 10 to 30 minutes under temperature-controlled conditions. Following centrifugation tubes were transferred to a N_2 filled glove bag where pore water was filtered (late-summer: 0.2 μm pore size polypropylene PALL filters; spring: 0.45 μm pore size polyethersulfone Orange Scientific filters). Pore water pH was determined directly on the filtrate. Filtrate aliquots for trace metal analysis were acidified with HNO_3 (50 μl conc. distilled HNO_3 per ml) and stored in high density polyethylene bottles at 4 °C until analysis by ICP-MS. Pore water blanks were determined by processing ultra-pure water from the laboratory in parallel with pore water samples in the field.

Sulfate and chloride were determined by Ion Chromatography (Dionex DX-120) on thawed filtrate sub-samples, and dissolved organic carbon (DOC) with a Shimadzu TOC-50550A analyzer on filtrate samples stored at 4 °C. Alkalinity was determined colorimeterically in the field (Sarazin et al. 1999). Sulfide pore water profiles were also measured using the Diffusive Gradient in Thin Films (DGT) method (Motelica-Heino et al. 2003; Naylor et al. 2004; Teasdale et al. 1999). With this method, sulfide is determined by quantifying the color change resulting from the reaction of a AgI (yellow) containing gel with pore water sulfide, producing AgS_2 (black). Sulfide concentrations in the pore water were calculated using the calibration of Naylor et al. (2004).

6.2.4 Solid phase analyses

Sediment water content and density were determined from the weight loss upon freeze drying, allowing for the determination of sediment porosity. Grain size analysis was conducted using a laser diffraction technique (Malvern Mastersizer S) on freeze dried sediment following a HCl and H_2O_2 pre-treatment. Total carbon, total sulfur, and organic carbon (C_{org}; following carbonate removal with 1 M HCl) were determined on freeze-dried sediment using an elemental analyzer (LECO SC-1440H).

A total digestion with HF-$HClO_4$-HNO_3 was conducted on freeze dried sediment samples as described in Hyacinthe and Van Cappellen (2004). Determination of major elements (Ca and Al) in the extractant was done with ICP-OES (Perkin-Elmer Optima 3000). Analysis of metals in all extractants was carried out with ICP-MS (Agilent 7500 series) unless otherwise noted. Acid Volatile Sulfide-Simultaneously Extractible Metal (AVS-SEM) extractions were conducted to determine concentrations of non-pyritic reduced sulfur, and metals bound to non-pyritic sulfides and other extractible phases (carbonates and amorphous oxides). AVS-SEM was performed on approximately 1 g wet sediment in an Ar-purged analysis train with room-temperature 6M HCl for 1 hour (van den Berg et al. 2001). The released H_2S was trapped in a 1 M NaOH solution from which sulfide concentrations were determined colorimetrically (Cline 1969).

The sequential extraction method of Huerta-Diaz and Morse (1990) was performed on freeze dried samples. The method includes three operationally defined Fe and trace metal pools: reactive (1N HCl, 16 h); silicate (10M HF,16 h); and pyrite (conc. HNO_3, 2 h). The degree of pyritization (DOP) and degree of trace metal pyritization (DTMP) can then be calculated as follows:

$$\text{DOP (\%)} = \left(\frac{(\text{pyrite - Fe})}{(\text{pyrite - Fe}) + (\text{reactive - Fe})} \right) \times 100 \quad (1)$$

$$\text{DTMP (\%)} = \left(\frac{(\text{pyrite - Me})}{(\text{pyrite - Me}) + (\text{reactive - Me})} \right) \times 100 \quad (2)$$

where the concentrations of Fe or trace metal (Me) measured in the reactive and pyrite pools of the extraction are used. DOP represents the percent of reactive Fe that is present as pyrite and DTMP is the percent of reactive trace metal bound in the pyrite phase. The degree of sulfidization (DOS), that is, the percent of reactive Fe that is bound to sulfide, is calculated as follows:

$$\text{DOS}\ (\%) = \left(\frac{(\text{pyrite} - \text{Fe}) + (\text{AVS} - \text{Fe})}{(\text{pyrite} - \text{Fe}) + (\text{reactive} - \text{Fe})} \right) \times 100 \qquad (3)$$

where (AVS-Fe) is the concentration of AVS, and reactive-Fe and pyrite-Fe are the Fe concentrations in the respective pools.

Additional extractions with citrate-dithionite bicarbonate (CDB, extraction solution analysis by ICP-OES; Slomp et al. 1996) and pH 7.5 ascorbate (Hyacinthe and Van Cappellen 2004; Kostka and Luther 1994) were performed on wet sediment to further characterize the reactive Fe(III) pool. The CDB extractant extracts all Fe-oxides while the near-neutral ascorbate extraction is limited to poorly crystalline and amorphous reducible Fe(III) phases. The reactive pool extraction in the Huerta-Diaz and Morse (1990) method (1N HCl) is less specific, as it also mobilizes reactive Fe(II) phases (Kostka and Luther 1994; Raiswell et al. 1994). The dissolution kinetics in pH 7.5 ascorbate of a freeze-dried surface sediment sample (0-0.5 cm) were followed by periodically sampling the sediment suspensions over the course of a 25-hour extraction period, following the procedure of Hyacinthe and Van Cappellen (2004).

Concentrations of Zn, Ni, Pb, and Cd, and grain size determinations for suspended matter (SPM), obtained during monthly water quality monitoring performed by RIZA, were downloaded from the publicly available database, www.waterbase.nl, and are reproduced here with permission. Metal concentrations in SPM reported in the data base were measured by ICP-OES after a HCl-HNO_3 extraction on freeze-dried samples. The RIZA provided SPM samples collected in 2001, on which we measured the concentrations of Fe and Mn, as these elements are not reported in the database.

6.2.5 Modeling

Reaction-transport model calculations were carried out with the Biogeochemical Reaction Network Simulator (BRNS; Aguilera et al. 2005; Jourabchi et al. 2005). The development and calibration of the model used to describe the sediment in Haringvliet Lake is presented in Canavan et al. (2006). The existing model, which includes a reaction network of 24 chemical species and 32 reactions, was expanded to include trace metal reactions. The discussion of reaction and transport processes in this paper is limited to those that directly involve the trace metals. Changes to model boundary conditions and rate constants for Fe, Mn, and S reactions were made to account for CDB fractions that were not included in the original model (Canavan et al. 2006). These changes are listed in the appendix. Trace metals in the model were subjected to the same transport processes as other constituents, namely molecular diffusion, bioirrigation,

bioturbation, and burial for solutes, and bioturbation and burial for solids. The model describes 1-D sediment profiles at steady-state.

Thermodynamic speciation calculations were conducted using Visual MINTEQ (Version 2.4, this program is an adaptation of MINTEQA2; Allison et al. 1991). Calculations included the following constituents: Na^+, Ca^{2+}, Mg^{2+}, K^+, NH_4^+, SO_4^{2-}, Cl^-, PO_4^{3-}, HS^-, Alkalinity, pH, Fe^{2+}, Mn^{2+}, Co^{2+}, Ni^{2+}, Zn^{2+}, Pb^{2+}. The ability of thermodynamic modeling to predict the speciation of dissolved metals is limited by the use of pure, end-member solid phases, the limited knowledge of metal-sulfide stability constants and, in this study, the exclusion of complexation by dissolved organic ligands.

6.3 RESULTS

6.3.1 Porewater

Pore water DOC displayed a gradual increase with depth in late-summer, while a subsurface maximum was observed in spring (Fig. 6.1). Alkalinity increased with depth in the upper 3 cm of sediment, and again below 10 cm. Pore water pH was higher in late-summer than spring; both profiles showed a gradual acidification with depth. Dissolved Fe in the pore water increased below 3 cm, with late-summer concentrations rising to 300 μM at depth. Sulfate concentrations rapidly declined in the upper 3 cm during both sampling periods. The highest sulfide concentrations were observed in late-summer in the depth range 2.5-5 cm, spring sulfide concentrations increased below 7 cm.

Pore water zinc concentrations were elevated in the uppermost centimeters of sediment, particularly in spring. Pore water concentrations of Pb and Cd were also greater in spring than late-summer in the upper 3 cm. No clear depth trend could be discerned in the pore water profiles of Pb. Note that the lowest pore water concentrations of Zn, Pb, and Cd approach the mean blank values, which represent practical detection limits. The pore water profiles of Mn, Ni, and Co showed sub-surface peaks that were most pronounced in spring. Pore water profiles of Co and Ni resembled those of Mn, for both sampling periods. The correlation with Mn was stronger for Co ($r^2 = 0.92$) than for Ni ($r^2 = 0.81$).

The pore waters were near equilibrium with amorphous FeS in late-summer, in the depth range 1.25-11 cm, and undersaturated in the upper 6.5 cm during spring (Fig. 6.2a). Supersaturation with respect to the monosulfides of Zn, Pb, and Cd was observed for both late-summer and spring, with calculated saturation indexes exceeding 2.5 (results not shown). The thermodynamic calculations predicted supersaturation to near-saturation with respect to CoS, but undersaturation with respect to NiS (Fig. 6.2b-c). The pore waters remained highly undersaturated with respect to MnS (saturation index < -3).

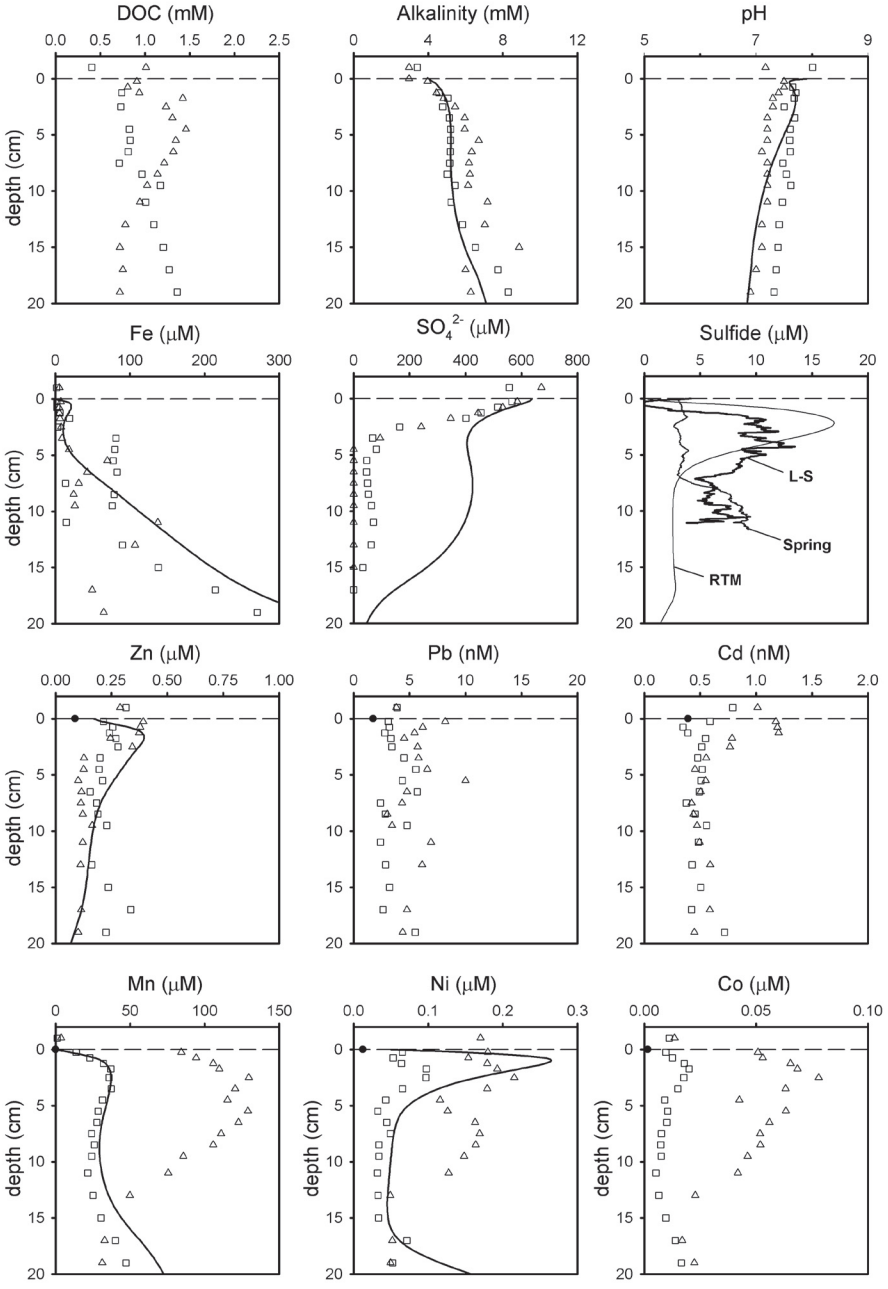

Figure 6.1 (see opposing page for description)

Figure 6.1 (opposite page) Porewater profiles of DOC, alkalinity, pH, Fe, SO_4^{2-}, sulfide, Zn, Pb, Cd, Mn Ni, and Co from late-summer (□) and spring (△). Sediment water interface (SWI) is given as a dashed horizontal line. Mean values of field blanks for Zn, Pb, Cd, Mn, Co, and Ni are given at the SWI (•). Model fits for alkalinity, pH, Fe^{2+}, SO_4^{2-}, sulfide, Zn^{2+}, Mn^{2+}, and Ni^{2+} are plotted as continuous lines in the plots. Results for sulfide as obtained using the AgI DGT probe (see methods), are also continuous. The sulfide results from late-summer, spring, and the model are labeled L-S, Spring, and RTM respectively.

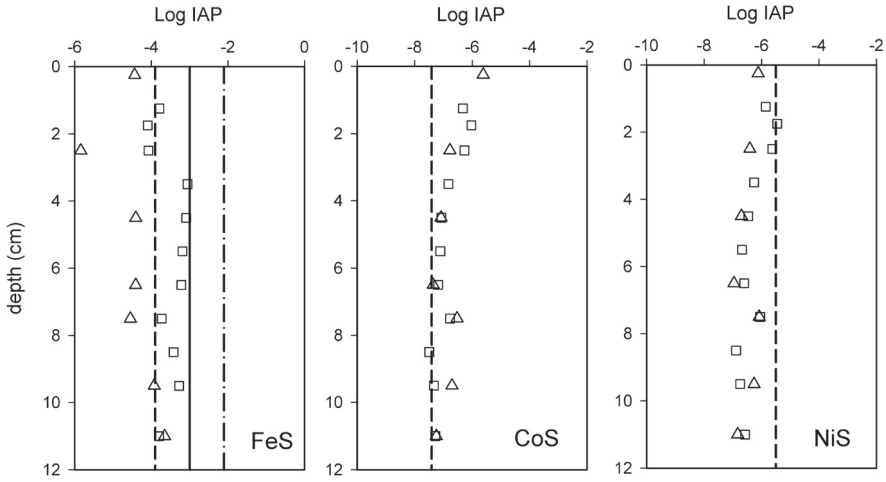

Figure 6.2 Log Ion Activity Product (Log IAP) for Fe^{2+} and HS^- (a), Co^{2+} and HS^- (b) and Ni^{2+} and HS^- (c) calculated using visual MINTEQ with pore water data from late-summer (□) and spring (△). Vertical lines represent solubility constant (Log K_{so}) for the metal sulfides. Values for FeS (a) determined by Davison et al. (1999; -3.0, solid line), Benning et al (2000; -3.9, dashed line), and Wolthers (Wolthers et al. 2005; -2.1, dash-dot line). The Log K_{so} values for CoS (b) and NiS (c) obtained from Huerta-Diaz et al. (1998; CoS = -7.4; NiS -5.5, dashed line) Solutions are super-saturated when the Log IAP value is greater than the Log K_{so}.

6.3.2 SPM Metal content

Trace metals in the water column of the Haringvliet Lake are mainly associated with the SPM. Concentrations of Zn, Ni, Pb, and Cd in the upper 2 cm of sediment were slightly enriched relative to the SPM (Fig. 6.3). This could be attributed to a grain size effect, as the sediment was enriched in the <63μm fraction, compared to the SPM (94% *versus* 67%). Concentrations of Fe and Mn in the SPM varied independently from one another (Fig. 6.4), as previously observed at other sites in the Rhine-Meuse Delta (Paalman and van der Weijden 1992). Both Fe and Mn SPM concentrations declined sharply in August 2001, as a result of dilution by an algal bloom in the lake.

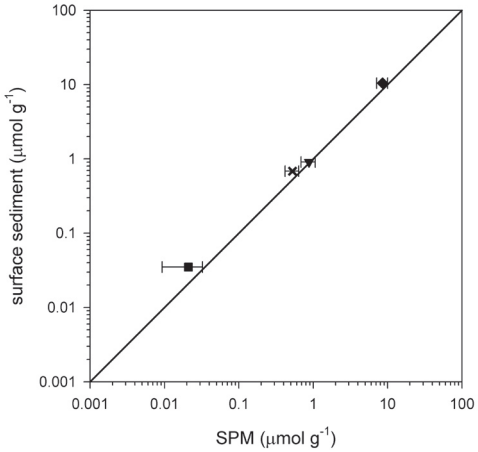

Figure 6.3 The mean concentration of Zn (◆), Ni (▼), Pb (×), and Cd (■) in suspended particulate matter (SPM) from monthly measurements between 2000-2004 (source: Rijkswaterstaat, www.waterbase.nl) versus total concentration in the upper 2 cm (average of 3 samples). The error bars represent one standard deviation of the SPM values. A solid 1:1 relation line is plotted to show where values are equal; note the log scales.

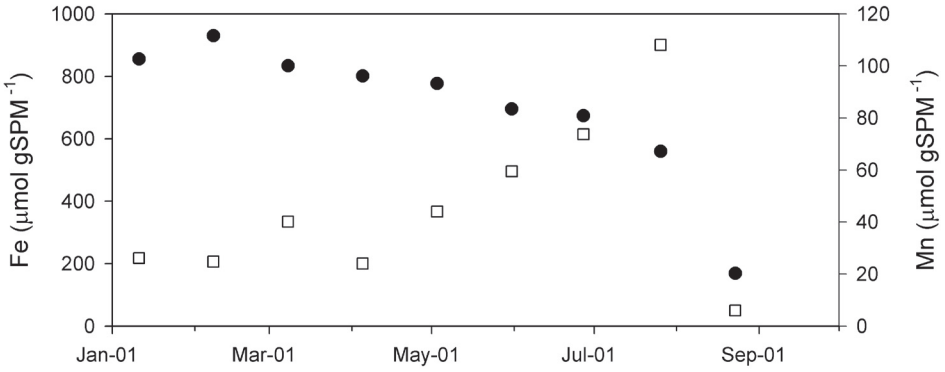

Figure 6.4 Concentrations of Fe (•) and Mn (□) in suspended particulate matter (SPM) over an 8-month period in 2001.

The SPM trace metal concentrations varied substantially in the period 2000-2004, with coefficients of variation ranging from 17% for Zn to 55% for Cd (see error bars on Figure 6.3). The concentrations of Zn and Pb followed similar trends during this period ($r^2 = 0.84$), while correlations between Zn and Ni ($r^2 = 0.43$), and Zn and Cd ($r^2 = 0.37$) were substantially weaker. The trace metal SPM concentrations displayed negative correlations with SPM organic matter, as organic matter produced in the lake during algae blooms had a lower trace metal content than the terrestrial derived SPM.

6.3.3 Sediment solid phase

The sediment is highly porous, fine grained and organic rich (Table 6.1). Sediment concentrations of total Al, Fe, C_{org} and porosity were correlated to grain-size, while the total Ca concentration was not (Table 6.1). The total sediment profiles of C_{org}, Fe, Mn, Zn, Pb, Co, and Cd displayed little variation with depth, particularly in the upper 10 cm of sediment (Fig. 6.5). The total Ni concentration showed a slight depletion in the uppermost cm of sediment.

Table 6.1 Depth weighted average concentrations of organic carbon (C_{org}), Ca, Al, Fe, porosity and grain size in the upper 10 cm of sediment and correlation with grain size

C_{org}	Ca	Al	Fe	Porosity	Grain Size <63μm
	(% dry weight)			(vol %)	(% total)
4.1 (0.11)	3.6 (0.10)	4.1 (0.05)	1.9 (0.03)	84 (2.15)	93 (2.00)
r^2 for regression with grain size less than 65 μm (%)					
0.62 ⋆	0.01	0.58 ⋆	0.89 ⋆	0.75 ⋆	-

Al and Fe were determined from 11 samples, the remaining values were determined from 12 samples. Values in parentheses are one standard deviation. Correlation determined with data from the upper 30 cm of sediment (19 samples). ⋆ Denotes significant correlation ($P < 0.05$).

As expected, the AVS-SEM concentrations for most metals were lower than the total concentrations. Extraction with 6M HCl does not dissolve silicates and pyrite, and may not release all organically bound metals. The SEM concentrations were nearly equal to the total concentrations for Cd, while the refractory pools not extracted by 6M HCl were most significant for Fe, Ni, and Co. The differences between the SEM and total concentrations declined with depth, except for Fe, S, and Co. The total sulfur concentration increased sharply below 10 cm to a peak concentration at a depth of approximately 15 cm. The concentration of AVS was near zero in the upper 2 cm of sediment and, like total S, increased with depth until 15 cm depth.

The concentrations released by the reductive extractions (ascorbate, CDB) declined with depth for all metals (Fig. 6.6). Significantly higher concentrations of Fe, Mn, Ni, and Co were extracted in CDB than in near-neutral ascorbate. For Zn, the two extractions yielded similar concentrations, which accounted for 15% of the total zinc at the sediment surface. The concentration profiles of CDB extractable Fe, Ni, and Co declined more sharply with depth than the ascorbate extractable concentrations. Both extractions suggested the persistence of reducible compounds at 20 cm depth. At the sediment surface (0-0.5 cm) the CDB fraction accounted for 68% of total Mn, 42% of total Fe, 34% of total Co and 23% of total Ni. Reducible phases appeared to be less important for Pb and Cd, as ascorbate extractions released only 7%

and 0.3% of the total surface sediment concentration, respectively (Pb and Cd concentrations were not determined in the CDB extraction).

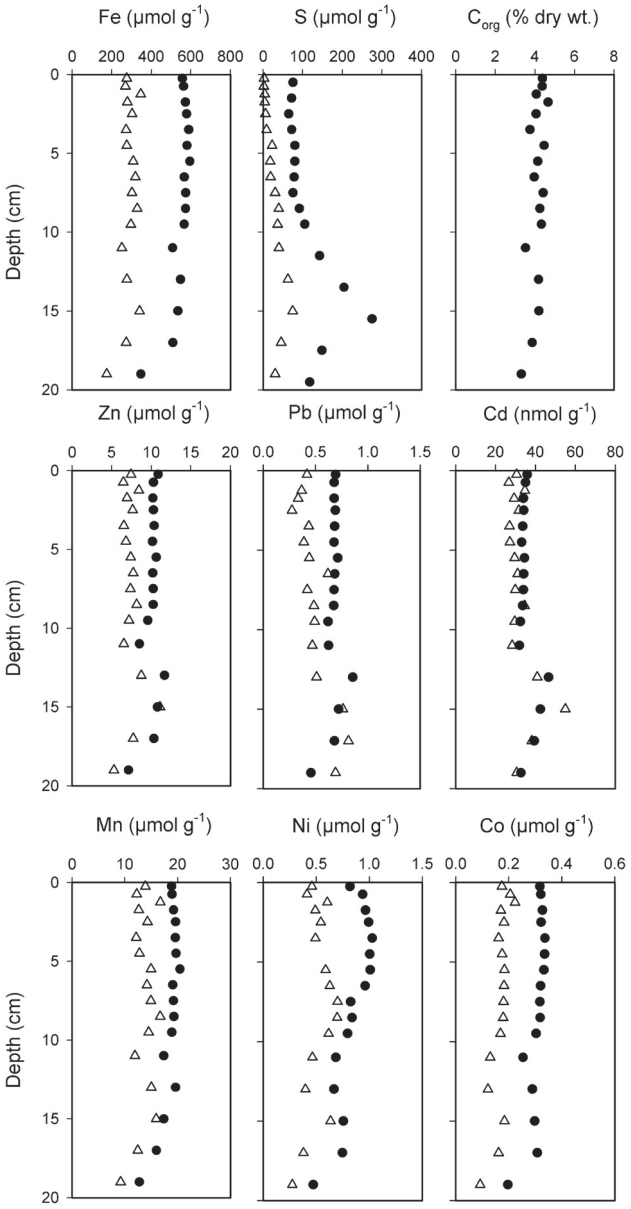

Figure 6.5 Depth distributions of Fe, S, C_{org}, Zn, Pb, Cd, Mn, Ni, and, Co, from sediment collected in late-summer. Total concentrations given with (•), and concentrations from the acid volatile sulfide-simultaneously extractable metals (AVS-SEM; 6M HCl) extraction are given with (△).

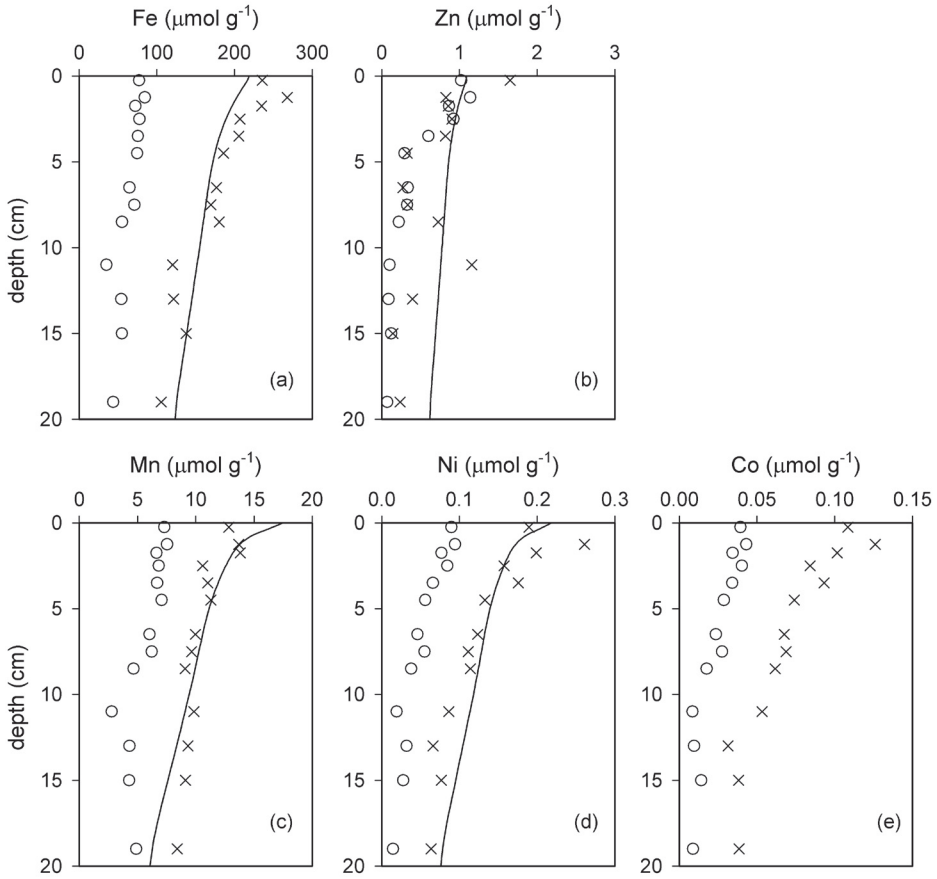

Figure 6.6 Sediment distributions of ascorbate (○) and CDB (×) extractable Fe (a), Zn (b), Mn (c), Ni (d), and Co (e) from sediment collected in late-summer. Model distributions of $\Sigma Fe(OH)_3$ (a), $Fe(OH)_3$-Zn (b), ΣMnO_2 (c), and MnO_2-Ni (d) are given as solid lines in the respective plots.

The release of trace metals during the pH 7.5 ascorbate extraction of the topmost (0-0.5 cm) sediment displayed a number of distinct patterns. These are shown in Fig. 6.7 where the extracted concentrations of dissolved trace metal are plotted versus the extracted concentration of dissolved Fe. The latter increased continuously over the 25 hours of extraction. The concentrations of extracted Zn, Co and Mn correlated positively with that of Fe during the entire extraction. Ni and Cr showed a near-instantaneous release to solution at the start of the extraction, followed by continuous release for the remainder of the extraction. Cu release was entirely uncorrelated to that of Fe, while Pb and Cd showed more complex patterns indicative of removal by precipitation when dissolved Fe exceeded 250 μM.

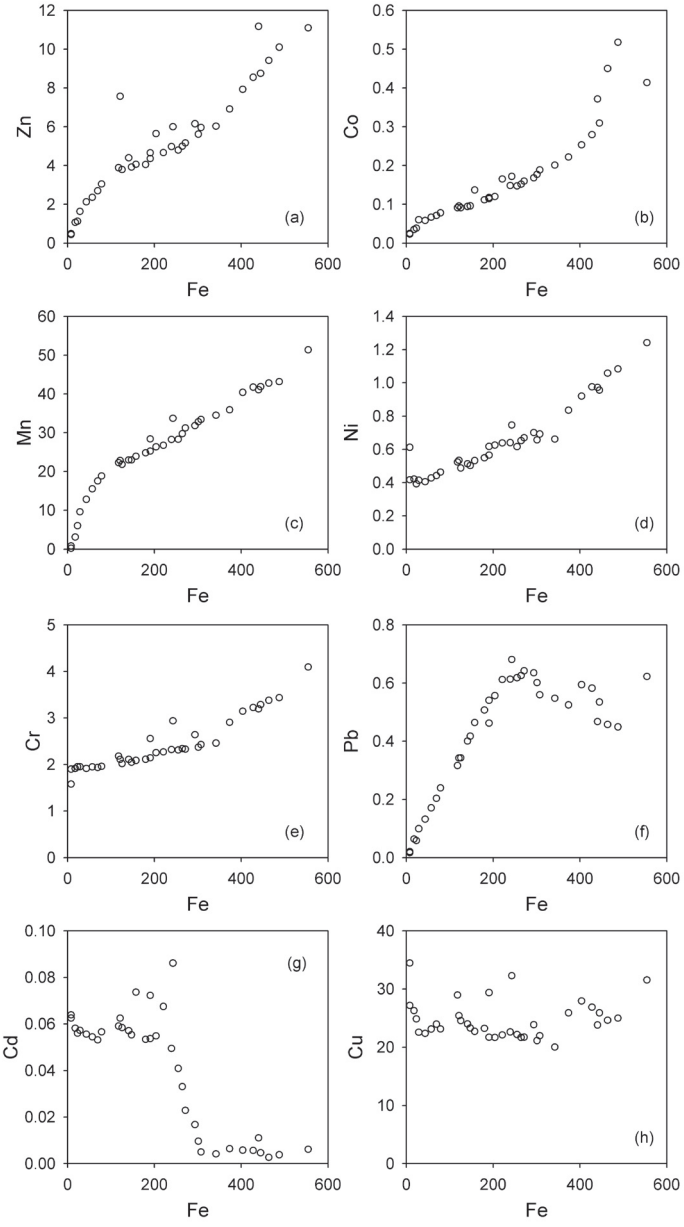

Figure 6.7 Extraction solution concentrations in μmol l^{-1} of Zn (a), Co (b), Mn (c), Ni (d), Cr (e), Pb (f), Cd (g), Cu (h) versus Fe from the kinetic ascorbate extraction. Samples were collected periodically over a 25-hour extraction conducted on a freeze-dried sediment sample from 0-0.5 cm depth collected in late-summer.

The degree of pyritization (DOP) in the upper 8 cm of sediment ranged between 12-16% (Table 6.2), followed by an increase to 35% at 15 cm. The degree of sulfidization increased between 2 to 15 cm, reaching a maximum value at the same depth as AVS. The degree of trace metal pyritization (DTMP) of Mn never exceeded 3%, while those of Zn, Pb, and Cd values remained below 10%. Higher DTMP values were obtained for Ni (10-21%) and Co (7-26%). In addition, the DTMP values of Ni and Co increased with increasing DOP, while those of the other metals did not correlate with DOP.

Table 6.2 Calculated Degree of Pyritization (DOP), Degree of Sulfidization (DOS), and Degree of Trace Metal Pyritization (DTMP)[a] from sediment collected in late-summer. DOP is calculated using the 1N HCl extraction (Huerta-Diaz and Morse, 1990).

			DTMP				
Depth range (cm)	DOP	DOS	Mn	Zn	Pb	Ni	Co
				(%)			
0-1	13.7	14.9	1.1	6.8	9.3	13.3	7.7
1-2	11.9	14.4	0.9	5.6	9.4	10.2	7.0
2-3	12.8	16.2	0.8	6.1	2.7		8.1
3-4	13.8	18.9	1.0	6.0	8.5	11.6	9.0
5-6	15.7	26.6	1.0	5.4	7.7	12.8	9.8
7-8	14.0	31.9	0.9	6.2	6.0	10.9	10.6
9-10	22.5	42.7	1.4	5.2	7.2	13.0	14.4
12-14	35.2	59.8	2.6	5.8	6.3	21.2	26.6
16-18	15.1	50.6	1.1	6.1	4.8	15.6	16.2

(a) DTMP values for Cd are not reported due to evidence of contamination. Values ranging from 0.4-8.0% were found at an additional sample site in the lake.

6.4 DISCUSSION

6.4.1 Pore water profiles

The build up of alkalinity in the pore waters reflects C_{org} mineralization (Fig. 6.1). The alkalinity increase with depth, however, is not monotonic because of pore water irrigation in the upper 10-15 cm (Canavan et al. 2006). The profiles of DOC, alkalinity, and pH vary between late-summer and spring, most likely because of seasonal differences in the deposition and mineralization of OM. Our previous work has shown that sulfate reduction is an important mineralization pathway (Canavan et al. 2006), which explains the rapid depletion of pore water SO_4^{2-} and the presence of measurable free sulfide. The pore water profiles of SO_4^{2-}, sulfide

and dissolved Fe imply overlapping zones of sulfate and Fe(III) reduction. Such overlap is observed in many sedimentary environments, and is attributed to the wide range of Fe-oxide properties in these environments (Postma and Jakobsen 1996; Roden 2003) and sediment mixing processes (Thullner et al. 2005).

Seasonal differences are also clearly seen in the pore water trace metal profiles (Fig. 6.1). Zn, Pb, and Cd pore water profiles in spring show a near-surface enrichment. While a smaller near-surface enrichment of dissolved Zn is also seen in late-summer, this is not the case for Pb and Cd. For Cd, enhanced release from freshly deposited OM is a possible mechanism explaining the near surface pore water enrichment in spring. The extraction results indicate that little Cd is associated with the reducible pool of Fe and Mn oxides (Fig. 6.5), and no correlation is observed between Cd and Fe release during the acsorbate extractions (Fig. 6.7). Furthermore, Cd has been reported to be associated with organic matter in estuarine sediments (Audry et al. 2006).

For Zn and Pb, the reductive extraction results indicate that the near-surface pore water enrichments can, in part, be explained by reductive dissolution of reactive Fe and Mn oxide phases right at the sediment-water interface. The concentrations of Zn and Pb in SPM of Haringvliet Lake are also strongly correlated ($r^2 = 0.84$), suggesting similar associations of the two metals in particulate matter settling to the lake bottom.

The pore water profiles of Mn, Ni, and Co show a broad, sub-surface peak that is more pronounced during the spring than late-summer sampling period (Fig. 6.1). The seasonal variations could be due to increased Mn-oxide deposition in spring. As shown in Figure 6.4, large variations in the Mn content of SPM are observed in Haringvliet Lake. The linear correlations between the pore water concentrations of Co and Ni with those of Mn, suggest that the release of the trace metals are coupled to Mn reduction. However, the concentration ratios of Mn to Co and Ni in the pore waters (approximately 2000 and 700, respectively) are much higher than those measured in the reductive extractions (Mn:Co = 100-450 and Mn: Ni = 50-155). This could reflect the more efficient removal of dissolved Co and Ni by sulfide precipitation (Fig. 6.2, Table 6.2), compared to Mn.

6.4.2 Sediment solid phase

The correlations of sediment C_{org}, Al, and Fe concentrations with grain size <63 μm (Table 6.1) indicate a close association of OM, metal oxides and clay minerals (Tessier et al. 1996). The surface sediment concentrations at the study site exceed the Dutch sediment quality target values by a factor of 6 for Co, and 3 for Zn and Ni. The concentration of Cd is approximately 1.6 times the target value, while Pb concentrations are just below the quality

target concentration of 0.7 μmol g^{-1}. The target values of the Dutch Soil Protection Act are calibrated to the clay and organic matter content at the sample site.

The total sediment concentration profiles do not display evidence of diagenetic remobilization, with the exceptions of S and possibly Ni (Fig. 6.5). Total sediment Ni concentrations are greater in the depth range 2-6 cm than in the sediment directly above and below this zone. This suggests either a changing total Ni input to the sediment over time, or post-depositional redistribution. Total S and AVS display a peak concentration at 15 cm, which is likely the result of sulfate reduction with subsequent FeS and FeS_2 precipitation. However, steady-state model simulations are unable to reproduce the observed peak, indicating that historical variations in depositional conditions may also have played a role (Canavan et al. 2006).

The decreasing concentrations with increasing depth of the ascorbate and CDB extractable Fe pools are consistent with reductive dissolution of Fe(III) in the sediment (Fig. 6.6). The reduction of chemically reducible Fe(III) mineral phases is not complete by 20 cm depth, indicating slow dissolution kinetics despite the reducing conditions. Similar results have been reported for other freshwater sediments (Hyacinthe and Van Cappellen 2004; Wersin et al. 1991).

Ascorbate at near-neutral pH extracts a fairly homogeneous, phosphate-rich Fe(III) pool. The molar P:Fe ratio of this pool is approximately 0.4, independent of the depth in the profile. In addition, the same P:Fe constant ratio is measured during the kinetic extraction of surface sediment by ascorbate. This phase may be similar to the ferric hydrous phosphate phase described in sediments of the nearby Scheldt estuary (Hyacinthe and Van Cappellen 2004). In the freshwater part of the Scheldt estuary, the phosphate-rich Fe(III) phase is preserved and accumulates in the sediments. In contrast, in sediments of the downstream brackish part of the estuary, reductive dissolution by sulfide produced by sulfate reduction prevents the preservation of the phosphate-rich Fe(III) pool (Hyacinthe and Van Cappellen 2004). Thus, present-day burial of reactive Fe(III) in Haringvliet sediment may reflect the limited sulfate reduction rate, a condition that should change upon restoration of estuarine conditions.

SPM concentrations of Fe and Mn in the water column are decoupled (Fig. 6.4). The increasing trend from winter to summer of the Mn SPM concentration in 2001 (Fig. 6.4) can be explained by increased release of Mn^{2+} from the more reducing sediments in summer and faster Mn^{2+} oxidation in the warmer water column (Paalman and van der Weijden 1992). However, in the sediment, reducible Mn and Fe concentrations appear to be coupled to one another (Figs. 6.6 and 6.7), probably because of co-precipitation during Fe and Mn oxidation in the uppermost sediment. Much of the reducible Mn is found in the ascorbate pool (Fig. 6.6),

which includes both oxide phases formed in the water column and in the sediment.

While the pore water profiles indicate a close coupling of Ni and Co to Mn, the kinetic ascorbate extractions reveal a different nature of the association of the trace metals with Mn (Fig. 6.7). In particular, Ni shows a significant initial release to solution that is not accompanied by similar releases of Mn and Co, suggesting the presence of a significant loosely sorbed fraction of Ni. These observations are consistent with the results of Kay et al. (2001), who report that Co uptake by Mn oxides is due to incorporation in the crystal structure, while Ni is removed through adsorption at the mineral surface.

In contrast to the other metals shown in Fig. 6.6, Zn concentrations are similar in the CDB and ascorbate extractions. Thus, Zn is incorporated into newly forming oxides in the surface sediment, but is not present in the more crystalline oxides extracted by CDB. Pb and Cd concentrations recovered in the ascorbate extraction are low relative to their total concentration (7% and 0.3%, respectively, in the 0-0.5 cm depth interval). As noted before, the release of Cd is not related to the reductive dissolution of Fe (Fig. 6.7).

The high DOP values of 12-16% throughout the sediment (Table 6.2) reflect active pyrite formation plus sediment mixing, which tends to homogenize solid-phase distributions. Our DTMP results are similar to the findings reported by Morse and Luther (1999), who attribute the commonly found low DTMP values for Zn, Pb, Cd to the tendency of these metals to form monosulfide phases. Ni and Co have higher DTMP values and are apparently incorporated into pyrite. Additionally, FeS may also bind Ni and Co (Huerta-Diaz et al. 1998; Morse and Arakaki 1993), while Zn, Pb, and Cd may substitute for Fe resulting in trace metal mono-sulfides (Di Toro et al. 1990). The low DTMP values found for Mn (Table 6.2) are characteristic for sediments with DOP values less than 35% (Morse and Luther 1999).

6.4.3 Diagenetic modeling

Reactive transport model calculations are used to simulate the changes in speciation of Zn and Ni with depth, explore the sensitivity of burial and sediment-water exchange fluxes of the metals, and predict their response to environmental changes that are expected to accompany estuarine restoration in the Haringvliet. The modeled steady state concentration profiles of the pore water reactive solid-state metals for present-day conditions generally fall within the range of measured values (Figs. 6.1 and 6.6). As the lake sediments obviously do not represent steady state conditions, a perfect match of the measured data is not expected.

The reaction and transport processes of Zn and Ni included in the model are described in Table 6.3 and parameter values are given in Table 6.4. For Zn, three parameters are used as fitting parameters. These are the rate constants for ZnS precipitation, Zn displacement of Fe in

FeS, and ZnS oxidation with O_2. For Ni, only the molar ratio describing Ni sorption to FeS was adjusted when fitting the data.

Table 6.3 A description of trace metal reaction-transport processes, the numbering corresponds with that given in Figure 6.8. Model parameters for trace metals are further defined in Table 6.4.

	Process	Description
1	Deposition	Influx of metals is related to the influx of Fe-oxides (Zn), Mn-oxides (Ni), or FeS_2 (Ni) by a ratio derived from extractions.
2	Reductive dissolution	Trace metal is released from oxides by reductive dissolution. The initial model includes two separate phases of Fe and Mn-oxides. One phase that can be reduced in conjunction with bacterial OM degradation and by reaction with sulfide. The second phase is only reduced by sulfide. A single oxide-trace metal ratio is applied to both oxide pools.
3	Oxide formation	Mn^{2+} and Fe^{2+} can be oxidized by reaction with O_2 and precipitate. This process was modeled to remove dissolved trace metal with the same oxide-trace metal ratio found in the incoming material.
4	Bioirrigation	The flushing of burrows by benthic organisms in the sediment is modeled by a non-local exchange reaction: α_x ($[Me]_x - [Me]_{OLW}$) where α_x is the bioirrigation coefficient at depth x, $[Me]_x$ is the concentration of dissolved trace metal at depth x, and $[Me]_{OLW}$ is the concentration of dissolved trace metal in the overlying water.
5	Diffusion	Transport by molecular diffusion of solutes is included in the model. The diffusion of trace metal is determined for the upper and lower boundaries.
6	Precipitation (ZnS)	The precipitation of ZnS is included by the reaction: $k_{ZnSprecip}$ (($[Zn^{2+}][HS^-]/[H^+]K_{ZnS}$)-1) where $k_{ZnSprecip}$ is a rate constant and K_{ZnS} is the equilibrium constant. This reaction is set to zero when ZnS is undersaturated.
7	Displacement	The displacement of Fe by Zn in FeS is included by the reaction: k_{disp} $[Zn^{2+}]$ FeS(s) where k_{disp} is a rate constant
8	Adsorption	The adsorption of Ni^{2+} to FeS and to FeS_2 is related to the rate of formation of FeS and FeS_2 by FeS:Ni and FeS_2:Ni ratios. The formation of FeS_2 is modeled as a reaction of FeS and sulfide. This process results in the release of Ni from FeS and subsequent removal by FeS_2, where the process results in a net removal.
9	Oxidative dissolution	ZnS oxidation with O_2 is included: k_{ZnSox} $[O_2]$ ZnS(s) where k_{ZnSox} is a rate constant. The release of Ni^{2+} is related to the dissolution and oxidation of FeS by the FeS:Ni ratio. Note that the oxidation of FeS_2 is not included in the model.
10	Burial	Burial of solids is determined at the lower boundary (20 cm).

Table 6.4 Description and values of model parameter that relate to processes affecting trace metals and the depth distributions of the bioirrigation coefficient, α. and bioturbation coefficient, D_b.

Parameter	Value	Units	Description
x	0-20	cm	depth in cm
α_0	10	yr^{-1}	The bioirrigation coefficient at the sediment surface. The value of α is depth dependant.
D_{b0}	5	$cm^2\ yr^{-1}$	bioturbation coefficient at sediment surface
λ	2.5	cm^{-1}	D_b depth attenuation coefficient
Fe:Zn	200	$mol\ mol^{-1}$	Ratio of Fe:Zn in Fe-oxides, based on extraction results and used in processes 1-3 (Table 6.3)
Mn:Ni	80	$mol\ mol^{-1}$	Ratio of Mn:Ni in Mn-oxides, based on extraction results and used in processes 1-3 (Table 6.3)
$k_{Znprecip}$	$1.0x10^{-10}$	$mol\ g^{-1}\ yr^{-1}$	rate constant for ZnS precipitation, used as a fitting parameter
K_{ZnS}	$10^{-9.02}$		The equilibrium constant for ZnS as reported in (Huerta-Diaz et al. 1998)
k_{disp}	$1.0x10^{3}$	yr^{-1}	rate constant for Zn displacement of Fe in FeS, used as a fitting parameter
k_{ZnSox}	$1.0x10^{5}$	$mol^{-1}\ L\ yr^{-1}$	rate constant for ZnS oxidation with O_2, used as a fitting parameter
FeS:Ni	833	$mol\ mol^{-1}$	molar ratio of Ni adsorption to FeS, used as a fitting parameter
FeS_2:Ni	600	$mol\ mol^{-1}$	Ratio of Fe:Ni found in the HNO_3 extraction step of the (Huerta-Diaz and Morse 1990) extraction
Depth distribution of α, D_b			Description
$\alpha = \begin{cases} \alpha_0 \left(1 - e^{(x-17)}\right) & (x \le 17\,cm) \\ 0 & (x > 17\,cm) \end{cases}$			Depth distribution of the bioirrigation coefficient α.
$D_b = D_b0\ e^{-(x/\lambda)}$			Distribution of bioturbation coefficient D_b

The model derived Zn^{2+} pore water profile exhibits a sub-surface maximum and generally follows the trend observed in the data (Fig. 6.1). The model $Fe(OH)_3$-Zn pool size declines with depth, although the model underestimates the drop in concentration observed in the reductive extractions (Fig. 6.6b). ZnS concentrations increase from 0.04 to 0.5 μmol g dry $wt.^{-1}$, in parallel to the decrease of the Fe-oxide bound pool. Since the pore waters are super-

saturated with respect to ZnS, very low values of the rate constant for ZnS precipitation are required to maintain Zn^{2+} concentrations in the observed range (Table 6.4). Processes that slow or inhibit the reaction between dissolved Zn and sulfide, such as Zn^{2+} binding to DOC, are implicitly included in this rate constant.

ZnS oxidation and Zn^{2+} scavenging by newly formed oxides in the sediment are important processes occurring in the upper millimeters of sediment, due to the shallow O_2 penetration depth (~4-7 mm; Canavan et al., 2006). The diffusive flux of Zn^{2+} from the sediment to the overlying water (OLW) is sensitive to the rates of these processes. ZnS oxidation contributes significantly to the release of Zn^{2+} in the upper millimeters of sediment and, consequently, strongly modulates Zn^{2+} fluxes at the SWI. In a simulation run without ZnS oxidation the flux of dissolved Zn^{2+} across the SWI changed from an efflux of 24 nmol cm^{-2} yr^{-1} to an influx of 9 nmol cm^{-2} yr^{-1} into the sediment. Model results suggest that 40% of the deposited Fe-oxide bound Zn is converted to ZnS (Fig. 6.8a).

The modeled Ni^{2+} pore water concentrations are in the range measured in the upper 16 cm of the sediment, although the modeled peak concentration is greater than observed and the peak occurs over a more narrow depth range (Fig. 6.1). Modeled concentrations of Ni^{2+} are greater than measured values below 16 cm. Model concentrations of Ni associated with Mn-oxides are in reasonable agreement with CDB-extractable Ni concentrations (Fig. 6.6d). The model derived FeS_2:Ni concentrations are similar to the extraction results in the upper 10 cm (Fig. 6.9a). The peak in FeS_2 (Table 6.2, DOP) and associated Ni below 10 cm cannot be reproduced by the steady-state model, however. The ratio of FeS:Ni is estimated at 833 through model fitting of pore water Ni^{2+}. This ratio is comparable to values found in sulfidic precipitations on Teflon sheets incubated in fresh water lakes (~1000-1100; Huerta-Diaz et al. 1993). The modeled Ni^{2+} concentration is quite sensitive to changes in the FeS:Ni ratio (Fig. 6.9b). Decreasing the ratio value results in complete removal of Ni from the pore water and alters the mass balance of Ni in the model. A FeS:Ni ratio of 1100 results in Ni^{2+} concentrations that were greater than all measured values.

Model results suggest that only 17% of the deposited Mn-oxide bound Ni is buried in that form (Fig. 6.8b). As Ni is released from Mn-oxides, 37% is bound to FeS or FeS_2. An additional 30% of the FeS_2:Ni pool is derived from deposition. Pore water Ni^{2+} that is not removed to sulfides mostly escapes from the sediment through diffusion or bioirrigation. Together the Ni^{2+} efflux from the sediment represents 50% of the modeled deposition flux of reactive Ni from the water column.

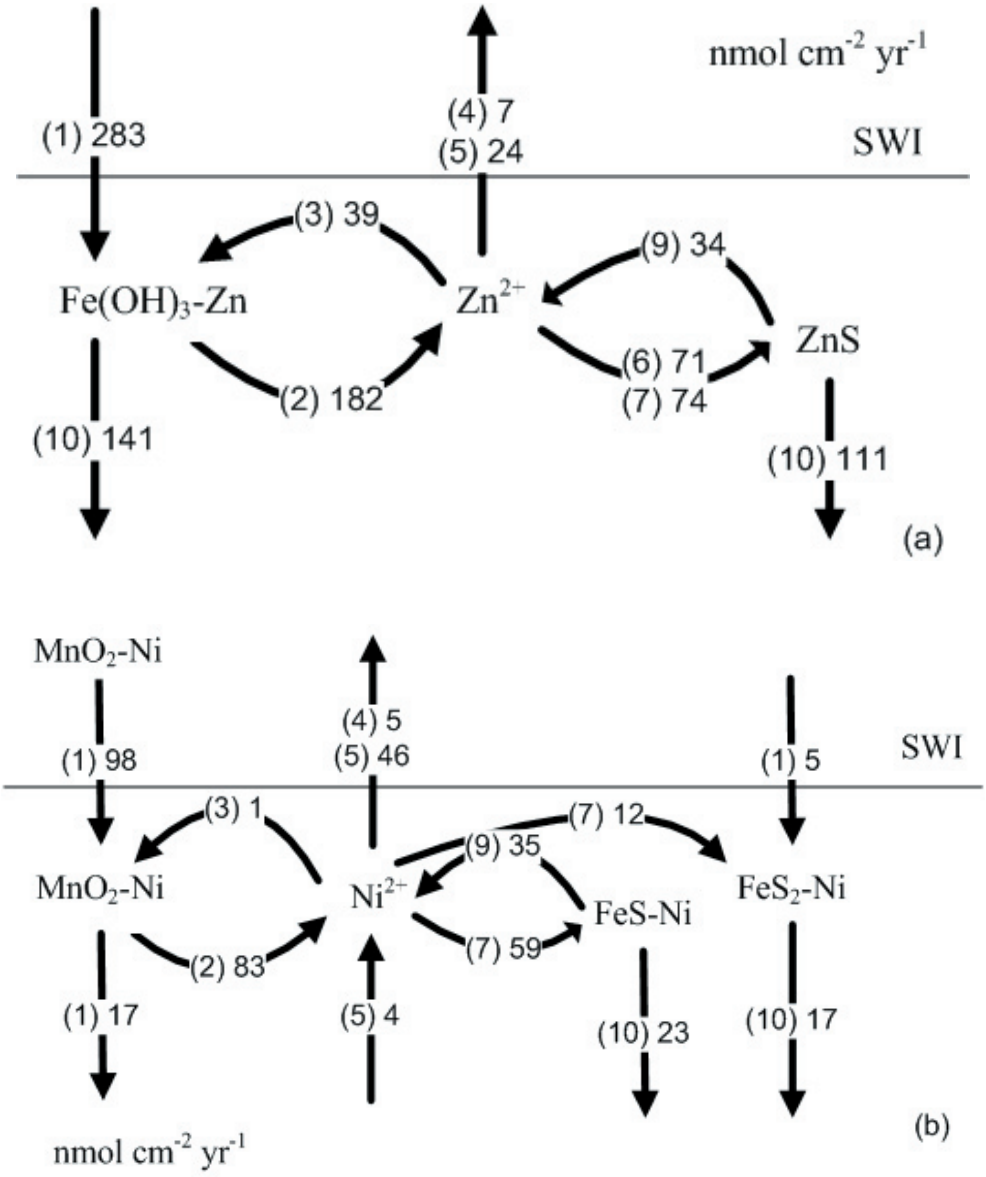

Figure 6.8 Schematic representations of the model reaction and transport processes for Zn (a) and Ni (b). The bracketed numbers refer to the description of processes given in Table 6.3. Depth integrated rates for the upper 20 cm of sediment are given on the arrows in units of nmol cm^{-2} yr^{-1}; discrepancies in mass balance are a result of rounding.

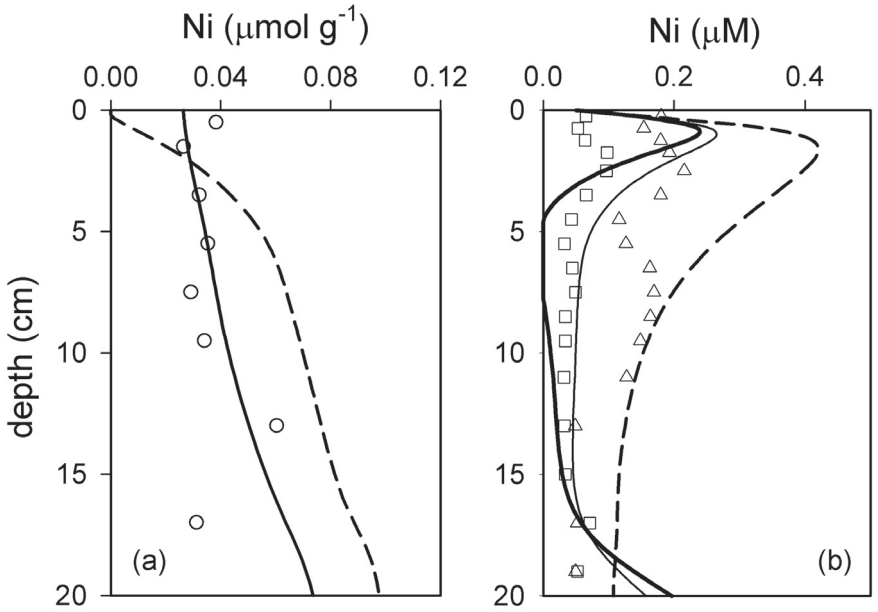

Figure 6.9. (a) Ni distribution from the pyrite fraction of the Huerta-Diaz and Morse (1990) extraction (o). A solid line represents the model concentration of FeS_2-Ni. The dashed line is the model concentration of FeS-Ni, which is not constrained by extraction data. (b) Pore water concentrations of Ni from late-summer (□) and spring (△). Modeled concentration of Ni^{2+} with FeS-Ni set to 588 (heavy line), 833 (thin line), and 1100 (dashed line).

The simple steady-state model in this study represents the initial step in the process of describing the complex and dynamic *in-situ* conditions. However, even at this stage the model results for Zn and Ni provide valuable information. While sediment efflux of Ni^{2+} corresponds to 50% of the reactive Ni input flux, it is only 11% in the case of Zn, implying a higher retention efficiency of Zn in the sediment (Fig. 6.8). It is important to remember that modeled input fluxes are only coupled to the Fe and Mn-oxide phases. Thus the total metal input fluxes are higher than the reactive metal input fluxes. The increased mobility of Ni relative to Zn can be explained by differences in removal by oxide formation and oxidative dissolution of sulfides. In the model, Ni^{2+} is removed by newly formed Mn-oxides, which precipitate at a slower rate than Fe-oxides. Therefore, the *in-situ* Zn and Ni behavior may not differ as greatly as suggested by the model calculations, because Zn^{2+} and Ni^{2+} can be scavenged by Fe and Mn-oxides. The sediment extractions further suggest a mixed Fe/Mn-oxide phase forming in the surface sediment.

The oxidation and dissolution of FeS occurs more readily than that of ZnS, allowing for a greater release of adsorbed Ni than precipitated Zn. Metal release via sulfide oxidation occurs primarily in the upper millimeters of sediment, which allows for diffusion across the SWI. Bioirrigation is responsible for less transport of metal to the OLW than diffusion for both Zn and Ni. The low rate of transport via bioirrigation is due to the similarity in concentration of bottom water and average pore water.

Additional simulations assess the sensitivity of the model to increased sulfate availability and bioturbation (Table 6.5). These changes are expected to accompany estuarine restoration as marine waters contain higher sulfate concentrations and higher bottom water salinity is expected to change the composition of the benthic community at the site, resulting in increased bioturbation. Increased sulfate concentrations in the OLW favor sulfate reduction in the sediment, elevating sulfide concentrations. Increasing sediment mixing also results in increased sulfate reduction as reactive OM is mixed below the depth of oxygen penetration. In these scenarios, the formation of ZnS and Ni adsorption to Fe-sulfides increases up to 35% and 26%, respectively, in response to the increased sulfide production in the sediment. Increased mixing at the sediment surface ($+D_{b0}$) leads to a greater rate of FeS oxidation allowing for a slight increase in Ni efflux, despite a greater adsorption of Ni to Fe-sulfides. This is not observed for Zn because ZnS oxidation occurs more slowly than FeS. The simulated changes to sediment processes resulting from estuarine restoration are shown to have a greater effect on the solid phase speciation than on metal efflux.

Table 6.5 The net rates of ZnS precipitation, Ni adsorption to Fe-sulfides, and release to the overlying water in simulations with increased sulfate availability in the overlying water, increased bioturbation intensity (D_{b0}) and deeper bioturbation (λ).

Scenario	ZnS precipitation	Zn^{2+} efflux to OLW	Ni^{2+} adsorption to FeS and FeS_2	Ni^{2+} efflux to OLW
	nmol cm^{-2} yr^{-1}			
Initial conditions[a]	110	31	62	51
$+SO_4^{2-}$ (10 mM)	122	27	63	51
$+D_{b0}$ (10 cm^2 yr^{-1})	133	31	74	54
$+\lambda$ (5 cm^{-1})	114	31	65	52
$+D_{b0}$ and $+\lambda$	137	30	78	55
$+D_{b0}$, $+\lambda$, $+SO_4^{2-}$	148	24	78	55

(a) Initial conditions: SO_4^{2-} in OLW 0.638 mM, D_{b0}=5 cm^2 yr^{-1}, λ = 2.5 cm^{-1}

6.5 CONCLUSIONS

The Haringvliet Lake sediment exhibits elevated concentrations of trace metals (Cd, Co, Ni, Pb, and Zn) derived from riverine suspended particles. Results of extractions show declining concentrations of reducible phases and an increase in sulfide species with depth. Pore waters are supersaturated with respect to Zn, Pb, Co, and Cd monosulfides, while Ni and Co are found to be associated with pyrite. These results illustrate a transition from oxide-bound to sulfide-bound trace metals with depth in the sediment. Total metal sediment profiles suggest that little metal release from the sediment is occurring with the possible exception of Ni. Diagenetic model simulations predict a greater mobility of Ni than Zn, as Ni does not form stable metal-sulfides, and is more slowly removed by oxidative precipitation at the sediment surface. Upon restoration of estuarine conditions, sulfide phases may become increasingly important for sediment trace metal speciation, while trace metal efflux should be relatively unaffected.

Appendix

The model concentrations of Fe and Mn-oxides in the original model (Canavan et al. 2006) were fit to the ascorbate extraction values because the CDB values were not available. The depositional flux of $Fe(OH)_3B$ and MnO_2B are increased in this simulation to approximate the results of the CDB extraction. (The model contains two pools of Fe and Mn-oxides: pool A can be reduced by reaction with organic matter and sulfide, pool B is only reactive with sulfide.) An input flux of FeS_2 is included in the model to better fit the concentrations obtained from the Huerta-Diaz and Morse (1990) extraction. The changes to the inputs of Fe and Mn necessitated the adjustment of other parameters to best fit the profiles of Fe^{2+}, Mn^{2+}, ΣHS^- H_2S, and FeS. The parameters are described and the new values are presented in Table A1.

Table A1. Changes in boundary conditions and parameter values from the model presented in Canavan et al., (2006)

Species	units	current	previous	Description
MnO_2B	μmol cm^{-2} yr^{-1}	3.7	2.1	depositional flux
$Fe(OH)_3B$	μmol cm^{-2} yr^{-1}	42.0	23.1	depositional flux
FeS_2	μmol cm^{-2} yr^{-1}	3.2	0.0	depositional flux
$KmFe(OH)_3$	μmol g^{-1}	500	200	limiting concentration for Fe-reduction with OM
kfemn	μM yr^{-1}	1 $x10^{-2}$	1 $x10^{-1}$	rate constant for the reduction of MnO_2 by Fe^{2+}
ktsmn	μM yr^{-1}	4 $x10^{-3}$	7.5 $x10^{-3}$	rate constant for the reduction of MnO_2 by sulfide
ktsfe	μM yr^{-1}	8 $x10^{-4}$	2.5 $x10^{-3}$	rate constant for the reduction of $Fe(OH)_3$ by sulfide
kfespre	mol g^{-1} yr^{-1}	7.5 $x10^{-4}$	1.5 $x10^{-3}$	rate constant for the formation of FeS(s) from Fe^{2+} and sulfide
kpyrpre	μM yr^{-1}	9 $x10^{-3}$	3.3 $x10^{-3}$	rate constant for the formation of FeS_2(s) from FeS(s) and sulfide

References

Aguilera, D. R., P. Jourabchi, C. Spiteri, and P. Regnier. 2005. A knowledge-based reactive transport approach for the simulation of biogeochemical dynamics in earth systems. Geochemistry, Geophysics, Geosystems 6**:** Q07012.

Allison, J. D., D. S. Brown, and K. J. Novo-Gradac. 1991. MINTEQA2/PRODEFA2, a geochemical assessment model for environmental systems: Version 3.0 Users Manual. U.S. Environmental Protection Agency,

Anonymous. 1998. MER beheer Haringvlietsluizen report (Environmental Impact Report- Haringvliet dam management). Rijkswaterstaat directie Zuid-Holland, APV 98.186. (in Dutch).

Audry, S., G. Blanc, J. Schafer, G. Chaillou, and S. Robert. 2006. Early diagenesis of trace metals (Cd, Cu, Co, Ni, U, Mo, and V) in the freshwater reaches of a macrotidal estuary. Geochimica et Cosmochimica Acta 70**:** 2264.

Baird, C., and M. Cann. 2005. Environmental Chemistry. 3rd. edition. W.H. Freeman and Company.

Benning, L. G., R. T. Wilkin, and H. L. Barnes. 2000. Reaction pathways in the Fe-S system below 100 degrees C. Chemical Geology 167**:** 25-51.

Boudreau, B. P. 1999. Metals and models: Diagenetic modelling in freshwater lacustrine sediments. Journal of Paleolimnology 22**:** 227-251.

Canavan, R. W., C. P. Slomp, P. Jourabchi, P. Van Cappellen, A. M. Laverman, and G. A. van den Berg. 2006. Organic matter mineralization in sediment of a coastal freshwater lake and response to salinization. Geochimica et Cosmochimica Acta 70**:** 2836-2855.

Cappuyns, V., and R. Swennen. 2005. Kinetics of element release during combined oxidation and pHstat leaching of anoxic river sediments. Applied Geochemistry 20**:** 1169.

Carbonaro, R. F., J. D. Mahony, A. D. Walter, E. B. Halper, and D. M. Di Toro. 2005. Experimental and modeling investigation of metal release from metal-spiked sediments. Environmental Toxicology and Chemistry 24**:** 3007-3019.

Carroll, S., P. A. O'Day, B. Esser, and S. Randall. 2002. Speciation and fate of trace metals in estuarine sediments under reduced and oxidized conditions, Seaplane Lagoon, Alameda Naval Air Station (USA). Geochemical Transactions 3**:** 81-101.

Cline, J. D. 1969. Spectrophotometric determination of hydrogen sulfide in natural waters. Limnology and Oceanography 14**:** 454-458.

Davison, W., N. Phillips, and B. J. Tabner. 1999. Soluble iron sulfide species in natural waters: Reappraisal of their stoichiometry and stability constants. Aquatic Sciences 61**:** 23-43.

Di Toro, D. M., J. D. Mahony, D. J. Hansen, and W. J. Berry. 1996. A model of the oxidation of iron and cadmium sulfide in sediments. Environmental Toxicology and Chemistry 15**:** 2168-2186.

Di Toro, D., J. Mahony, D. Hansen, K. Scott, M. Hicks, S. Mayr, and M. Redmond. 1990. Toxicity of cadmium in sediments: The role of acid volatile sulfide. Environmental Toxicology and Chemistry 9**:** 1487-1502.

Douglas, G. B., and J. A. Adeney. 2000. Diagenetic cycling of trace elements in the bottom sediments of the Swan River Estuary, Western Australia. Applied Geochemistry 15**:** 551-566.

Ferguson, H. A., and W. J. Wolff. 1984. The Haringvliet-Project: The development of the Rhine-Meuse Estuary from tidal inlet to stagnant freshwater lake. Water Science and Technology 16**:** 11-26.

Gallon, C., A. Tessier, C. Gobeil, and M. C. Alfaro-De La Torre. 2004. Modeling diagenesis of lead in sediments of a Canadian Shield lake. Geochimica et Cosmochimica Acta 68**:** 3531-3545.

Holmer, M., and P. Storkholm. 2001. Sulphate reduction and sulphur cycling in lake sediments: a review. Freshwater Biology 46**:** 431-451.

Huerta-Diaz, M. A., R. Carignan, and A. Tessier. 1993. Measurement of trace-metals associated with acid volatile sulfides and pyrite in organic fresh-water sediments. Environmental Science & Technology 27**:** 2367-2372.

Huerta-Diaz, M. A., and J. W. Morse. 1990. A quantitative method for determination of trace metal concentrations in sedimentary pyrite. Marine Chemistry 29**:** 119-144.

Huerta-Diaz, M. A., A. Tessier, and R. Carignan. 1998. Geochemistry of trace metals associated with reduced sulfur in freshwater sediments. Applied Geochemistry 13**:** 213-233.

Hyacinthe, C., and P. Van Cappellen. 2004. An authigenic iron phosphate phase in estuarine sediments: composition, formation and chemical reactivity. Marine Chemistry 91**:** 227-251.

Jourabchi, P., P. Van Cappellen, and P. Regnier. 2005. Quantitative interpretation of pH distributions in aquatic sediments: A reaction-transport modeling approach. American Journal of Science 305**:** 919-956.

Kay, J. T., M. H. Conklin, C. C. Fuller, and P. A. O'Day. 2001. Processes of nickel and cobalt uptake by a manganese oxide forming sediment in Pinal Creek, globe mining district, Arizona. Environmental Science & Technology 35**:** 4719-4725.

Kostka, J. E., and G. W. Luther. 1994. Partitioning and speciation of solid-phase iron in salt-marsh sediments. Geochimica et Cosmochimica Acta 58**:** 1701-1710.

Morse, J. W., and T. Arakaki. 1993. Adsorption and coprecipitation of divalent metals with mackinawite (FeS). Geochimica et Cosmochimica Acta 57**:** 3635.

Morse, J. W., and G. W. Luther. 1999. Chemical influences on trace metal-sulfide interactions in anoxic sediments. Geochimica et Cosmochimica Acta 63**:** 3373-3378.

Motelica-Heino, M., C. Naylor, H. Zhang, and W. Davison. 2003. Simultaneous release of metals and sulfide in lacustrine sediment. Environmental Science & Technology 37**:** 4374-4381.

Naylor, C., W. Davison, M. Motelica-Heino, G. A. van den Berg, and L. M. van der Heijdt. 2004. Simultaneous release of sulfide with Fe, Mn, Ni and Zn in marine harbour sediment measured using a combined metal/sulfide DGT probe. Science of the Total Environment 328**:** 275-286.

Otero, X. L., and F. Macias. 2002. Variation with depth and season in metal sulfides in salt marsh soils. Biogeochemistry 61**:** 247-268.

Paalman, M. A. A. 1997. Processes affecting the distribution and speciation of heavy metals in the Rhine/Meuse Estuary. PhD Thesis. Utrecht University.

Paalman, M. A. A., and C. H. van der Weijden. 1992. Trace metals in suspended matter from the Rhine/Meuse estuary. Netherlands Journal of Sea Research 29**:** 311.

Perret, D., J. F. Gaillard, J. Dominik, and O. Atteia. 2000. The diversity of natural hydrous iron oxides. Environmental Science & Technology 34**:** 3540-3546.

Postma, D., and R. Jakobsen. 1996. Redox zonation: Equilibrium constraints on the Fe(III)/SO4-reduction interface. Geochimica et Cosmochimica Acta 60**:** 3169-3175.

Raiswell, R., D. E. Canfield, and R. A. Berner. 1994. A comparison of iron extraction methods for the determination of degree of pyritisation and the recognition of iron-limited pyrite formation. Chemical Geology 111**:** 101-110.

Reinhold-Dudok van Heel, H. C., and P. J. den Besten. 1999. The relation between macroinvertebrate assemblages in the Rhine-Meuse delta (The Netherlands) and sediment quality. Aquatic Ecosystem Health and Management 2**:** 19-38.

Roden, E. E. 2003. Fe(III) oxide reactivity toward biological versus chemical reduction. Environmental Science & Technology 37**:** 1319-1324.

Sarazin, G., G. Michard, and F. Prevot. 1999. A rapid and accurate spectroscopic method for alkalinity measurements in sea water samples. Water Research 33**:** 290-294.

Slomp, C. P., E. H. G. Epping, W. Helder, and W. Van Raaphorst. 1996. A key role for iron-bound phosphorus in authigenic apatite formation in North Atlantic continental platform sediments. Journal of Marine Research 54**:** 1179-1205.

Smit, H., R. Smits, G. van der Velde, and H. Coops. 1997. Ecosystem responses in the Rhine-Meuse delta during two decades after enclosure and steps toward estuary restoration. Estuaries 20**:** 504-520.

Smith, S. L., and P. R. Jaffé. 1998. Modeling the transport and reaction of trace metals in water- saturated soils and sediments. Water Resources Research 34**:** 3135-3147.

Taillefert, M., B. J. Macgregor, J. F. Gaillard, C. P. Lienemann, D. Perret, and D. A. Stahl. 2002. Evidence for a dynamic cycle between Mn and Co in the water column of a stratified lake. Environmental Science & Technology 36**:** 468-476.

Teasdale, P. R., S. Hayward, and W. Davison. 1999. In situ, high-resolution measurement of dissolved sulfide using diffusive gradients in thin films with computer-imaging densitometry. Analytical Chemistry 71**:** 2186-2191.

Tessier, A., D. Fortin, N. Belzile, R. R. Devitre, and G. G. Leppard. 1996. Metal sorption to diagenetic iron and manganese oxyhydroxides and associated organic matter: Narrowing the gap between field and laboratory measurements. Geochimica et Cosmochimica Acta 60**:** 387-404.

Thullner, M., P. Van Cappellen, and P. Regnier. 2005. Modeling the impact of microbial activity on redox dynamics in porous media. Geochimica et Cosmochimica Acta 69**:** 5005.

Turner, A., G. E. Millward, and S. M. Le Roux. 2004. Significance of oxides and particulate organic matter in controlling trace metal partitioning in a contaminated estuary. Marine Chemistry 88**:** 179-192.

van den Berg, G. A., S. E. J. Buykx, M. van den Hoop, and L. M. van der Heijdt. 2001. Vertical profiles of trace metals and acid-volatile sulphide in a dynamic sedimentary environment: Lake Ketel, The Netherlands. Applied Geochemistry 16**:** 781-791.

van den Berg, G. A., J. P. G. Loch, L. M. van der Heijdt, and J. J. G. Zwolsman. 1999. Mobilisation of heavy metals in contaminated sediments in the river Meuse, The Netherlands. Water Air and Soil Pollution 116**:** 567-586.

van Griethuysen, C., J. van Baren, E. Peeters, and A. A. Koelmans. 2004. Trace metal availability and effects on benthic community structure in floodplain lakes. Environmental Toxicology and Chemistry 23**:** 668-681.

Wersin, P., P. Hohener, R. Giovanoli, and W. Stumm. 1991. Early Diagenetic Influences on Iron Transformations in a Fresh-Water Lake Sediment. Chemical Geology 90**:** 233-252.

Wolthers, M., L. Charlet, P. R. van der Linde, D. Rickard, and C. H. van der Weijden. 2005. Surface chemistry of disordered mackinawite (FeS). Geochimica et Cosmochimica Acta 69**:** 3469.

Young, L. B., and H. H. Harvey. 1992. The Relative Importance Of Manganese And Iron-Oxides And Organic-Matter In The Sorption Of Trace-Metals By Surficial Lake-Sediments. Geochimica et Cosmochimica Acta 56**:** 1175-1186.

Zhang, H., W. Davison, S. Miller, and W. Tych. 1995. In-Situ high-resolution measurements of fluxes of Ni, Cu, Fe, and Mn and concentrations of Zn and Cd in porewaters by DGT. Geochimica et Cosmochimica Acta 59**:** 4181-4192.

Chapter 7

The effect of estuarine restoration of Haringvliet Lake on sediment water exchange of nutrients and trace metals: implications for surface water quality

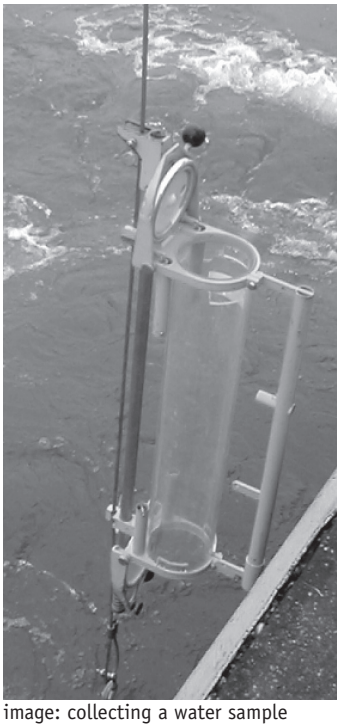

image: collecting a water sample

In this chapter the processes controlling changes in sediment-water exchange of nitrogen, phosphorus, and trace metals expected after restoration of estuarine conditions in the Haringvliet are briefly reviewed. Additional experimental data are provided to supplement the results of Chapters 2-6. These experiments assess the effects of salinization on N, P, and trace metal release. Finally the possible effects of these changes for surface water quality in the Haringvliet are reviewed. The experimental and analytical procedures are as described in Chapters 2-6.

7.1 Sediment-water exchange of nitrogen

Haringvliet sediments are currently a sink for NO_3^- and source of NH_4^+ (Chapter 4). The experimental and modeling results presented in Chapters 3 and 4 indicate that estuarine restoration may enhance the release of dissolved inorganic nitrogen (DIN) from the sediment, in particular in the form of NH_4^+.

Results obtained with Flow Through Reactors (FTRs) containing intact sediment slices show a pulse release of NH_4^+ following exposure to increased salinity. This is a well-documented phenomenon (e.g. Gardner et al. 1991; Seitzinger et al. 1991) which results from the competition of NH_4^+ with other cations, such as Na^+, for exchange sites in the sediment. The process is rapid and would be limited to the first days to months of bottom water salinization (Fig. 4.4). The addition of NaCl to the FTR inflow solution also resulted in an increased release of NO_2^- (Chapter 3). This release declined after 40 hours (Fig. 7.1), suggesting it is also a transient feature. Short-term release of NH_4^+ and NO_2^- may be toxic to some organisms (Hargreaves 1998), and contributes to oxygen consumption through nitrification. Oxygen consumption may also be stimulated by the transient salinity induced mobilization of sediment-bound organic matter (Chapter 3).

Long-term changes in sediment N-cycling following restoration could result from a salinity-induced shift in nitrate reduction pathways from denitrification to dissimilatory nitrate reduction to ammonium (DNRA). This is important for water quality because denitrification releases N_2, which is not immediately bioavailable, while DNRA releases NH_4^+, which is readily available for primary producers (Chapters 3 & 4). Actual changes with rates of nitrate reduction will also be influenced by the variation in availability of NO_3^- and reactive organic matter. Nitrate concentrations in the adjacent North Sea water are significantly lower (~ 90 μM) than those currently found in the Haringvliet (~160 μM). Thus, total nitrate reduction rates in the sediment are expected to decrease after the restoration.

Changes in organic matter supply and reactivity are more difficult to predict. The addition of nutrient poor, turbid coastal water may lower primary production rates and decrease the deposition rate of labile organic matter. On the other hand, increased salinity could also lead to

flocculation and increased deposition of organic matter. An additional change in environmental conditions that would affect benthic N cycling is a decrease in bottom water oxygen concentration upon salt intrusion in the Haringvliet. This would tend to decrease nitrification in the sediment and further reduce the contribution of nitrate reduction to organic matter breakdown

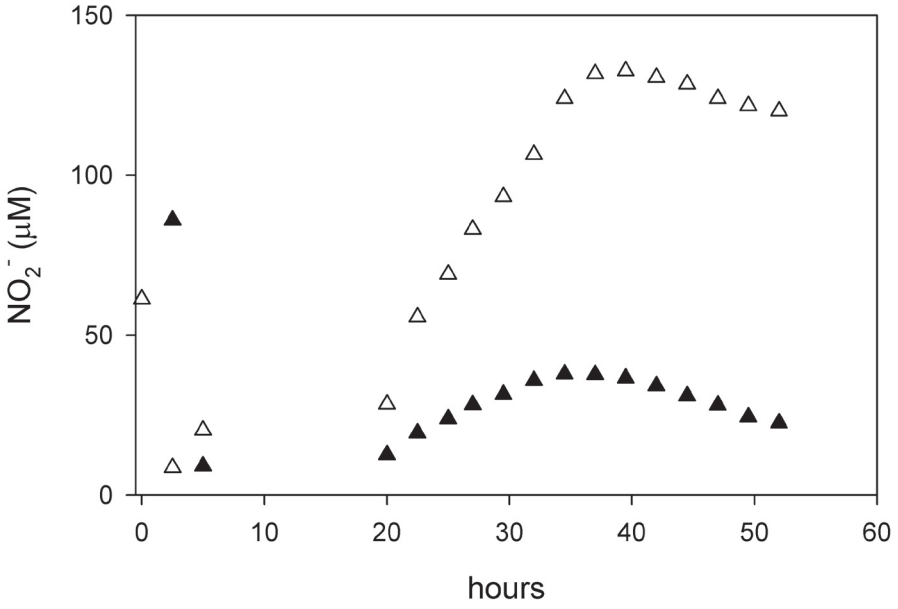

Figure 7.1 Nitrite (NO_2^-) concentrations in FTR outflow solutions from reactors obtained during the spring sampling (0-1 cm) and incubated at ambient temperature (12°C) at a flow rate of 6 ml $hour^{-1}$. The input solution to the FTR contained 0.5 mM KNO_3 (▲) or 0.5 mM KNO_3 and 10‰ NaCl (△).

7.2 Sediment-water exchange of phosphorus

A significant proportion (~60%) of the organic and Fe-bound P deposited at our site, is currently being released to the overlying water as dissolved P (Chapter 5). Estuarine restoration is expected to enhance this release of P by causing a shift in Fe speciation from Fe-oxides to pyrite in the sediment on a decadal time scale (Chapters 2 and 5). The cause of this change is increased sulfate reduction, driven by both increased sulfate availability in the brackish waters and increased bioturbative mixing of organic matter below the oxic and suboxic zones. A salinity-induced increase in the organic matter degradation rate (Chapter 3) may also lead to enhanced organic-P mineralization.

The changing chemistry of the overlying water will also influence the solubility of P-minerals, for example, abundant sulfide may lower Fe^{2+} concentrations and inhibit the formation of vivianite. The initial increase in pore water salinity will lead to the release of exchangeable or adsorbed-P and may release dissolved organic-P through the plasmolysis of bacterial cells (Gardolinski et al. 2004). These processes may explain the increased P release rates in FTR experiments particularly at NaCl concentrations above 5‰ (Fig. 7.2).

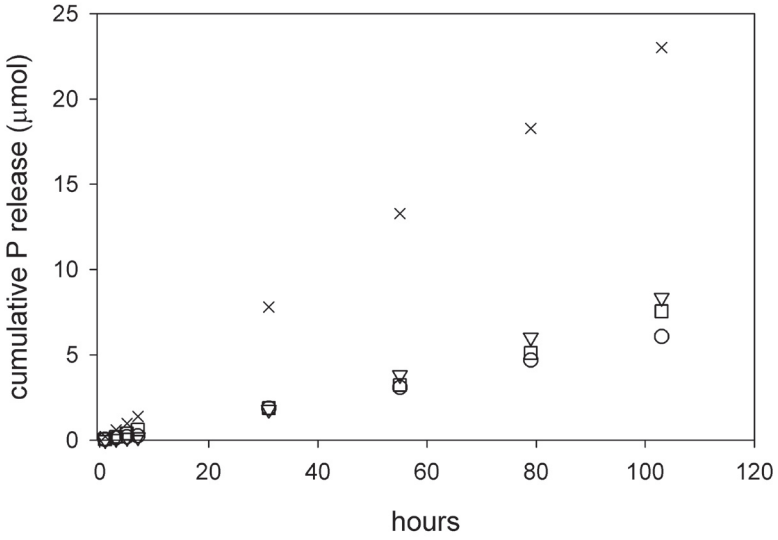

Figure 7.2 The release of total dissolved P from FTRs where inflow solution salinity was 0‰ (□), 2‰ (○), 5‰ (▽), and 10‰ (×) as NaCl. Sediment from depth intervals of 1-2 cm was collected in April, 2004. The input solution flow rate was approximately 5.5 ml $hour^{-1}$.

7.3 Sediment-water exchange of trace metals

Total sediment profiles of trace metals suggest efficient retention in the sediments at present (Chapter 6). Diagenetic modeling of Zn and Ni dynamics suggests that increased rates of sulfate reduction rate may further decrease the long-term Zn efflux to the overlying water and increase the accumulation of sulfide-bound Zn. The Ni efflux is less sensitive to the various restoration scenarios and might increase slightly in response to increased mixing at the surface. Generally, the model results suggest that Ni is more mobile than Zn due to the fact that sulfide-bound Ni is more readily oxidized than sulfide-bound Zn.

Overall, trace metal stability in the sediment is expected to increase with increased sulfate reduction rates; however increased mixing by benthic organisms or turbulent flow could enhance

sulfide oxidation and trace metal release. The release of exchangeable metals due to increased salinity may also result in the release of trace metals to solution, particularly during the early stages of estuarine restoration. This was confirmed for Cr, Zn, Ni and Cd in FTR experiments in which surface sediment was exposed to NaCl concentrations of 5‰ (Fig. 7.3). In contrast to the other metals, the salinity response of Cu did not diminish throughout the 24-hour experiment. Lead concentrations did not exhibit a salinity response in this experiment.

Cadmium is particularly sensitive to increasing salinity because cadmium chloride ion pairs can form in solution (e.g. Paalman et al. 1994). Slurry incubations of sediment with increased salinity showed increased Cd solubility (Fig. 7.4). Cadmium sulfides are also highly insoluble ($K_{SO} = 10^{-14}$; Daskalakis and Helz 1992), thus increased sulfate reduction may limit the release of Cd caused by the formation of chloride-complexes.

The release of exchangeable trace metals in response to salinization is expected to be primarily a transient response, while other processes such as the rates and distributions of organic matter decomposition, sulfate reduction, sulfide oxidation, and sediment mixing are expected to be import processes for the long-term sediment water exchange of trace metals. While the expected increase in sulfate reduction rate suggests long-term trace metal stability in the sediment, this is not a certainty. Metals such as Cr, Mn, and Ni are less likely to form sulfide precipitates than Zn, Pb, and Cd and therefore may respond differently to the changing sediment conditions. Monitoring following restoration is needed to assess the new conditions of the sediment with regards to trace metal solubility.

7.4 Restoration Area

The area of the lake that will be salinized by the restoration is a critical factor in determining the net potential efflux of nutrients and trace metals. The actual extent of salinization of bottom waters is dependent on, among other factors, lake bathymetry, river stage, wind-stress, and the degree and configuration of the opening in the gates of the dam (Jacobs et al. 2003). The sediment response will also depend on the chemical content of the sediment. Sandy sediment is also present in the restoration area and is likely to be less reactive than the fine-grained sediment that was the focus of this study. The deeper basins in the lake are the areas which have accumulated recent fine-grained sediments (van Wijngaarden et al. 2002) and are also most likely to develop salinity stratification. Longer-term management plans include the possibility of expanding the range of restored tidal brackish water conditions to much of the Haringvliet and adjacent Volkerak by 2030, which would be a significant expansion of the initial restoration area. The initial restoration area will be approximately 30 km^2. In future this could increase up to 60 km^2 in the Haringvliet and ultimately include an additional 60 km^2 in the Volkerak.

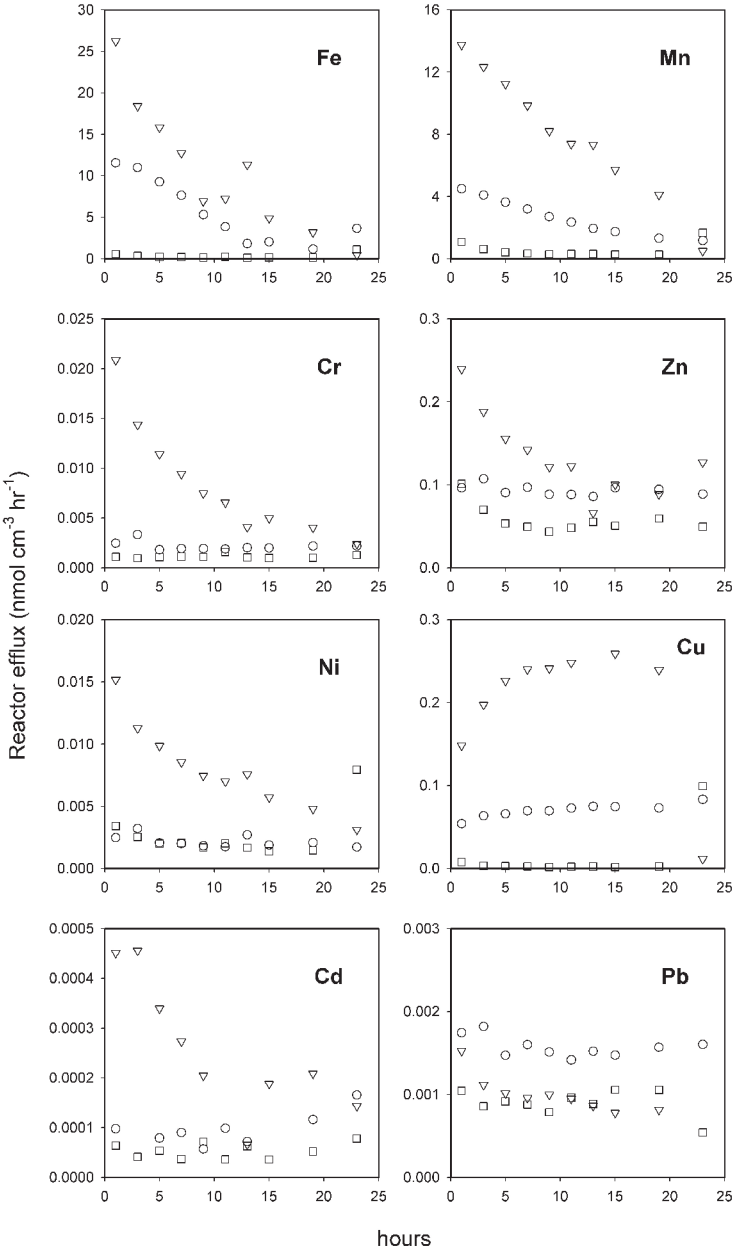

Figure 7.3 The efflux rate (nmol cm^{-3} $hour^{-1}$) of total dissolved Fe, Mn, Cr, Zn, Ni, Cu, Cd, and Pb from FTRs where inflow solution salinity was 0‰ (□), 2‰ (○), and 5‰ (▽) as NaCl. Sediment was collected in April, 2004 at a depth range of 1-2 cm and the input solution flow rate was approximately 5.5 ml $hour^{-1}$.

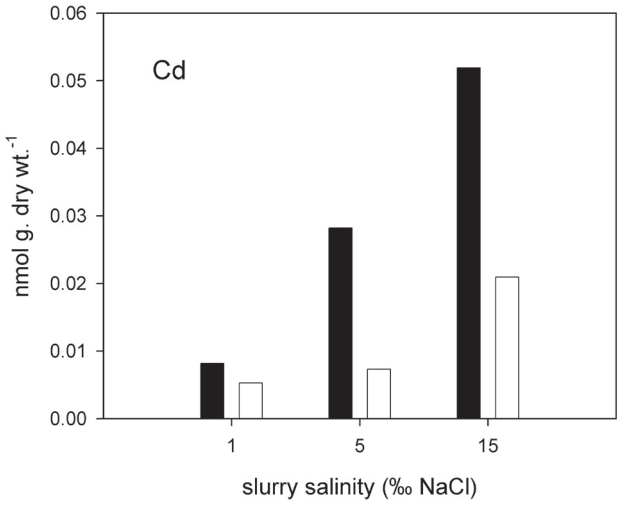

Figure 7.4 Cadmium concentration in the water phase of slurry incubations normalized to weight of sediment in slurry. The slurries were prepared with sediment from 0.5-1.5 cm depth, where NaCl solutions were mixed 2:1 by volume with sediment and incubated for 36 hours under oxic (white bars) or anoxic (black bars) conditions.

7.5 Water flow

The Haringvliet maintains a fluvial nature despite the closure to the sea. Flow rates of fresh water through the dam are variable and are determined by the river discharge rates (Fig. 7.5a). Water flow is seasonal based on precipitation and snow melt in the watershed with greater flow in winter and spring than summer. In the period of 1999-2004 the mean flow rate at the Haringvliet dam was 859 m^3 s^{-1} and the median rate was 442 m^3 s^{-1}, although during dry weather in the summer of 2003 no flow was recorded for an entire month (Rijkswaterstaat, www.waterbase.nl). This variability in discharge from the lake leads to a variable water residence time. Smit et al. (1997) calculate an average residence time of approximately 6-days for the western Haringvliet with a range of 0.6-42 days based on Rhine discharges from 8000 to1200 m^3 s^{-1}.

7.6 The role of sediment-water exchange for surface water quality

Surface water concentrations of nutrients and organic matter in the lake are well-monitored (Fig. 7.5; Rijkswaterstaat, www.waterbase.nl). Nitrate concentrations in the surface water of the lake display a seasonal pattern with lower concentrations in warmer months. Concentrations of

ammonium show a less distinct seasonal trend, with higher concentrations in winter months but also sharp increases in June and July. The increased NH_4^+ levels in summer may result from wastewater discharge to the rivers when low river flow limits dilution. Our results however, also suggest that NH_4^+ efflux from bottom sediments may contribute to higher concentrations during summer months. Lower concentrations of ammonium compared to nitrate are likely due to preferential removal by algae (Middelburg and Nieuwenhuize 2000) and nitrification in the water column. The dissolved P concentrations in surface water decline in spring, preceding the decline in NO_3^- (Fig. 7.5). Declining P concentrations roughly correspond with periods of increasing organic matter in lake suspended matter suggesting P removal is the result of biological uptake in the lake and river basin.

Table 7.1 combines estimated changes in nutrient efflux rates (Chapters 3-6), restoration surface areas, and flow rates to determine an estimated change in surface water concentrations based on a 30 km^2 restoration area and a median flow rate (440 $m^3\ s^{-1}$). For example, at median flow rates the maximum increase in DIN due to benthic efflux is 2.7 μM, which represents a 1.8% increase in concentration (Fig. 7.5). Sediment efflux of nutrients and trace metals will have the greatest influence on water quality if low flow river conditions result in extended closure of the dam, or if salinity stratification results in stagnant bottom waters. These two conditions are likely to occur simultaneously. The release of reduced species from the sediment under stagnant conditions could also lower oxygen concentrations in the bottom water. Future water quality monitoring in the restored estuary should therefore include bottom water chemistry in stratified areas during low flow conditions, when they arise.

The results of this thesis show that salinization will have a significant impact on the biogeochemical processes in the sediments of the Haringvliet on both the short- and long-term. However, given the relatively high water fluxes and small impact area, the influence of these changes in the sediment on surface water concentrations of nutrients and trace metals is expected to be relatively limited.

Figure 7.5 Water quality data for the period 1999-2004 from the Haringvliet. The flow rate, Q, in $m^3\ s^{-1}$ is from daily measurements and plotted as a solid line (a). Filtered surface water concentrations of NO_3^- (b), NH_4^+ (c), and ortho-Phosphate ($o\text{-}PO_4$; d) as μM and mg l^{-1} and the organic carbon content of the suspended particulate matter (e; % dry weight) from monthly or bi-monthly sampling. The sampling dates of November 2001 (fall), September 2002 (late-summer), and April 2003 (spring) are marked with vertical lines across the plots. Data were obtained from the publicly available database of the Rijkswaterstaat (www.waterbase.nl) and are reproduced with permission.

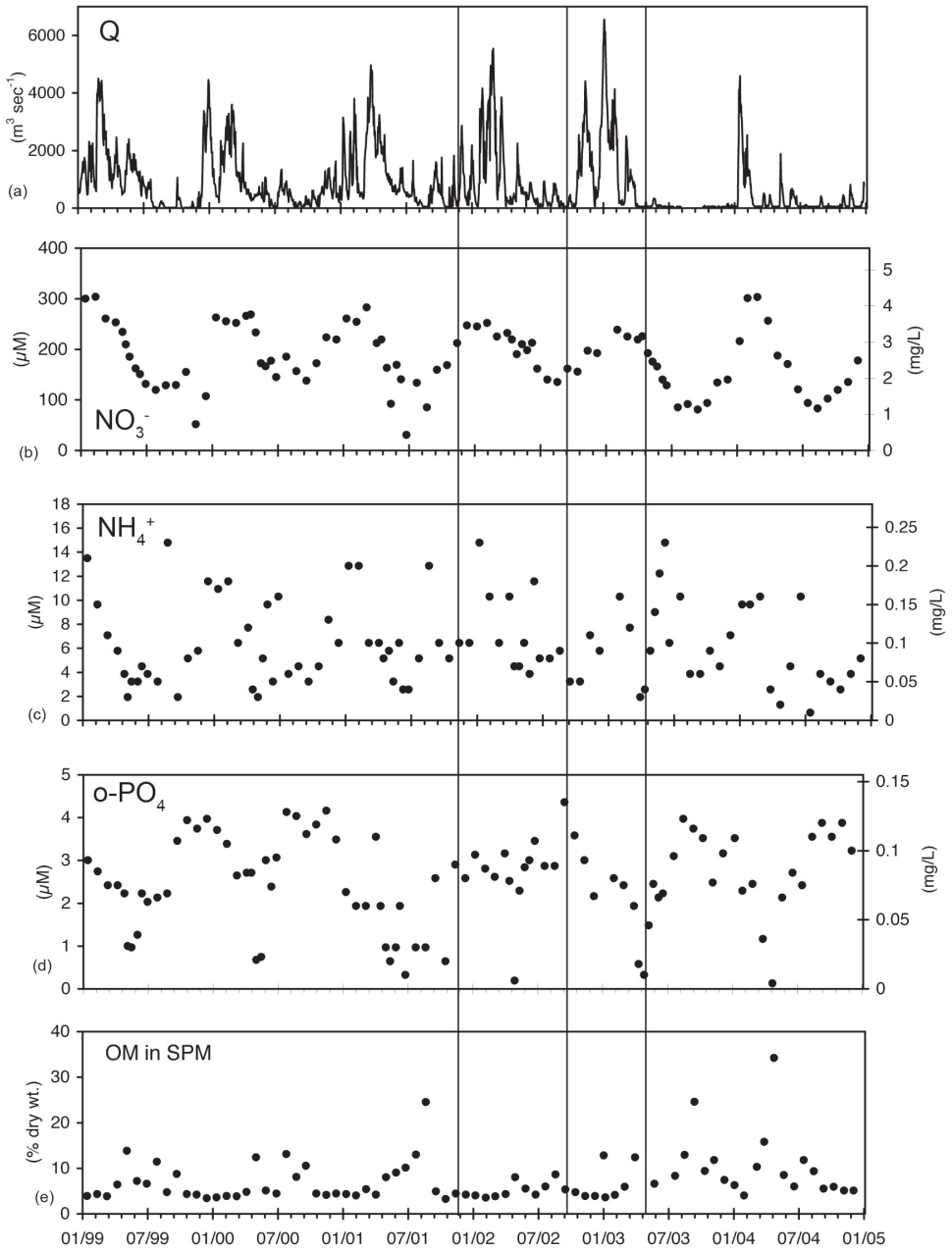

Figure 7.5 see previous page for description

Table 7.1 Expected changes in nutrient and trace metal efflux based on model and experimental studies. Efflux rates are multiplied by the estimated restoration area to derive a rate in moles per day. Estimated changes in surface water concentrations are derived for the median flow rate of 440 m^3s^{-1}. Example flow rates are also provided and converted into units of liters per day for reference.

Change in efflux due to salinization[a]			Restoration area 30 (km^2) efflux x area [b]	Estimated conc. change
species	μmol cm^{-2} yr^{-1}	mol km^{-2} day^{-1}	mol day^{-1}	Δ μmol l^{-1}
DIN	45	1224	3.7×10^4	0.97
DIN	125	3425	1.0×10^5	2.7
P	3	82	2.5×10^3	0.06
Zn	-7	-192	-5.8×10^3	-0.15
Ni	4	110	3.3×10^3	0.09

example flow rates	
Flow rate (Q)	
m^3 s^{-1}	L day^{-1}
3000	2.59×10^{11}
860	7.43×10^{10}
440	3.80×10^{10}
50	4.32×10^9
1	8.64×10^7

(a) Key to efflux estimates

species	source
DIN	Figure 3.5; Δ NH_4^+ Production Rate (APR) in +NaCl reactors, 30-55 hours
DIN	Table 4.4; maximum Δ DIN
P	Figure 5.6; maximum Δ efflux
Zn	Table 6.5; maximum Δ efflux
Ni	Table 6.5; maximum Δ efflux

(b) Note that the combination of a single efflux value and surface area is made as a simple estimation of the maximum possible restoration effects. The natural system includes a range of sediment characteristics and will be exposed to a varying degree of salinization depending on depth and location in the lake.

References

Daskalakis, K. D., and G. R. Helz. 1992. Solubility of CdS (Greenockite) in sulfidic Waters at 25 degrees-C. Environmental Science & Technology 26**:** 2462-2468.

Gardner, W. S., S. P. Seitzinger, and J. M. Malczyk. 1991. The effects of sea salts on the forms of nitrogen released from estuarine and freshwater sediments: Does ion pairing affect ammonium flux. Estuaries 14**:** 157-166.

Gardolinski, P. C. F. C., P. J. Worsfold, and I. D. McKelvie. 2004. Seawater induced release and transformation of organic and inorganic phosphorus from river sediments. Water Research 38**:** 688-692.

Hargreaves, J. A. 1998. Nitrogen biogeochemistry of aquaculture ponds. Aquaculture 166**:** 181.

Jacobs, P., B. P. C. Steenkamp, and S. De Goederen. 2003. Van zoet naar zout in 5 dagen? RIZA, RIZA rapport 2003.001. (in Dutch).

Middelburg, J. J., and J. Nieuwenhuize. 2000. Uptake of dissolved inorganic nitrogen in turbid, tidal estuaries. Marine Ecology-Progress Series 192**:** 79-88.

Paalman, M. A. A., C. H. van der Weijden, and J. P. G. Loch. 1994. Sorption of cadmium on suspended matter under estuarine conditions - competition and complexation with major sea-water ions. Water Air and Soil Pollution 73**:** 49-60.

Seitzinger, S. P., W. S. Gardner, and A. K. Spratt. 1991. The effect of salinity on ammonium sorption in aquatic sediments: Implications for benthic nutrient recycling. Estuaries 14**:** 167-174.

Smit, H., R. Smits, G. van der Velde, and H. Coops. 1997. Ecosystem responses in the Rhine-Meuse delta during two decades after enclosure and steps toward estuary restoration. Estuaries 20**:** 504-520.

van Wijngaarden, M., L. B. Venema, and R. J. de Meijer. 2002. Radiometric sand mud characterisation in the Rhine-Meuse estuary part B. In situ mapping. Geomorphology 43**:** 103-116.

Acknowledgements

I am very grateful to have worked with so many different people during this project. While the wide scope of the project meant that I worked with nearly everyone in our group at various times over the last four plus years, I must particularly thank Caroline Slomp for maintaining involvement and providing direction in all phases of the project. I am glad to have been able to work with you and appreciate all your hard work on my behalf.

I thank Caroline, Philippe Van Cappellen, Gerard van den Berg, and Gertjan Zwolsman for developing the project. Philippe, thank you for letting me be a part of the great international group you have brought together and for guidance throughout the project. Gerard and Gertjan thank you for your support through the project: including securing funds for the field work, supporting Madelon van den Hooven for her masters work at the RIZA, and providing data. I also benefited from your advice and perspective. Jos Vink made sure that the project continued to run smoothly after Gerard and Gertjan left the RIZA for KIWA. I also thank Anniet Laverman for being a major contributor to the project. Thank you for letting me include your paper in this thesis (Chapter 3), and I also greatly appreciate your help in the field and in the lab. Het was heel fijn om met jullie samen te werken. Meestal was dat in het Engels, maar af en toe ook in het Nederlands, dus ik schrijf ook graag: hartelijk bedankt.

The three major research cruises were very important to the project and could not have been successful without the help of many additional people. The cruises were staffed primarily with UU geochemistry group members and students who spent several long days on the boat collecting and analyzing samples, and conducting experiments. Cruise participants included: Caroline, Anniet, Gerard, Gertjan, Helen de Waard, Yvonne van Lith, Ralf Haese, Pieter Kleingeld, Thilo Behrends, Christelle Hyacinthe, Celine Pallud, Jacqueline Claessens, Debby Los, Andy Dale, Claudette Spiteri, Fraukje Steffen, Steeve Bonneville, Laurent Voitel, and Parisa Jourabchi. Thank you all very much! Het werk op het R.V. Navicula ging soepel en was heel gezellig. Met dank aan Kees van der Star, Leon Wuis, Tony van der Vis, Johan Tuntelder, en Hein de Vries. Dank aan Gert de Lange voor het gebruik van Marine Geochemistry apparatuur tijdens het veldwerk. Ik wil Pieter, Madelon, Jeffrey Abell, and Ton van Druten bedanken voor de korte veldwerk in maart 2004.

Ik wil Helen, Pieter, Dineke van de Meent, Erik van Vilsteren, Bertil van Os, Rob van Galen, Arnold van Dijk, en Gijs Nobbe graag bedanken voor het analyseren van monsters, voor alle advies en uitleg en voor de opbouw en het onderhoud van de apparatuur. Thanks to Anniet, Debby, Celine, Christelle, and Yvonne for conducting experiments, extractions, and for help with flow through reactor experiments. Thanks to for help with extractions. I enjoyed working

with the marine geochemists in their lab and thank Paul Mason for giving me access to his lab space. I was fortunate to be able to visit Lancaster University to learn the DGT technique and thanks to Hao Zhang for organizing the visit and to Chris Naylor for discussions regarding sulfide analysis with DGT and AVS determination. My work with DGT and AVS analysis also benefited from cooperation with Rob Cleven, Suzan Bukyx and Liesbeth van Dorn at RIVM. Ik wil graag Madelon bedanken voor al je werk in het lab op dit project tijdens je masters. I am also pleased to have been part of the visit of Idoia Sáenz Arteche to our group in Utrecht.

I am indebted to Parisa for the use of her steady-state solver for the BRNS: thanks for all of your careful answers to my questions. Additional advice in model development came from Caroline, Philippe, Andy, Claudette, David Rodríguez Aguilera, Christof Meile, Martin Thullner, and Pierre Regnier. Thank you to Thilo and Mariëtte Wolthers for help with chemical speciation models.

Thanks for the 'gezelligheid' to the rest of the geochemistry group who were not previously mentioned: Anke, Anja, Dennis, Diana, Doug, Gernot, Gert Jan, Goulven, Guus, Iana, José, Kagan, Katja, Marjolijn, Natalia, Nikolaj, Niels, Pien, Rinske, Sandra, Sanela, Shauna, Simon, Socratis, Tom, Vasso, Vincent, and Yanchun.

I have really enjoyed my time in Utrecht. I have thought about how to describe this sometimes while biking home from work, but of course its not possible to do everything justice here. I will list a few of the people and activities that I wish to remember and acknowledge as part of my good 'Utrecht experience'. Becoming a father with two healthy kids born at home. Having the opportunity to have a 'Papa-dag' once a week. Plezier hebben met mijn medecursisten en leraren tijdens mijn inburgeringcursus, genieten van mijn nieuwe Nederlanderschap, van de ouders en leidsters bij kinderopvang de Kikker, bij het frisbeeën met UFO en vooral van het 'Driem Team'. Verder denk ik aan de spelletjesavonden en vriendschappen met Manuel, Francesco(a), Jeroen en Paula. Els en Arafan en Marleen en Iris zijn niet alleen goede buren, maar ook goede vrienden geworden. De familie Groenewegen is vanaf onze eerste dag in Nederland een vaste steun geweest voor Anouk en mij. Wat hebben wij met veel plezier samen Pasen, Sinterklaas, Thanksgiving en verjaardagen gevierd. Ik ben vooral dankbaar voor de vriendschap die is ontstaan met Sara en Philo en ben vereerd dat zij mijn paranimfen zijn. I am grateful for the visits and support of friends and family from the US including my Mom & Dad, Sue, Joosje & Maarten, Katinka, and Florentien. Joosje vooral bedankt voor je hulp rondom de geboorte van Isabella and Lucas. Thanks to my sister Sue for doing the cover layout and helping with the design and layout of this thesis.

My final words of thanks are for my Mom & Dad and Anouk for all your love and support through the years.

Curriculum Vitae

Richard William Canavan IV was born on February 6th 1971 in Putnam, Connecticut in the United States of America. He was the salutatorian of his high school class in 1989 at Woodstock Academy in Woodstock, CT. In 1993 he received a Bachelor of Arts degree in Botany from Connecticut College in New London, CT. During this study he conducted an examination of water quality in 56 lakes for his bachelors honors thesis. This work was awarded the Ames Prize for the best thesis in the graduating class of 1993 and was used to calibrate paleolimnological and watershed land-use studies. Richard received a Masters of Science degree from the Soil, Crop, and Atmospheric Science Department of Cornell University in 1997. Following the completion of the masters he taught university level laboratory classes, worked briefly at the US Geologic Survey in Menlo Park, California, and as an environmental consultant for Vanasse Hangen Brustlin, Inc. in Watertown, Massachusetts. In November, 2001 he began work on this thesis in the geochemistry department of Utrecht University.